

**MODELING AND OPTIMIZATION OF OFF-GRID SOLAR
STREET LIGHTING SYSTEM**

by

Behzad Barzegar Bafrouei

Submitted in partial fulfilment of the requirements
for the degree of Master of Applied Science

at

Dalhousie University
Halifax, Nova Scotia
August 2014

© Copyright by Behzad Barzegar Bafrouei, 2014

Table of contents

List of tables.....	v
List of figures.....	vii
Abstract.....	x
List of abbreviations and symbols used.....	xi
Acknowledgments.....	xiii
Chapter 1 Introduction	1
Chapter 2 Literature review.....	5
2.1 Photovoltaic cells	5
2.2 Photovoltaic systems	6
2.3 Charge controller	9
2.4 Lead acid batteries.....	14
2.5 Street light.....	17
2.5.1 Incandescent lamp	17
2.5.2 Fluorescent lamps.....	17
2.5.3 Low pressure sodium (LPS)	17
2.5.4 High intensity discharge (HID).....	18
2.5.5 LED lamp	19
2.6 Standalone application in street lighting systems	20
2.7 Sizing of battery based stand-alone photovoltaic systems	24
Chapter 3 Simulation methods.....	27
3.1 Introduction	27
3.2 Weather database.....	29
3.3 PV panel component.....	32
3.3.1 Validation of five-parameter model	38
3.4 Battery.....	41
3.4.1 TRANSYS battery model	41
3.4.2 Copetti battery model.....	44
3.4.3 Developed Battery model (self-coded component)	45
3.5 Charge controller (Self coded)	46
3.6 Light controller.....	50
3.7 Model description.....	52

3.8	Simulation results	54
3.8.1	PV	55
3.8.2	Battery.....	56
3.8.3	Temperature	61
Chapter 4	Experiment.....	63
4.1	LED lamp	65
4.2	PV	66
4.3	Battery.....	67
4.4	Charge controller	68
4.4.1	Charge controller features.....	68
4.4.2	Charge controller test	71
4.4.3	IPN ProRemote.....	72
4.5	Data logger.....	78
4.6	Voltage divider.....	82
4.7	Electric shunt.....	84
4.8	Battery box.....	84
4.9	Thermocouples	85
4.10	Wiring and connector	86
4.11	Experiment board	87
4.12	System installation.....	90
4.13	Experimental results	96
4.13.1	PV	97
4.13.2	Battery.....	100
Chapter 5	Results and discussion	108
5.1	Simulated performance for various configurations.....	119
5.2	Simulated performance for various locations	121
Chapter 6	Conclusion and recommendations	125
6.1	Conclusion.....	125
6.2	Summary of contribution.....	127
6.3	Recommendations	128
6.4	Future research.....	128
Reference.....		129

Appendix A	Detailed simulation and measured results	140
Appendix B	Matlab codes for charge controller and battery components	150
Appendix C	IPN ProRemote setting menus.....	152

List of tables

Table 1: Maximum needed depth of discharge for different types of battery [40].....	13
Table 2: Street lighting technology comparison [69]	20
Table 3: TRNSYS weather database stations over the world [3]	30
Table 4: Maximum power values of the polycrystalline cell type from NIST measurements, King and five-parameter models [4].....	39
Table 5: PV input	40
Table 6: PV output	40
Table 7: PV parameters.....	41
Table 8: Battery input	43
Table 9: Battery output	43
Table 10: Battery parameters	43
Table 11: Columbic capacity (Ah) of discharge and charge cycles (May14-22)	59
Table 12: Columbic capacity (Ah) of discharge and charge cycles (May23-31)	60
Table 13: Columbic capacity (Ah) of discharge and charge cycles (June 1-6)	60
Table 14: Columbic capacity (Ah) of discharge and charge cycles (June 6-12)	60
Table 15: equipment list for main setup and measurement board	63
Table 16: Site features	64
Table 17: LED lamp feature	65
Table 18: Photovoltaic panel key features	67
Table 19: Battery weight and dimensions.....	67
Table 20: Charge status indicator	69
Table 21: Data logger energy consumption	79
Table 22: Data logger channel wiring.....	82
Table 23: Voltage divider specification.....	83
Table 24: Setup and measurement equipments specification	95
Table 25: Details of wattage usage by LED lamp	106
Table 26: Detailed information for ambient and components temperature	107
Table 27: Selected days for model verification	108
Table 28: Monthly average of columbic capacity (Ah)	118
Table 29: PV and battery size for newconfigurations.....	121

Table 30: Site and weather information for Doha, Qatar [104, 105]	122
Table 31: Site and weather information for Montreal, Canada [104, 106]	123
Table 32: Failure matrix for various configurations (Qatar)	124
Table 33: Failure matrix for various configurations (Montreal).....	124
Table 34: PV daily maximum current, voltage and power	140
Table 35: PV daily maximum current, voltage and power	140
Table 36: PV daily maximum current, voltage and power	140
Table 37: Daily maximum current, voltage and power	141
Table 38: Daily produced Ah by PV	141
Table 39: Daily produced Ah by PV	141
Table 40: Daily produced Ah by PV	141
Table 41: Daily produced Ah by PV	141
Table 42: Maximum current & power during charging and discharging	142
Table 43: Maximum current & power during charging and discharging	142
Table 44: Maximum current & power during charging and discharging	142
Table 45: Maximum current & power during charging and discharging	143
Table 46: Initial and final voltage for charge and discharge cycles	143
Table 47: Initial and final voltage for charge and discharge cycles	143
Table 48: Initial and final voltage for charge and discharge cycles	144
Table 49: Initial and final voltage for charge and discharge cycles	144
Table 50: Columbic capacity (Ah) of discharge and charge cycles.....	144
Table 51: Columbic capacity (Ah) of discharge and charge cycles.....	145
Table 52: Columbic capacity (Ah) of discharge and charge cycles.....	145
Table 53: Columbic capacity (Ah) of discharge and charge cycles.....	145
Table 54: LED operating data.....	145
Table 55: LED operating data.....	146
Table 56: LED operating data.....	146
Table 57: LED operating data.....	146
Table 58: Wattage usage by LED lamp	147
Table 59: Wattage usage by LED lamp	147
Table 60: Wattage usage by LED lamp	147
Table 61: Wattage usage by LED lamp	147
Table 62: PV, ambient, box and battery temperature	148

List of figures

Figure 1: Breakdown of the components of solar street light system [2]	1
Figure 2: Cumulative photovoltaic installations, 1992–2013 [16]	6
Figure 3: Failure rates of battery based standalone PV in Puno-Peru [32].....	9
Figure 4: Charging pattern of a 12V battery [39]	11
Figure 5: Battery charging efficiency for PWM in compared with ON/OFF controllers [42]	12
Figure 6: Spiral and flat palate electrode [49]	14
Figure 7: TRNSYS simulation studio	28
Figure 8: Meteonorm station over the world [87].....	31
Figure 9: PV panel equivalent circuit [3].....	33
Figure 10: Current vs voltage predicted by the five parameter model, the king model and measured by NIST for the poly crystalline cell type [4]	39
Figure 11: Current and voltage profiles for battery charging process [101].....	48
Figure 12: Simulation model flowchart	49
Figure 13: Simulation model (with TRNSYS battery component)	51
Figure 14: Simulation model (with self-coded battery component)	51
Figure 15: Simulation components' inputs and output	53
Figure 16: Halifax solar horizontal radiation (May 14-31)	54
Figure 17: Halifax solar horizontal radiation (June 1-14)	54
Figure 18: PV output current, voltage and power (May 14-31)	55
Figure 19: PV output current, voltage and power (Jun 1-14).....	55
Figure 20: Battery current, voltage and power (May 14-31).....	56
Figure 21: Battery current, voltage and power (Jun 1-14).....	57
Figure 22: Ampere hour depletion (May 14-June 14)	57
Figure 23: Battery state of charge (May 14-31).....	58
Figure 24: Probability distribution of battery state of charge (May 14-31).....	59
Figure 25: Columbic capacity (Ah) of discharge and charge cycles	61
Figure 26: Ambient and PV temperature (May 14-31).....	62
Figure 27: Ambient and PV temperature (June 1-14).....	62
Figure 28: Experiment setup (Sexton Campus roof)	64
Figure 29: LED lamp dimensions	66

Figure 30: Top and rear view of PV	66
Figure 31: Battery bank connected in series (Type Hoppecke solar. bloc 6V)	68
Figure 32: Charge controller (Front plate and internal kit).....	69
Figure 33: Pre-installation setup for testing charge controller operation	72
Figure 34: IPN Pro-Remote	73
Figure 35: UCM device and website homepage (Start page)	75
Figure 36: UCM setup page for adjusting system communications.....	76
Figure 37: Data log file descriptions.....	77
Figure 38: FTP file data description	78
Figure 39: Data logger [103].....	81
Figure 40: Voltage divider equivalent circuit	83
Figure 41: Voltage divider	83
Figure 42: Electrical shunt for measuring voltage and current.....	84
Figure 43: Battery box	85
Figure 44: Installed thermocouples for (a) battery bank (b) PV panel (c) Ambient (d) box inside.....	86
Figure 45: Experiment board stand dimensions.....	87
Figure 46: Experiment board (Including current shunt, charge controller and data logger)	88
Figure 47: Setup wiring diagram	89
Figure 48: Bracket for installing PV array.....	90
Figure 49: Front and rear view of installed PV panel & PV panel diagram.....	91
Figure 50: Dimensions and measurements for PV stack	92
Figure 51: Installed street light (Day/Night).....	93
Figure 52: Enclosure mounting plates & box attachment angles	93
Figure 53: Solar street light setup (Day/Night).....	94
Figure 54: Experimental result sample	96
Figure 55: PV output voltage, current and power.....	98
Figure 56: Maximum PV output current, voltage and power.	99
Figure 57: Daily and cumulative electricity production	100
Figure 58: Battery voltage, current and power profile.....	101
Figure 59: Maximum battery current and power for charging cycles.	102
Figure 60: Initial and final battery voltage for charging cycles.....	103

Figure 61: Initial and final battery voltage for discharging cycles.	103
Figure 62: Columbic capacity (Ah) of discharge and charge cycles	104
Figure 63: Battery Ah depletion (May 13-31)	104
Figure 64: Battery Ah depletion (June 1-16)	105
Figure 65: Daily operation of LED lamp	105
Figure 66: PV, ambient, box and battery temperature (May 13-31).....	106
Figure 67: PV, ambient, box and battery temperature (June 1-16).....	107
Figure 68: PV output current-voltage (Cloudy day)	109
Figure 69: PV output current-voltage (Hazy day)	110
Figure 70: PV output current-voltage (Sunny day).....	111
Figure 71: Measured initial and final battery voltage and AHD diagram	112
Figure 72: Battery current-voltage profile for fully charged cycle.....	113
Figure 73: Ampere hour depletion diagram for fully charged cycle	114
Figure 74: Battery current-voltage profile for half charged cycle	115
Figure 75: Ampere hour depletion diagram for half charged cycle.....	116
Figure 76: Simulated ampere hour depletion.....	117
Figure 77: Experimental ampere hour depletion	117
Figure 78: Frequency distribution for charging and discharging cycles.....	118
Figure 79: Simulated battery current-voltage profile (October 1-31).....	120
Figure 80: Simulated ampere-hour depletion (October 1-31).....	120
Figure 81: Comparison of simulated ampere-hour depletion (October 1-31)	121
Figure 82: Monthly columbic capacity of charge-discharge (Qatar).....	122
Figure 83: Monthly columbic capacity of charge-discharge (Montreal)	123

Abstract

Off-grid solar street lighting presents an opportunity to illuminate specific sections of areas and roads which are not served by the electricity grid. Proper sizing of components may lead to decreasing capital cost as well as ensuring quality and continuity of supply. Optimized sizing depends on accurate modeling and simulation of both daily and annual output performance. To this end a new model was developed to optimize the sizing of the photovoltaic module and battery, and the lighting controller strategy, to improve the performance and utilization of the system, for a range of climatic conditions. Comparing simulation and experimental results for average of columbic charge and discharge shows 5 % and 2 % error respectively. According to simulation model, estimated number of failures for installed solar street light with 540 W photovoltaic panel, 375 Ah battery capacity and 55 W lamp in Halifax is 49 nights over the year.

List of abbreviations and symbols used

Abbreviations

AGM – Advanced Glass Mat
ANN – Artificial Neural Network
ANN-GA – Artificial Neural Network Genetic Algorithm
DDOD – Daily Depth of Discharge
DF – (PV's) De-rating Factor
DOD – Desired Depth of Discharge
FSEC – Florida Solar Energy Center
FTP – File Transfer Protocol
EBA – Global Energy Balance Archive
HPS – High Pressure Sodium (lamps)
HTTP – Hypertext Transfer Protocol
HVAC – Heating, Ventilation and Cooling
LPS – Light Pressure Sodium (lamps)
MLP – Multi-Layer Perceptron
MPPT – Maximum Power Point Trackers
NIST – National Institute of Standards and Technology
PSH – location's Peak Sunshine Hours (h)
PV – Photovoltaic
PWM – Pulse Width Modulation
RBF – Radial Basis Function
SAPV – Stand Alone Photovoltaic
SNL – Sandia National Laboratories
SOC – State of Charge (battery)
THD – Total Harmonic Distortion
UCM – Universal Communication Module
WMO – World Meteorological Communication

Symbols

$\alpha_{I_{SC}}$ – Short circuit current temperature coefficient
 $\beta_{V_{OC}}$ – Open circuit voltage temperature coefficient
 η_b – Battery charging efficiency
 θ_z – Zenith angle (deg)
 $\mu_{V_{OC}}$ – Open circuit voltage temperature coefficient
a – Modified identify factor
 a_i – Cell material coefficient
AM – Air Mass modifier
 C_b ; C – Battery capacity (Ah)
 C_T – Limit capacity when discharge current tends to zero (Ah)

C_{10} – Capacity rated (Ah)
 E_{day} – Total daily load (Ah)
 E_g – Material band gap
 e_{qc} – Open circuit voltage of full charge on charge mode (V)
 e_{qd} – Open circuit voltage of full charge on discharge mode (V)
 g_c – Small valued coefficient of H for charge mode (V)
 g_d – Small valued coefficient of H for discharge mode (V)
 H – Fractional state of discharge
 $I_{\text{controller}}$ – Maximum current from PV array which pass through the controller (A)
 I_{DC} – Continuous DC current (A)
 I_L – Light current (A)
 $I_{\text{mp, ref}}$ – Maximum power point current (A)
 I_O – Diode reverse saturation current (A)
 I_{sh} – Shunt current (Ω)
 I_{sc} – Short circuit current of PV module (A)
 K – Boltzmann's constant
 m – Cell type coefficient
 M – Air mass modifier
 N – Number of electrical device
 n_i – Identify factor
 N_p – Number of modules connected in parallel
 N_s – Number of cells in series
 P – Power rating of electrical device
 $P_{AC, \text{tot}}$ – Total power of AC load (W)
 q – Electron charge
 Q_a – Required generated power from PV (W)
 Q_c – Capacity parameter in charge mode (Ah)
 Q_d – Capacity parameter in discharge mode (Ah)
 Q_{day} – Daily load demand (Ah)
 R – Resistance parameter value
 R_{dir} – Ratio of the load directly met by PV array to the the total load demand
 r_{qc} – Internal resistances at full charge when battery is charging (Ω)
 r_{qd} – Internal resistances at full charge when battery is discharging (Ω)
 R_s – Series resistance (Ω)
 R_{sh} – Shunt resistance (Ω)
 S – Absorbed solar irradiance (W/m^2)
 t – Daily number of hours
 T_c – Cell temperature ($^{\circ}\text{C}$)
 $V_{b, \text{nom}}$ – System's nominal battery voltage (V)
 V_d – Discharge voltage (V)
 V_{in} – Circuit input voltage (V)
 $V_{\text{mp, tot}}$ – Maximum power point voltage (V)
 V_{out} – Circuit output voltage (V)
 W_p – Maximum power output of array (W)
 ΔT – Temperature difference from reference temperature (25°C)

Acknowledgments

First and foremost, I would like to convey my warmest gratitude to my supervisor Dr. Lukas Swan, for the continuous support of my study and research, for his patience, motivation, enthusiasm, and immense knowledge. His guidance helped me in all the time of research and writing of this thesis. I could not have imagined having a better advisor and mentor for my master study. The difficulties of designing and implementing the project would have been far more difficult without your persistent drive for excellence. The guidance during the long and sometimes difficult parts of the simulation process provided a learning curve that allowed me to gain confidence and a strong background to fall back on. Also, thanks you for making this study possible by providing the financial support of not only this research, but also my entire master program.

I have to thank PoleCo Inc. for providing part of the necessary items to build a solar powered project. I am also thankful to Sean Fleming from aforementioned company that without his invaluable help the project would not have gone as smoothly as it did.

I would also like to show gratitude to all of those in the Mechanical Engineering department who have helped me along the way including, Darrel Doman, Dominic Groulx, Peter Jones, Mark MacDonald, Albert Murphy, Angus MacPherson and Selina Cajolais.

During the period of two years, many friends have helped to color my life. To my colleagues in the laboratory/office and all RESL team, thank you for your assistance on this project. Without you, believing in me, this would have been so much harder.

Last but not the least important, I owe more than thanks to my family members. To my Mum, Dad and my brother, I appreciate the love and care you showed during my two year stay away from you. Every time I was ready to quit, you did not let me and I am forever grateful. Above all, I give honor and glory to Almighty God for giving me good health and intellectual power to successfully complete this study.

CHAPTER 1 INTRODUCTION

Roadway lighting is considered as essential subject in road traffic safety, which plays crucial role in decreasing the number of fatal accidents and ensure the security and comfort of pedestrians and motorists [1]. Conventional street light, dependent on electricity grid as a power source to supply the required load so they would not be applicable in the area which are not served by electricity grid. Self-sustaining system (e.g. standalone photovoltaic system (PV)) would be appropriate solution for the remote and isolated regions with no access to electricity grid. Due to inherent predictability and reliability of solar cycles, standalone solar street light would be considered as an appropriate alternative for conventional street light. The solar street light system consists of a photovoltaic module, charge controller (equipped with maximum-power-point tracking functionality), battery bank, lighting controller, and LED lamp.

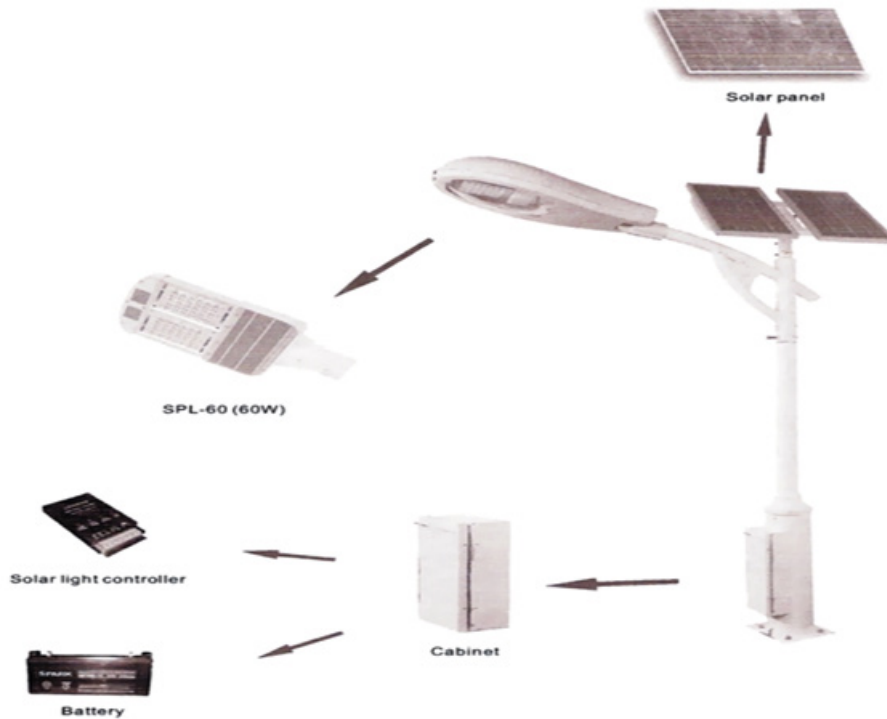


Figure 1: Breakdown of the components of solar street light system [2]

Due to site dependence feature of photovoltaic (solar insolation) and battery (ambient temperature) systems, major components should be designed based on installation site's

features. Climatic conditions of the installation site should be considered as the most important parameter to achieve more reliable and efficient system. Capital cost also has notable impact on penetration rate of solar street light which can be reduced through optimum sizing. Testing the system in various real climates is both costly and time consuming. Thereby, simulation as a low cost solution can be utilized in order to attain reliable results for optimized design through following objectives:

- Evaluating the solar energy potential to accommodate off-grid solar street light
- Generating loading profile
- Sizing optimization of battery and PV for selected locations
- Comparing different charge algorithms on battery operation

The main objective is making new model of off-grid solar street light with capability to be used for various locations and configurations. The second objective is building experiment setup unit for evaluating model performance for Halifax. According to provided information by TRNSYS [3] components manual it was found that battery and charge controller have failure in simulation of corresponding components behavior under real operating conditions. The ambient temperature is not considered as input data for TRNSYS battery component which leads to less accurate results in operating condition with temperature far from reference temperature. TRNSYS charge controller component is an On/Off switch, which is not capable of modeling the constant-power/constant-voltage of real charge controller operation. In this research, the aforementioned component were redesigned and modified for more accurate and reliable results compared to present simulation tools the verified experimentally.

TRNSYS is a transient system simulation program with a modular structure which is well suited for detailed analyses of photovoltaic systems. TRNSYS libraries include components commonly utilized in thermal and electrical systems. Modular structure of the program facilitates adding new or modified components, in addition to provide link with other software such as MATLAB and Microsoft Excel. The performance of PV is site dependent and efficiency varies with various parameters such as incidence angle, daily temperature and wind velocity. Consequently operating conditions are completely dynamic and cannot be modeled without access to temperature and radiation data for area

of interest. TRNSYS has a comprehensive weather database and powerful five-parameter PV model [3] able to predict long term output power under real dynamic conditions for many locations over the world. The five-parameter model can accurately predict the I-V curve for wide range of operating conditions. Contrary to other simulation software and previous PV models, five parameters model accurately predicts output power in lower irradiance (less than 200 W/m^2) [4].

Battery components in TRNSYS are programmed based on Shepherd and Hyman [5] model to specify how the battery state of charge varies over time and given the rate of charge or discharge. However ambient temperature has great impact on battery voltage and available capacity, and presently is not entered in the aforementioned model. Consequently, temperature is not considered as an input for battery component which make it unreliable for locations where the daily mean temperature is far from reference temperature ($25 \text{ }^\circ\text{C}$) (e.g. Qatar at $45 \text{ }^\circ\text{C}$ daily average).

A new battery component was coded in MATLAB based on accurate charge/discharge equations which involve ambient temperature to predict the battery behavior (e.g. battery voltage, state of charge and available capacity) during long term charge/discharge cycles. These equations are set to be compatible with different type of lead-acid batteries based on the manufacturer's battery specification data sheet. Light controller and LED lamp is modeled by modifying existing components in TRNSYS libraries to predict the load profile data. The light controller switch has capability to control LED lamp through solar radiation or PV produced electricity current. LED lamp component's features can be set based on provided data by manufacturer. It is critical that the installed street light should accommodate required luminance level based on pertinent standards (e.g. main road (1.5cd/m^2), freeway (0.75cd/m^2)) [6].

The research study is divided into simulation and experimental parts and each part follows its own methods and uses relevant tools.

TRNSYS 17 and MATLAB are linked together to model the typical off-grid street light. The system will be simulated for the period of one year by specified time step (interval time). At every time step each component will send to or/and receive data from its

connected components. Failure occurs when stored energy in batteries is not sufficient to accommodate the lighting load during zero solar-illumination hours (failure to provide) or when PV panels have to be shut down and battery capacity does not allow for more charging (i.e. too much PV or too little battery capacity). The model estimates the frequency of each type of failure separately and optimized design could be achieved based on minimum number of failures.

The experimental setup comprised PV panels, charge controller, batteries, LED lamp, battery box and electrical measurement equipment. The setup was designed and installed in Halifax, NS to collect the data in order to analyze the performance, calibrate and validate the simulation model.

This thesis has five content chapters. A detail report of the relevant literature reviewed is given in Chapter 2. Chapter 2 is subdivided into 4 sections which respectively reports on the literature reviewed in relation to PV panel background, lead-acid battery application at solar system, technical performance and algorithms of charge controller, efforts for developing accurate model for optimum sizing of major components and the procedure of battery based standalone photovoltaic system (BSPVS) sizing. Chapter 3 briefly describes the TRNSYS software components used in simulation of solar street light and reports step by step methods followed in the simulation. At the end of this chapter, the result related to simulation part is presented. Chapter 4 reports in detail the device, methods and materials were used for test setup preparation in order to meet the objective of this study by evaluating TRNSYS model. A brief explanation on how data was analyzed is outlined at the end of this chapter which is followed by experimental results. A comprehensive discussion about model accuracy is presented in Chapter 5 through comparison among simulation and experimental results. Chapter 6 draws conclusion from the study. It further gives list of new contribution this study has offered; recommendations and finally further research areas are suggested.

CHAPTER 2 LITERATURE REVIEW

Comprehensive review on battery based standalone photovoltaic systems, major components and street light is presented in this Chapter.

2.1 PHOTOVOLTAIC CELLS

Due to the finite supply of fossil fuel sources and the environmental destructive effects, the technological development of harvesting renewable energy has greatly increased over the past century. First time, Edmund Becquerel, a French experimental physicist, discovered the photovoltaic effect when experimenting with an electrolytic cell made up of two metal electrodes, in 1839 [7, 8]. Willoughby Smith in 1873 and Adams and Day in 1877 discovered the photoconductivity and photovoltaic effect of selenium, respectively [9, 10]. Six years later, Charles Fritts, an American inventor, describes the first solar cells made from selenium wafers [11]. His Selenium solar cell gave less than 1% efficiency. In 1905, Albert Einstein published paper on theory behind “photoelectric effect” along with paper on relativity theory [12] and received the 1921 Nobel Prize in Physics for his discovery of this law [13]. The first conventional photovoltaic cells were produced in the late 1950s [14, 15]. In 1954, the invention of the first practical silicon solar cell was announced by Bell Labs [14]. These cells have about 6% efficiency. Hoffman Electronics creates the 8%, 9% and 10% efficient solar cells in 1957, 1958 and 1959, respectively [16]. Throughout the 1960s these cells were used to provide electrical power for Telstar satellites [17]. In the 1970s, improvements in manufacturing, performance and quality of PV modules helped to reduce costs and created numerous opportunities for powering remote terrestrial applications, including battery charging for navigational aids, signals, telecommunications equipment and other critical, low-power needs [16, 18, 19]. Significant endeavors such as worldwide photovoltaic production exceeds 21.3 megawatts, and sales exceed \$250 million began to enhance PV power systems in 1980s, for residential and commercial uses, for both stand-alone and utility-connected applications [16, 20]. During the same period, the off-grid households using PV increased dramatically. In 1990, laboratory cells with more than 30% efficiency were fabricated with areas of many square meters and a new field had peak generating capacity of 50

MW. Today, the industry's production of PV modules is growing at approximately 25 percent annually [21], and major programs are rapidly accelerating the performance of PV systems to benefit networks, in the U.S., Japan and Europe [22]. If the trend of doubling of consumption in every two years which happened from 2001 to 2012 continues, the solar power would reach 10% of total global power generation by 2018 [23], and would provide 100 percent of the current world energy needs by 2027 [24]. Figure 2 shows trend of Photovoltaic array installations and production in a range of years, respectively.

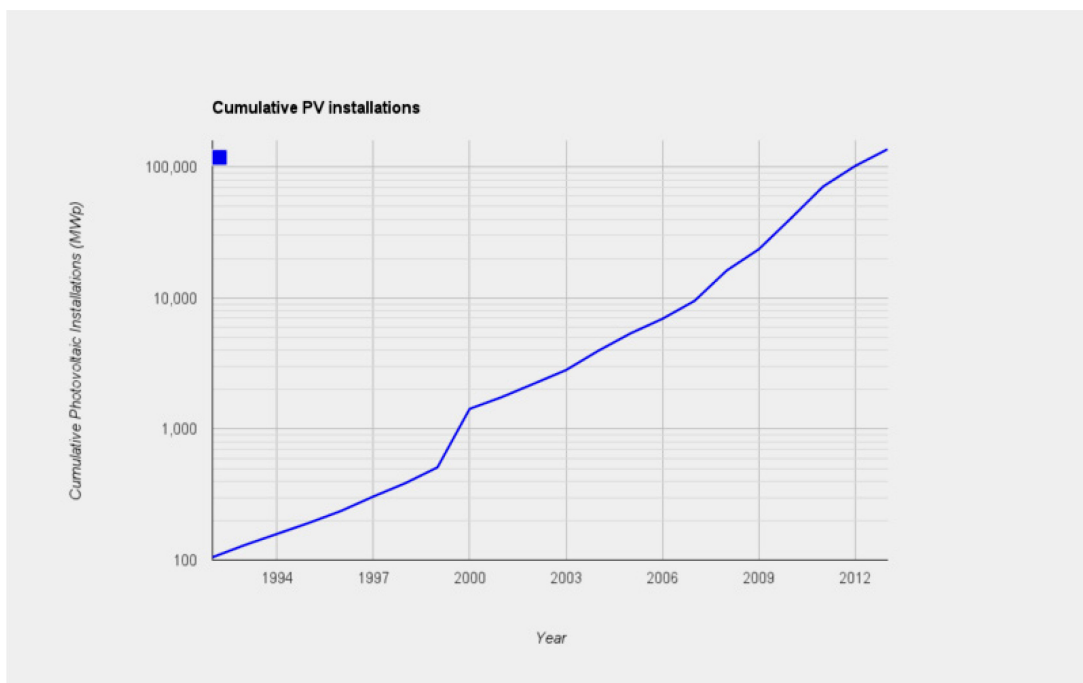


Figure 2: Cumulative photovoltaic installations, 1992–2013 [16]

2.2 PHOTOVOLTAIC SYSTEMS

PV systems are often built in different configurations [25]:

- Off-grid without battery (array-direct)
- Off-grid with battery storage for DC-only appliances
- Off-grid with battery storage and inverter for AC and DC appliances
- Grid-tie without battery

- Grid-tie with battery storage

Battery Based Stand-Alone PVs can be classified into three categories, namely systems with purely DC loads; systems with purely AC loads; and systems with both DC and AC loads. With exception of purely DC load system, this type of PV contains DC/AC inverter component.

In battery based PV system, performance ratio is an indicator for measuring system efficiency in terms of using PV panel potential power. Jahn et al. [26] conducted comprehensive performance analysis of installed PV in France. They defined new indicator (performance ratio) for comparing different PV systems, which shows the daily ratio of energy delivered to the load to in plane irradiation. It was observed that performance ratio of systems without back-up varied from 0.1 to 0.6 while providing back-up leads to rise in performance ratio which varied from 0.3 to 0.6. Regarding to performance ratio of grid tied systems which ranged from 0.6 to 0.8, it can be concluded that battery based performance ratio which just depends on solar energy for its battery charging is less efficient.

On the other hand, systems with purely DC loads are more efficient than systems with AC loads since there is not any extra power loss in the inverter. Nevertheless, as DC operated appliances are rarely available on market, the purely DC load system has been upgraded to purely AC load system by incorporating DC/AC inverter into the system. Unfortunately, choosing the cheapest inverters by non-specialists without considering technical implications had led to poor performance of such modified systems. This inappropriate performance is the result of coupling incompatible components and they operate below their capacities. In addition, as Celik et al. reported [27], climate condition of installation site has significant impact on PV performance, consequently it should be considered beside the economic perspective. So, the professional one must pay attention to weather data to optimize PV system design.

In performance of diverse components, solar panel is the least problematic, while its energy conversion efficiency still remains low. For the silicon based solar cell, which are

widely used in battery based standalone Photovoltaic System (PVS), the efficiency is 15%, approximately. Despite being less problematic in terms of component's break down, the performance of solar panel is site dependent and its efficiency get affected by daily temperature. On the other hand, as Bucher reported [28], if the module is mounted with latitude tilt, the reflection losses are independent of geographical latitude. Furthermore, the performance of this panel is decreased by shading resulting from poorly located panels and additionally dust accumulates due to the lack of routine maintenance.

Svoboda investigated that in battery based standalone PVs, due to the long period at low battery state-of-charge (SOC), partial cycling in low SOC, rare full charges, and elevated temperatures, battery is the weakest performing component and is prone to short life [29]. Batteries which are only designed for using in solar systems can stay in operation even more than 5 years by well managing. However, as it is experienced in Lundazi, Zambia [30], because of using the cheap and inappropriate automobile batteries, the dramatic reduction of battery's capacity occurred, after just one year of operation. Moreover, due to financial constraints, self-installed battery based standalone PVs are commonly installed without battery charge controllers. Charge controller controls charging and discharging current in order to avoid any overcharging and over discharging. The lack of charge controller usage results in significant descending of the battery life because of excessing gassing and thereby lowering system performance.

Munoz and Lorenzo reported a high conversion efficiency of 91% for the DC/AC inverters which performs at the rated nominal power output and falls within the grid frequency fluctuation of 2% [31]. In order to assure the technical quality of PV systems, the effects of contributing to possible configuration, procurement specifications and testing procedures of inverter feature on these systems are reviewed. However, the amount of the output voltage regulation of their case was not acceptable and the total harmonic distortion (THD) reaches to 50%.

Egido et al. [32] study the field evaluation of PV rural electrification project in Titicaca Lake Island. Regarding the evaluation of their battery based standalone PVs in Puno-Peru, Figure 3 showed high rate of failure in fuses and batteries after 1 year. Lamp

becomes the second most replaced component after fuses at the end of third year. Also, failure of charge controllers was relatively negligible while PV modules remained reliable component in the systems with no failure condition.

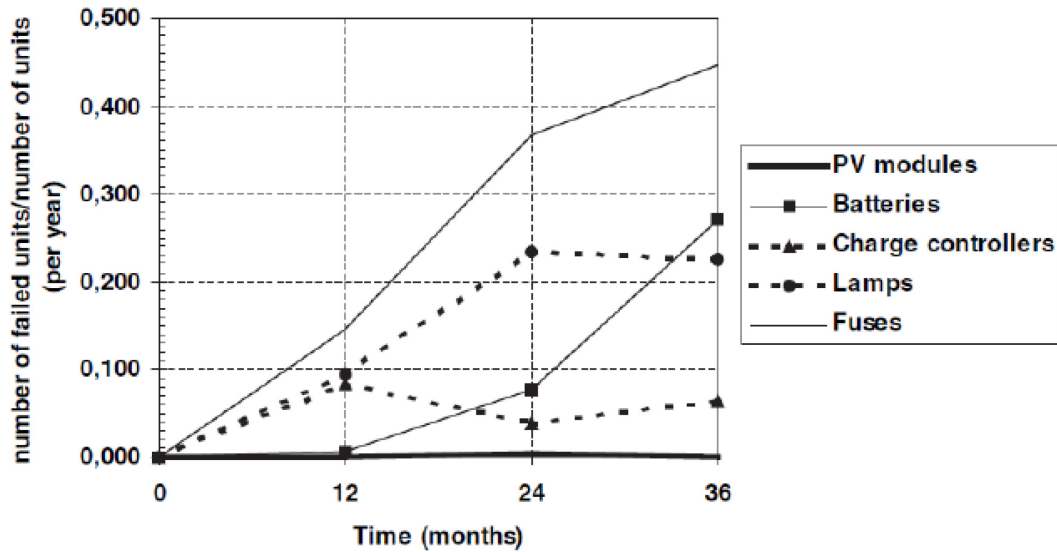


Figure 3: Failure rates of battery based standalone PV in Puno-Peru [32]

2.3 CHARGE CONTROLLER

A charge controller is needed in photovoltaic system to control the rate of electric current which is added to or drawn from electric batteries. It improves battery performance as well as life expectancy through preventing overcharging and over-discharging.

All systems which have to encounter with unpredictable power source or loads require charge controller or low-voltage load disconnect panel [33]. Overcharging with high charging voltages generates oxygen and hydrogen gas by electrolysis of water, which is lost from the cell. Commonly over discharge can make cell inner pressure raise, and the reversibility of activity materials both in positive and negative will be damaged. Over charging/discharging occurs as a result of inappropriate sizing or end users intervention which leads to notable impact on decreasing battery life time. On the other hand systems with small, predictable, and continuous loads and power supply can be employed without utilizing any charge controller [33]. It is worth mentioning that under particular operating

conditions charge controller can be omitted from PV systems. For instance, when system is coupled with oversized battery storage, and battery charging currents are defined for safe finishing charge rates at an appropriate voltage [34, 35, 36, 37].

Regardless of any changes in size of system components, load profile or temperature in different seasons, a charge controller must support battery by providing continuous over-charge/over-discharge protection. The algorithm of a battery charge controller plays important role in increasing effectiveness of battery performance and PV operation which results more efficient system through reduction in number of system failures. Moreover, other features such as temperature compensation, accurate light controlling and particular charging algorithms (two or three stages charging) improve functionality of charge controller. Aforementioned features maximize system reliability and continuity as well as extending battery life time [33].

The process of voltage-based charging for lead acid batteries consists of three steps. During first step, the battery is charged with the solar module maximum power. After reaching the battery voltage up to the preset voltage setpoint, in the second step, the charging mode is modified to the constant-voltage algorithm [38]. Based on charge controller adjustments second step continue after specified time or when battery current drops to pre-set threshold. Float charging is the last step for compensating the unwanted self-discharge. During third step the battery voltage drops to lower voltage.

Figure 4 shows the voltage-based charging pattern for a 12 V battery system.

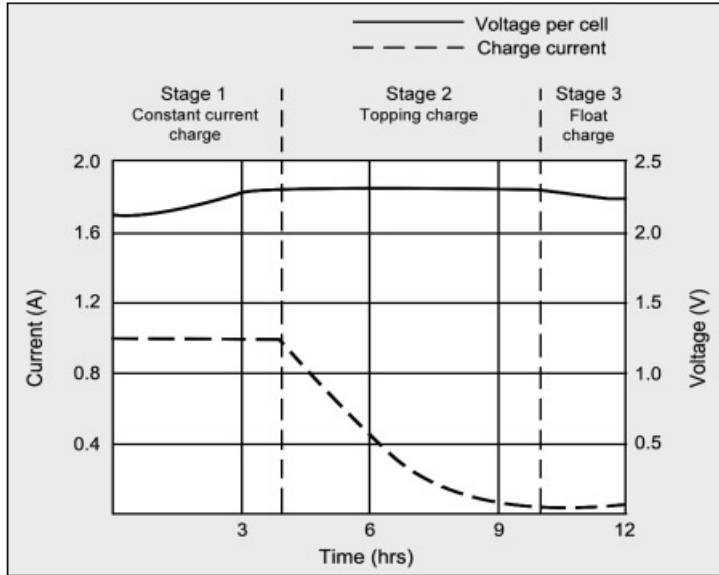


Figure 4: Charging pattern of a 12V battery [39]

Diaz and Egido [40] investigated the influence of charge controllers on the performance of battery based standalone PVs. They observed that the mismatching of battery and charge regulator types has notable impacts on battery performance and consequently the system's efficiency. In addition, performance of systems also is affected by the regulation of voltage set points.

At the beginning, simple On/Off charge controllers were used to limit battery charging when a solar panel produced excess energy. By increasing in penetration rate of solar systems, it became clear how much these simple devices results in ascending battery failures which increase the number of load disconnection. Stevens et al. [41] in their research article investigated the limitation of PV system performance which are using the ON/OFF charge regulator. As it can be seen in Figure 5, Morningstar Corporation [42] showed that charge controllers with pulse width modulation (PWM) increases the charge acceptance of the battery and consequently increasing battery life time. When a battery voltage reaches the regulation setpoint, the PWM algorithm slowly reduces the charging current to avoid heating and gassing of the battery, yet the charging continues to return the maximum amount of energy to the battery in the shortest time. The result is a higher charging efficiency, rapid recharging, and a healthy battery at full capacity. In addition to aforementioned privileges, PWM charge controllers have other advantages; For instance,

recovering lost capacity, retaining average of battery capacities at higher level, equalizing drifting cells, decreasing the heating and gassing phenomenon, and auto compensation for probable change in voltage and temperature.

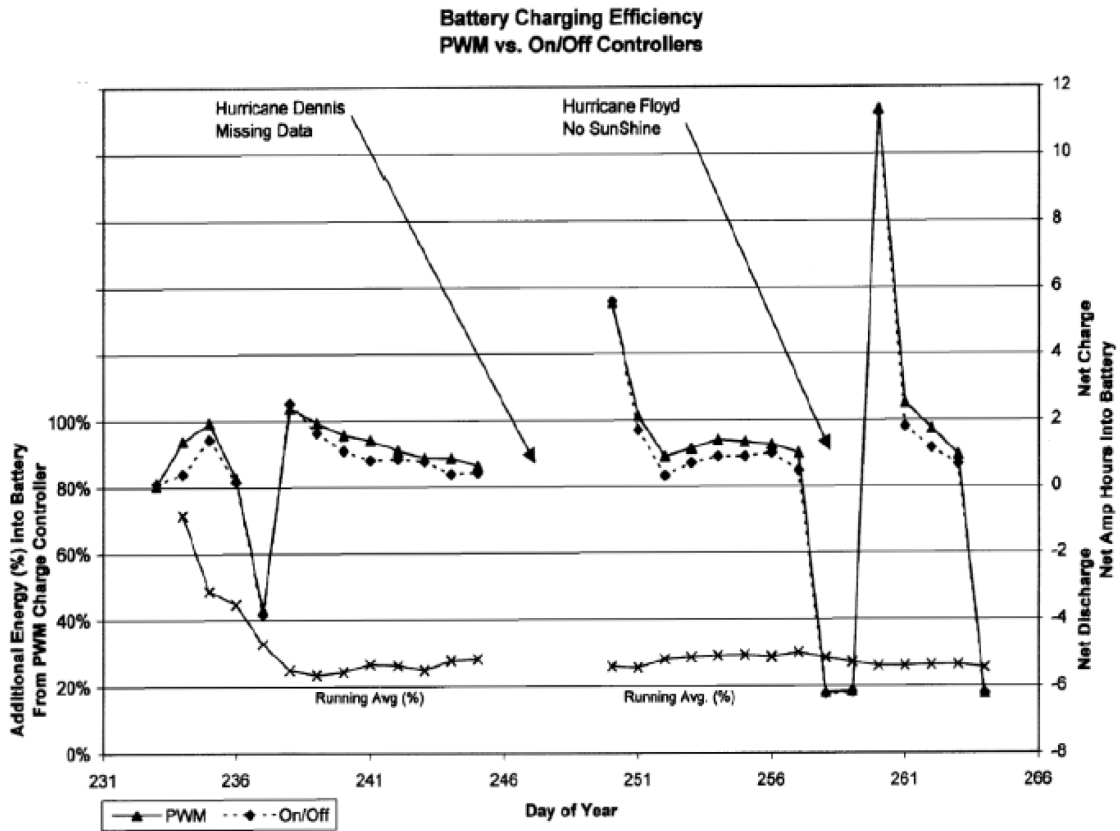


Figure 5: Battery charging efficiency for PWM in compared with ON/OFF controllers [42]

Sanidad et al. [43] proved that coupling On/Off charge controllers results in PV energy curtailment and consequently keeps battery state of charge at lower level. In 2003, Diaz and Egido [40] found that achieving more efficient energy supply for batteries which provides longer life cycles depends on the ending voltage in ON/OFF charge controllers. The ending voltage should be maintained between 13.8 to 14.4 V for a nominal 12 V system at 25°C. In addition to ending voltage, the load connection voltage set point should be set around 0.9 to 1.2 V higher than load disconnection voltage. As can be seen information related to maximum depth of discharge for different kinds of batteries is tabulated in Table 1.

Table 1: Maximum needed depth of discharge for different types of battery [40]

Battery type	DOD _{max} (%)
SLI automotive	50
Solar modified	60
Tubular stationary	80

As it is mentioned above, the battery bank should be protected against overcharge or over discharge through appropriate charge controller which operates based on battery voltage and temperature. Charge controller disconnects the wind turbine, solar panel or other types of power supply when the high voltage set-point of battery bank is reached. On the other hand, when the battery bank reaches the low voltage set-point, the charge controller disconnects the load to avoid over discharge [44]. Corbus et al. [45] defined the battery/wind ratio as the battery capacity divided by charge current at rated wind power and investigated the relationship between this ratio and high voltage set-point of the charge controller. In addition, they demonstrated that the high voltage set-point of the charge controller is reached prematurely in systems with a low battery/wind capacity ratio (between 3 and 10 h), accordance to voltage ascends on the DC bus. This condition is caused by low values (60% or less) of the battery bank state of charge.

In 1990, Sandia National Laboratories (SNL) and the Florida Solar Energy Center (FSEC) surveyed on eight different models of small (approx. 10 amps) charge controllers [46]. They were carried out a comprehensive test program including complete electrical characterizations at selected temperatures, photovoltaic inputs, and load levels.

Then in 1992, the same centers continued their efforts to gain a better understanding of charge controllers' impacts on these batteries. In addition to utilize diverse algorithms, they changed voltage set points, charging algorithms and maintaining methods [33]. The typical strategies for battery charging regulation and load controlling which is utilized in standalone PV systems have been presented in their article.

In 2010, Weichen Li et al. [47] provided a simple PV charger circuit for the portable applications, which is simply composed of several analog chips to enhance the system structure. Three mode of charging solution consists of: maximum power point tracking (MPPT) mode, the constant-voltage mode and the current-limited mode are used to meet the requirements of the PV array and the lithium battery.

2.4 LEAD ACID BATTERIES

Battery is a critical component in a stand-alone photovoltaic system. The function of battery is storage of excess energy from the PV array as a damper and providing energy during night or non-sunny days. In addition, because battery feeds the loads with a relatively fixed voltage, it can be considered as a stabilizer. Nowadays, lead acid battery is the typical type of batteries which is often used in PV systems [48].

There are two categories of lead-acid batteries: flooded and valve regulated. Also, electrode designs have two types, including prismatic (flat plate) and spiral wound. For better judgment the two types of electrode is illustrated in Figure 6.

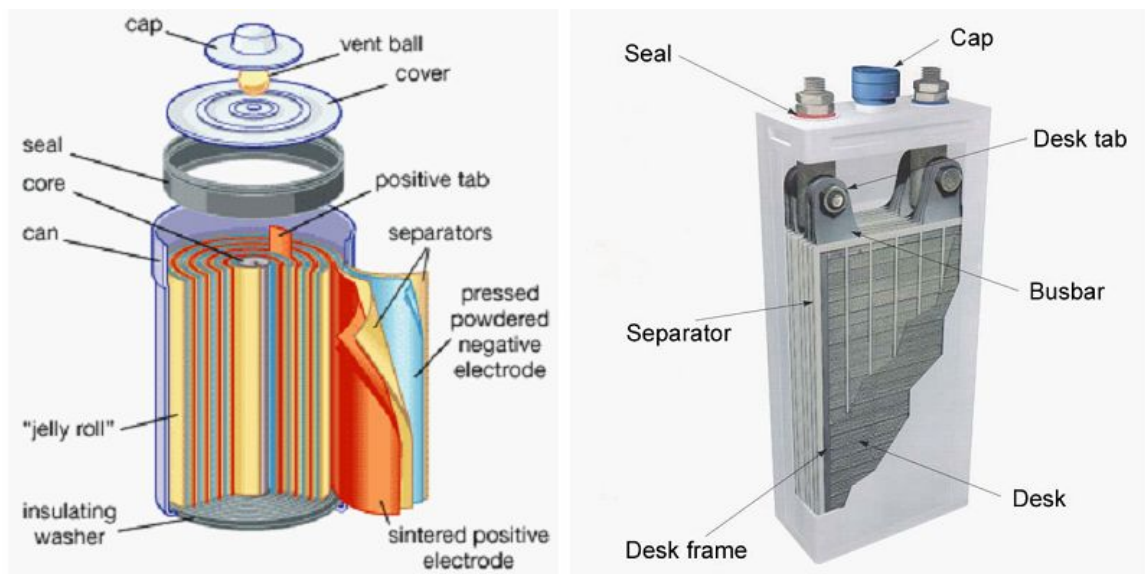


Figure 6: Spiral and flat palate electrode [49]

Spiral type batteries usually have been used in heavy cycling, since they better compress the electrodes which increase cycle life through improved cohesion of the positive active

mass [50]. In contrast with heavy cycling applications such as grid support ones, lead-acid batteries have the significant application in float service or infrequent cycle applications such as uninterruptible power supplies and demand peak shaving, primarily due to low cost.

Because of participating to both active materials and the electrolyte in the reaction, corroding the positive plate during overcharge, and the passivation of the negative electrode due to sulfation, lead acid battery has relatively lower cycle life than other chemistries [51].

Many attempts have been done to predict the lead acid battery lifetime. These lifetime models can be categorized in three main groups: a physico-chemical aging model, a weighted Ah aging model, and an event-oriented aging model [52]. The brief explanation about these models' characteristics is presented in following:

- The physico-chemical aging model is based on the detailed knowledge of the chemical and physical process of electrochemical system.
- The weighted Ah aging model considers that the lifetime is proportional to the total columbic Ah throughput.

The event-oriented aging model calculates the loss of lifetime by recognizing extreme operating conditions.

However, it should be considered that often, the experimental information established through laboratory tests is essential in implementation of these aging models [53].

During the process of charge and discharge, many parameters such as voltage, current, density, temperature, resistivity, etc. can be changed. Consequently predicting battery behavior which depends on battery voltage and state of charge is complicated. Shepherd, Monegon, Mayer, Facinelli, Hyman, CIEMAT [54] and many other authors have investigated the battery behavior in their literatures.

In this regard, many efforts have been done for modeling the lead acid batteries, in last century. In 1993, Manwell and McGowan [55] presented the model which has been used

in many simulation and optimization models such as those submitted in [56, 57, 58]. In their model the influence of current on battery capacity based on the interpretation of chemical kinetics is considered as two storage tanks. While a tank shows the energy immediately available, another one represents the energy that is chemically bound. For calculating the voltage of the battery, the aforementioned model can be used jointly with the model proposed by Shepherd [59]. The model which is presented by Protogeropoulos et al. [60] can estimate the state of charge and voltage trend regarding the battery capacity as a function of the charge and discharge currents. Ross et al. [61] investigated a simplification of the electrochemical model in which the cell is fabricated of a number of sub-cells connected in parallel. Therefore the flow of acid between cells is specified by the impedance and concentration of the acid. Schiffer et al. [62] developed a model in which comparison of the diverse parameter impacts on battery lifetime such as operating conditions, system sizing and battery technologies are considered.

In contrast with the models presented in [54-57] which experimental data is required to fit the model parameters, the model presented in [62] can be adjusted to any battery types with using data that has been proposed by the manufacturers. However, since it is based on a detailed analysis of the aging processes in the lead acid battery, this model cannot be considered as an appropriate model for a hybrid system.

In 1993, the general model has been proposed by Copetti and Chenlo [63] and Copetti et al. [54] that only required the rated capacity. By normalizing equations with respect to the experiment results that were carried out on lead acid batteries at a large range of operating situations, they presented the model which is valid for any type and size of lead-acid batteries. Because of solving a nonlinear equation system for each hour of simulation, mathematical formulation of this model is complex to obtain the voltage and state of charge of the battery bank. The results show less than 3% error for the charging and discharging. In this work, Copetti's model was used [54, 63] for modeling lead acid battery.

2.5 STREET LIGHT

Street lights are used as the source of light on the edge of road or walkway in order to provide luminance when it is required. Street light are witnessing lots of changes from invention of initial candle to the contemporary LED lamp. Roman and Greek were the first places where the primary lamp had been utilized [64]. In 1792 William Murdoch utilized flammability of gas for the application of lighting. After 15 years in 1807, the first street light with gas was demonstrated in London by Frederick Winsor [64]. In 1853, kerosene was used in the first modern street lamp in Lviv. Pavel Yablochkove produced the first power street light in 1875. This new invention had arc lamps and called Electric candle. The initial electric light in the USA was installed in Cleveland, Ohio, in 1879. The main types of light sources have been used since 1950s are Incandescent, Fluorescent, Low Pressure Sodium and High Intensity Discharge [64].

2.5.1 Incandescent lamp

This type of lamps was the most popular option for street lighting until the 1950s [65]. As the first generation of light sources, this type had the least efficiency compared to other types.

2.5.2 Fluorescent lamps

Due to higher efficiency and lower necessary maintenance compared to their Incandescent counterparts, fluorescent lamp has been widely used in downtown areas and parking lots. They were appropriate solution for any place requiring a lot of light over a large area. High Intensity Discharge lamp technology was the next generation of light sources with higher efficiency more compact and lower maintenance [65].

2.5.3 Low pressure sodium (LPS)

Among all available light sources, the Low pressure Sodium lamps have the most efficiency [65]. Aforementioned type produces a monochromatic orange-yellow light by long and skinny lamp. Color rendering is considered as drawback for this type of street

lights. When the lamp is on, everything around it looks either orange-yellow, black or shades in between. As the lamp ages, lamp uses more wattage while the lumen level stays relatively constant.

2.5.4 High intensity discharge (HID)

High intensity discharge (HID) lamps are categorized in three main groups [65]:

- Mercury Vapor
- Metal Halide
- High Pressure Sodium

HID lamps need an external ballast to operate and usually between 1 to 5 minutes take till they reach their maximum brightness. A sufficient cooling is necessary for this particular type of light source which takes between 1 to 10 minutes.

2.5.4.1 Mercury vapor

Mercury Vapor was the first type of HID lighting sources. Clear mercury vapor produce blue-green light. Phosphors layer on the outer glass globe of the lamp replace this green-blue light with clear white light.

Compared to fluorescent lamp, mercury vapor were smaller and had longer life span with almost same efficiency. Operating in extremely cold climatic is considered as one of the positive aspects of this light source.

2.5.4.2 Metal halide

Metal halide lamps are the same as mercury vapor but other metallic elements added which result in good quality white light. It is mostly used in parking area and inside the commercial and industrial buildings. However it has more efficiency compared to mercury vapor its life span is slightly shorter. Slight variation in color of produced light by metal halide lamps leads to color shift which is considered as the main problem for this type.

2.5.4.3 High pressure sodium (HPS)

The lamps were developed in the early 1970s and are more energy efficient compared to other types of HID lamps [65]. The lamps give off an amber color, have virtually no problem with color shift, and last for long periods of time.

According to notable improvements in equipment effectiveness and the advancement of new technologies, some studies have been carried out for designing and surveying the performance of electronic ballasts for high-pressure sodium (HPS) lamps [66]. In 2003, Wu Libo et al. [67] presented a high-efficiency stand-alone photovoltaic lighting system which could provide functional illumination through high-pressure sodium (HPS) lamp. The isolated regions with limited or no access to electricity grid are the best places to study the abilities of stand-alone lighting systems.

2.5.5 LED lamp

An LED lamp is a light-emitting diode (LED) product that is assembled into a lamp (or light bulb) for use in lighting fixtures. LED lamps have a lifespan and electrical efficiency that is several times better than incandescent lamps, and significantly better than most fluorescent lamps, with some chips able to emit more than 100 lumens per watt [68]. LEDs do not emit light in all directions, and their directional characteristics affect the design of lamps. The light output of single LEDs is less than that of incandescent and compact fluorescent lamps; in most applications multiple LEDs are used to form a lamp. The primary appeal of LED street lighting is energy efficiency compared to conventional street lighting fixture technologies such as high pressure sodium (HPS) and metal halide (MH). Comparison between available technologies for street light is provided through Table 2 [69].

Table 2: Street lighting technology comparison [69]

light technology	life time (hours)	lumens per watt	color temperature	CRI (color rendering index)	Start time	considerations
incandescent light	1000 -5000	11 - 15	2800K	40	instant	very inefficient, short life time
mercury vapor light	12000 - 24000	13 - 48	4000K	15 - 55	up to 15 min	very inefficient, ultraviolet radiation, contains mercury
metal halide light	10000 - 15000	60 - 100	3000-4300K	80	up to 15 min	high maintenance UV radiation, contains mercury and lead, risk of bursting at the end of life
high pressure sodium light	12000 - 24000	45 - 130	2000K	25	up to 15 min	low CRI with yellow light, contains mercury and lead
low pressure sodium light	10000 - 18000	80 - 180	1800K	0	up to 15 min	low CRI with yellow light, contains mercury and lead
fluorescent light	10000 - 20000	60 - 100	2700-6200K	70 - 90	up to 15 min	UV radiation, contains mercury, prone to glass breaking, diffused non-directional light
LED light	50000 - 100000	70 - 150	3200-6400K	85 - 90	instant	relatively higher initial cost

2.6 STANDALONE APPLICATION IN STREET LIGHTING SYSTEMS

The approach of utilizing solar energy in lighting streets has been started in 1990's. The primary systems were fabricated for lighting paths or walkways. Aforementioned systems were comprised of lamp with less than 50 W output power [70]. Commonly, the low pressure sodium or fluorescent lamps were coupled with these systems in order to provide luminance for area of installation. The locations such as New Mexico, California, Thailand, and Spain with high amounts of solar insolation as well as adequate number of sunny days in a year, have been selected as appropriate sites to conduct research study on the powering street lights with solar energy [70]. One of the earliest studies was surveyed in New Mexico by Harrington et al. in 1996. In this research study the reliability of the system with two 50 W photovoltaic panels, 35 W low pressure sodium lamp and valve regulated lead-acid (VRLA) gel batteries has been evaluated through accurate experiment setup [71]. The results of this study showed the potential of solar energy for powering street lights at the site of interest. This preliminary setup illustrated solar energy

independently is capable of accommodating required energy for street light which broadened horizons for future design [71].

In 2002, Salas et al. [72] investigated the control strategies enclosed in photovoltaic charge controller, including maximum power point trackers (MPPTs). It is obvious that PV panel efficiency plays crucial role in enhancing the solar system performance. They found that coupling PV panels with charge controller which is equipped by MPPT feature, maximizing the output power considerably. Comprehensive tests have been designed and implemented in Thailand by using basic photovoltaic system with seven hours daily operation. In this research, Hiranvardom et al. [73] compared three various types of lamp in PV street lighting system: low pressure sodium lamp, high pressure sodium lamp and fluorescent lamp. These various lamps have been tested in order to determine suitable option for installation in a typical rural area [73]. Considering cost of lamps, system performance and possibility for purchasing the components of the system, the fluorescent lamp has been selected as the most appropriate option for installation in the region. Although, the HPS lamp worked more efficiently than the other two lamps, its cost was seven times more than the fluorescent lamp [73]. The low-pressure-sodium (LPS) lamp was the worst candidate in considering both cost and availability in Thailand [73]. Light-Emitted Diode (LED) is the newest light source which uses semiconductors and electroluminescence to create light. LED uses a small semiconductor crystal with reflectors and other parts to make the light brighter and focused into a single point. In 2003, Tetra Tech EM Inc. in San Diego debated the LED as a solution to the high running cost of HPS lights [74]. According to their result, this new technology was not adequate for lighting city streets; but led to further development in future applications [74].

In last decade, some studies have been conducted to optimize the size of stand-alone photovoltaic (SAPV) systems. For instance, in 2004, Mellit et al. have done effective efforts to develop accurate model for sizing the system with minimum number of inputs. In this study an adaptive Artificial Neural Network (ANN) has been used to investigate optimum size for major system components [75]. They defined new experimental sizing coefficients (K_{PV} , K_B) for comparing obtained results with new developed models such as

feed-forward (MLP), radial basis function (RBF), etc. The estimation of the PV-array area and the storage capacity from a minimum input data and short simulation time were some of the advantages of their model. With a correlation coefficient of 98%, their sizing estimation accuracy was good. However the results were related to Algerian sites, their methodology has capability to be applied at any geographical area over the world [75]. Two years later, they developed their model to be adaptive with various climatic conditions [76]. They stated that their obtained correlation coefficient varied from 90% to 96% for any site and climate conditions. Just one year later, in order to enhance the results obtained in [75, 76], the same authors studied the eligibility of the adaptive radial basis function network with infinite impulse response filter to estimate the sizing coefficient of stand-alone PV [77]. Due to great match between actual and new model's results (97 % correlation), proposed model can be successfully utilized for any locations in Algeria and any other locations in the world. Proposed numerical model was not capable of simulating components behavior over the year. Although their model is compatible for different operating conditions, adequate experimental data is required for training ANN. Consequently the model cannot estimate optimum size of components without experimental data from selected site. Additionally designers prefer to test the effect of each single component on system performance and aforementioned feature is not provided in this model. However the model has capability to be used for other locations, still complicated calculations corresponding to artificial neural network is required. Thereby using this model for various configurations and locations associated with new adjustments on ANN. Contrary to aforementioned model the developed TRNSYS model in this research study can be used by users with selecting site location from weather database. The TRNSYS modular structure also allows users to select battery capacity and PV size for adjusting model with various configurations.

In 2008, Lagorse et al. [78] coupled solar systems with fuel cell to enhance system reliability and continuity. According to their research study classical configuration, which is comprised of photovoltaic cells (PV) and battery cannot work all the year round in regions that are far from the equator; because the solar power is weak and varies significantly according to the seasons and high number of autonomy days. Therefore an

auxiliary power source was coupled with system to avoid probable failure. They tried to obtain accurate model to simulate system operation from energy point of view. Their hybrid system comprised of photovoltaic cells, battery bank, and fuel cell supplying a stand-alone street lighting system. In order to design the optimal hybrid system, a genetic algorithm was utilized. The obtained results showed that stochastic optimization methods are the most suited strategy to achieve an optimal design for these types of systems (FCs and PVs). Later, the same authors provided new model (simplex model) and compared that with their former model in order to investigate optimum sizing [79]. Furthermore, they took into the account more parameters such as PV tilt angle, number and size of fuel cell, start and end of cycles as well as control parameters like battery SOC thresholds which control FC operation. Finally, they exhibited an optimal configuration which is comprised of 60 watt street light, 148W photovoltaic panel, 128W fuel cell and 2.54 kWh battery bank. The hydrogen consumption every 6 years would be 1650 L with pressure of 200 bar. Their cost estimation for whole system was approximately 7150€. Components' lifespan depends on operating conditions but in normal conditions PV panels and fuel cells should be replaced after 25 and 6 years respectively. In 2010, Mellit et al. [80] applied an artificial neural network-based genetic algorithm (ANN-GA) model to generate sizing curve for stand-alone photovoltaic (SAPV) systems. Aforementioned curve has capability to be used at 40 sites located in Algeria [80]. Experiment data were compared with obtained results from the numerical method and conventional regression models. This comparison ascertained that the proposed exponential regression model is more accurate compared to conventional regression models. Due to outstanding match between simulation and experiment results with high correlation factor, it could be concluded that this model has been satisfactory. Costa et al. [81] proposed a high efficiency autonomous street lighting system which was powered by solar energy as primary source, batteries as secondary source, and LEDs as lighting source. In addition, since all power stages are implemented in DC current, it exhibited high efficiency. In their work, the control modes for charging the batteries depended on battery state of charge, and solar irradiance level. This charging strategy was including three stages, bulk charge mode (using maximum power point tracking (MPPT) feature), constant current mode, and constant voltage mode. In same year, Nunoo et al. [82] investigated the solar

power as an appropriate alternative source of electrical energy for street lighting in Ghana. They proposed LED-based lighting systems which stores solar energy during the day through bank of lead-acid batteries to provide light during night time. In the final analysis, they concluded that the usage of LED technology can help government for solving the problems of budgetary and environmental challenges. They investigated the performance of LED lamp against high-pressure sodium and mercury vapor lamp in view of some parameters such as: flux, power consumption, system efficiency, average lux, lifetime, etc. Finally, they found that this approach enhances streetlight quality by decreasing glare and preparing better color rendering.

2.7 SIZING OF BATTERY BASED STAND-ALONE PHOTOVOLTAIC SYSTEMS

Sizing of battery based stand-alone photovoltaic system (BSPVS) can be approached in different ways but all approaches have at least three common steps and these are: 1) load estimation; 2) battery sizing; 3) PV array sizing. The procedure given by Solar Energy International [83] is to sequentially examine solar resources and estimates the electric load, battery size, PV size, specify charge controller and perform system wire sizing. The approach given in Australian Standards [84] follows 7 steps given in their order of occurrence as load determination; selection of battery capacity, first approximation of tilt angle; determining insolation of the location; initial approximation of array size optimizing array tilt angle and optimizing array size. On the other hand, Chapman [85] approaches the PV system sizing by firstly defining site-specific and application-specific parameters then determining battery storage and finally determining the array size.

The following sub-sections will give a detail BSPVS sizing basing on approach by Malawi Bureau of Standards [86] for load estimation, battery sizing and array sizing while using approach by Solar Energy International [83] for charge regulator sizing.

Step 1: Load estimation

The daily load estimation is accomplished if the electrical devices, their power rating, number of operated hours in a day are known. If P is the power rating of electrical device in Watts (W), N is the number of electrical devices of type i and t is the daily number of hours for which a particular device operates then the total daily load (E_{day}) in W_h is

estimated by equation (1). Equation (2) is then used to calculate the daily load (Q_d) demand in terms of electrical charge in Ah.

$$E_{day} = \sum_i P_i N t \quad (1)$$

$$Q_{day} = \frac{E_{day}}{V_{b,nom}} \quad (2)$$

where $V_{b,nom}$ is the system's nominal battery voltage.

After the daily load is estimated, the actual hours of the day at which the electrical load is expected to be operated should be established in order to know the loading profile to which the system will be subjected to.

Step 2: PV array sizing

First it is assumed that during solar window¹ load demand is directly met by PV array output and from the loading profile established in Step 1, the load demand expected to be directly met by PV array is known. The required generated power from PV array (Q_a) is then calculated by

$$Q_a = Q_{day} \left(R_{dir} + \frac{(1 - R_{dir})}{\eta_b} \right) \quad (3)$$

Where R_{dir} is the ratio of the load directly met by PV array to the total load demand and η_b is the battery charging efficiency. If DF is the PV's de-rating factor and PSH is location's peak sunshine hours then equation (4) is used to calculate the expected maximum power output of the array:

$$W_p = \frac{Q_a \times V_{b,nom}}{DF \times PSH} \quad (4)$$

¹ Solar window is the timeframe within which solar radiation is optimally collected which is generally between 9am to 3pm

Step 3: Battery sizing

The battery is used to supply electrical energy during night and cloudy days. In cloudy days there is little if any battery charging. Therefore, depending on location, any BSPVS must be designed with battery capacity to meet certain number of autonomy days. Therefore, if the desired depth of discharge is DOD and the desired days of autonomy are n then the battery is subjected to daily depth of discharge ($DDOD$) equal to DOD divided by n . From the daily load charge demand and $DDOD$, the expected battery capacity (C_b) is calculated by equation (5):

$$C_b = \frac{Q_{day}(1 - R_{dir})}{DDOD} \quad (5)$$

Step 4: Sizing of charge controller

Since the controller is specified by the operating current, then maximum current from the PV array which is expected to pass through the controller must be determined. This is calculated by equation (6).

$$I_{controller} = 1.25I_{sc}N_p \quad (6)$$

Where I_{sc} is the short circuit current of PV module, N_p is the number of modules connected in parallel and 1.25 is the factor of safety recommended by Solar Energy International [83].

CHAPTER 3 SIMULATION METHODS

Chapter 3 is centered in simulation model and methodology which was followed to meet the objectives of this research. It later describes operation of TRNSYS software and components which were used in this model. The achieved results from simulation model are presented at final section.

3.1 INTRODUCTION

There are several common simulation software used to design, simulate and verify solar systems (e.g. TRNSYS, POLYSUN, TSOL, etc.). Due to modular basis, TRNSYS software [3] is considered as the most flexible and powerful tool among the commercially available software for designing and simulating battery based standalone photovoltaic systems. TRNSYS is an acronym for “transient system” given to combination of various thermal, mechanical and electrical libraries which are linked to extendable environment in order to simulate the behavior of transient systems. It includes graphical interface, simulation engine, powerful weather database of more than 1200 locations, and library of components are used in wide range of applications ranging from alternative energy (wind, solar, hydrogen and etc.) to HVAC (heating, cooling and ventilation) to low energy building to renewable energy and cogeneration system.

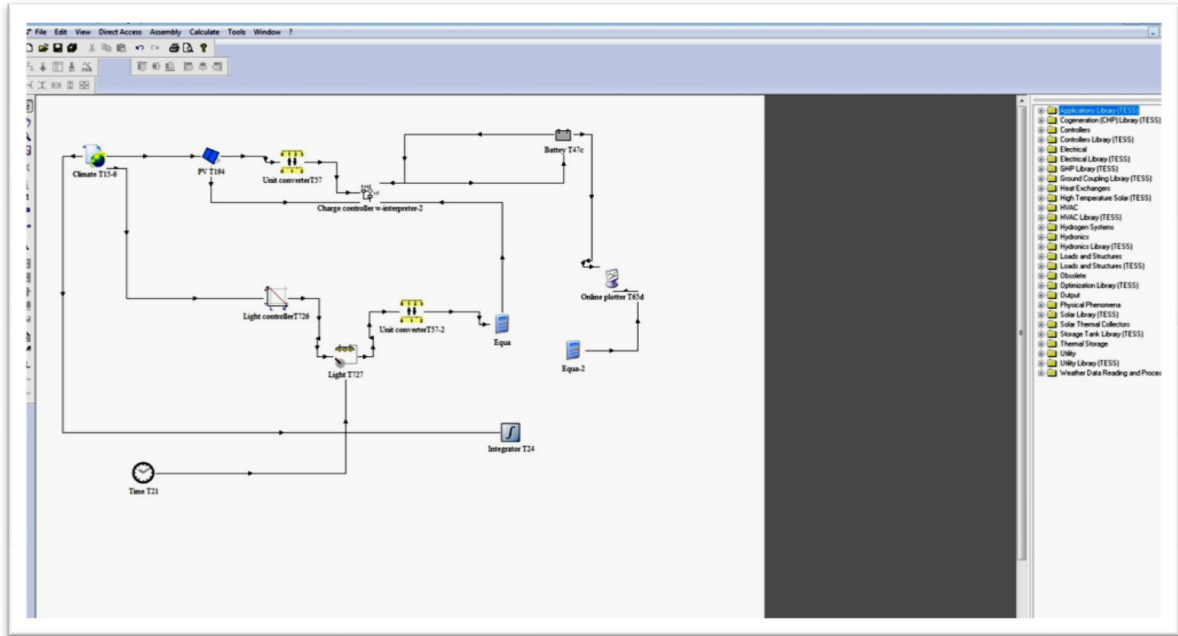


Figure 7: TRNSYS simulation studio

TRNSYS has unique feature in comparison to other simulation software which allows users adding custom component through common programming language such as C++, FORTRAN and MATLAB. Aforementioned attribute enrich the accuracy and compatibility of the simulation with real operating condition. The new project would be set up by drag and dropping components and connecting them together through flexible visual interface (called simulation studio). All available components are categorized in fourteen major types. Each type of these components is defined in TRNSYS simulation engine by the certain mathematical model and linked to simulation studio through set of matching performance (TRNSYS component). Each component includes description box which shows values and units of inputs, outputs and constant parameters. In addition, brief description is available about the component functionality. The powerful output manager gives the user ability to control which variables are integrated, plotted and/or printed. Also, the detailed study of what happened during simulation is provided for the user through the log/error manager.

Due to aforementioned features and availability of major components of the off-grid solar street light includes PVs, light controller, battery and charge controller, system performance can be simulated. However, charge controller and battery were modified or

redesigned in order to meet the project objectives. Ambient temperature has great impact on battery voltage and available capacity, while presently is not entered in TRNSYS battery model equations [3]. Consequently temperature is not considered as an input for battery component which makes it unreliable for locations where the daily mean temperature is far from reference temperature of 25 °C (e.g. Qatar at 45 °C daily average). Additionally present charge controller component in TRNSYS library acts as on/off switch [3] which is not appropriate for modeling the constant-power/constant-voltage of real charge controller operation.

The mathematical algorithms associated with involved components in simulation model are explained in the following sections.

3.2 WEATHER DATABASE

Solar array is the only energy source of the system and the PV output power depends on weather parameters such as solar irradiation, ambient temperature and wind velocity. The weather component is set to read data in various standard formats (TMY2, TRY, CWEC, IWEC, TMY3, etc.) for various time steps from external weather data file. Currently there are two data sources are organized in weather directory:

- US-TMY2 (National Renewable Energy Laboratory)
- METEONORM

The US-TMY2 was produced by NREL Analytic Studies Division under the Resource Assessment Program which includes 237 locations in the US (contiguous states, Hawaii and Alaska) [87]. METEONORM database is considered as one of the most comprehensive meteorological reference with 8300 station worldwide [87]. The METEONORM database is the result of evaluating and combining numerous global and regional databases such as GEBA (Global Energy Balance Archive) [88], the World Meteorological Organization (WMO/OMM) [89] and the Swiss databases compiled by MeteoSwiss [90]. Also, Satellite data is used for area with low density of weather stations. Following measured parameters are available for about 1200 locations around the world (the list of locations is prepared in appendix) as average of 1960-2005 [3]:

- Global Horizontal radiation (TRNSYS Processor component calculate tilted and diffuse radiation)
- Ambient dry bulb temperature
- Wind velocity and direction
- Relative humidity

Summary of available data is tabulated according to data source and region in Table 3.

Table 3: TRNSYS weather database stations over the world [3]

Source	World Region	Available locations
US-TMY2	United States only	237 locations in the US (contiguous states + Alaska and Hawaii), and 2files for Puerto-Rico and Guam.
Meteonorm	Africa	174 locations in 46 countries
	Asia	227 locations in 43 countries
	Australia-Oceania	55 locations in 9countries
	Central and South America	141 locations in 29 countries
	Europe	369 locations in 35 countries
	North America (excluding US)	67 locations in 3 countries

The available locations are illustrated in following figure where the US-TMY2 stations are shown by blue triangle and black and white dots represent METERONOM stations with and without solar radiation data respectively.

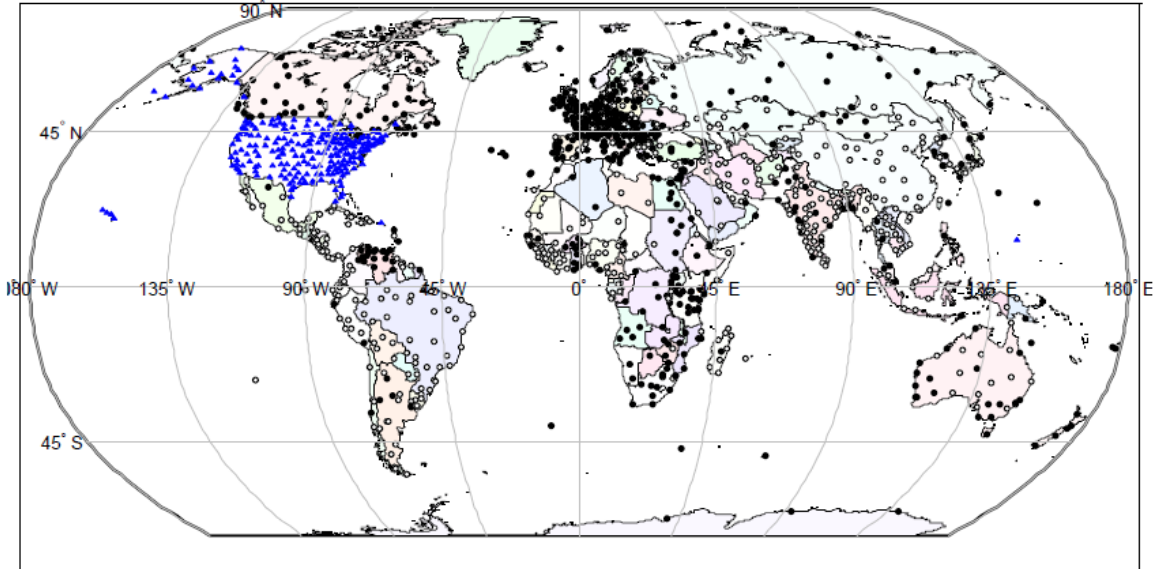


Figure 8: Meteorological stations over the world [87]

The weather components act as solar radiation processors with the ability to calculate total, beam, sky diffuse and ground reflected solar radiation as well as azimuth and incidence angle of beam radiation for slope surfaces with arbitrary orientation and inclination. Most weather stations can record total horizontal irradiance, ambient temperature and relative humidity while only a few are equipped to measure beam or diffuse radiation. The radiation processing mode to calculate radiation components on a tilted surface can be selected from the following models [91]:

- Isotropic Sky model
- Hey and Davies model
- Reindl model
- Perez model

The aforementioned models require at least two components of solar radiation in order to calculate radiation on tilted surfaces. The various combinations of required parameters are listed below:

- Direct beam irradiance and diffuse irradiance
- Total global horizontal irradiance and diffuse irradiance
- Total global horizontal irradiance and Direct normal beam irradiance

- Total global horizontal irradiance, ambient temperature and relative humidity (Reindl's [91] reduced correlation is used to estimate the diffuse radiation)

Also, the component can be set for various sun tracing modes:

- Fixed surface
- Surface with sun tracking feature (rotation about vertical or user defined axes)
- Surface with 2-axis tracking system (beam radiation is always normal to surface)

Effect of snow on ground reflectance is considered for period of year in which ground is covered by snow.

Fifty nine parameters are calculated by this component as output such as effective sky temperature, relative humidity and atmospheric pressure, only ten of them are effective in this modeling. Site latitude is used as input that is sent to other component (self-coded) in order to set the slope of PV panels. Aforementioned component adjusts the PV slope for maximum output according to prepared PV installation guide by manufacturer. Total Horizontal Radiation is the other parameter required for light controller in order to investigate luminance level and control the LED lamp. A part from these two parameters other outputs are sent to PV panels component. As mentioned earlier solar radiation components (beam, diffuse and ground reflected radiations) on tilted surface and solar angles (azimuth angle and incidence angle) are calculated by this component through reading data from data file, converting them into a desired system of units and sending them to PV panel. Wind velocity and ambient temperature are also considered as crucial parameters on estimation of PV output so weather component serve to read these data from weather database and import them to PV panels.

3.3 PV PANEL COMPONENT

The performance of PV is site dependent and efficiency varies with daily temperature and operating voltage/current, so real operating conditions are completely dynamic and cannot be modeled without access to temperature and radiation data for area of interest. TRNSYS has a powerful five-parameter PV model able to predict long term output power under real dynamic conditions for many locations.

PV panel manufacturers commonly measure and state electrical parameters for only standard rating condition (SRC). These parameters are open circuit voltage (V_{OC}), short circuit current (I_{SC}), maximum power current (I_{mp}) and voltage (V_{mp}) the temperature coefficient at open circuit voltage and short circuit current ($\beta_{V_{oc}}$ and $\alpha_{I_{sc}}$, respectively) and the nominal operating cell temperature (NOCT). Except NOCT which is measured at constant irradiance of 800 W/m^2 and an ambient temperature of $20 \text{ }^\circ\text{C}$ other parameters are determined when irradiance and cell temperature are fixed on 1000 W/m^2 and $25 \text{ }^\circ\text{C}$ respectively. Due to the fact that PV panels are site dependent device and normally working over wide range of conditions, manufacturer's data is not sufficient to model their overall performance especially under low irradiance condition. The model proposed by King et al. [92, 93] precisely predicts the energy production over wide range of operating condition but it requires parameters that are not normally available from manufacturer". So it is necessary to apply reliable and accurate model with ability to estimate energy production of PV panels in various operating conditions using only manufacturer's data. "Five-parameters model developed by W. De Soto et al. [94] accurately predict energy production of array for four different cell technologies (single crystalline, poly crystalline, Silicon thin film and triple-junction amorphous). Five-parameters model considered as powerful tool for modeling PV panel because contrary to previous models requires only small amount of data which are normally prepared by manufacturer; the model circuit will be presented in Figure 9.

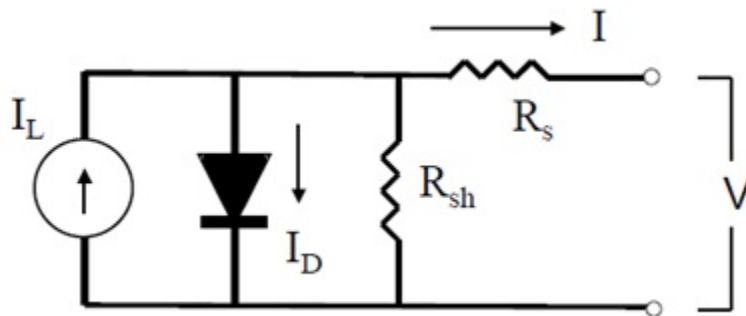


Figure 9: PV panel equivalent circuit [3]

TRNSYS library includes three different types of PV generator:

- Type 94 series (4 parameters model)

- Type 180 series (4 parameters model)
- Type 194 series (5 parameters model)

These types are used to simulate PV output power in various operation conditions. Type 94 and 180 are programmed based on four parameters model, simplified version of five parameters model which is used in type 194. Extensive database of model parameter for many array types is provided by Sandia National Laboratory [95] and PV array type can be selected among available models. For array types that are not included in the database, required inputs must be entered manually. Duffie and Beckman [96]; Nelson [97] proposed the equivalent circuit to model available electrical power of PV array. The current-voltage relationship for the illustrated circuit in Figure 9 in certain temperature and solar irradiance is expressed in equation (7). Current, voltage and finally delivered output power are estimated by determining following five parameters. These parameters are: the light current I_L , the diode reverse saturation current I_0 , the series resistance R_S , the shunt resistance R_{Sh} and the modified ideality factor 'a' defined in Equation (8).

$$I = I_l - I_D - I_{sh} = I_l - I_o \left[e^{\left(\frac{V+IR_s}{a} \right)} - 1 \right] - \frac{V + IR_s}{R_{SH}} \quad (7)$$

where:

$$a \equiv \frac{N_s n_1 K T_c}{q} \quad (8)$$

The electron charge q and Boltzmann's constant K are known, n_1 is the ideality factor, N_s is the number of cells in series and T_c is the cell temperature. Five pair of independent pairs of data is required to identify the model parameters. These parameters are dependent on cell temperature and solar irradiance. As mentioned earlier, three pairs of information are available by manufacturer at standard radiation condition: short circuit current, open circuit voltage and current/voltage at the maximum power point. Based on I-V chart and recognizing the fact that derivation of power at maximum power point is zero the fourth pair is resulted. Open voltage temperature coefficient (β_{Voc}) shows voltage

trend versus temperature and it is used as the fifth pair of data to satisfy the current-voltage equation and identify the whole five parameters. These five known pair of current and voltage are substituted to Eq. (9) to identify the five appeared parameters (a , I_0 , I_L , R_S and R_{SH}).

For short circuit current: $I = I_{SC}$, $V = 0$

$$I_{SC,ref} = I_{L,ref} - I_{0,ref} \left[e^{\frac{I_{SC,ref} R_{S,ref}}{a_{ref}}} - 1 \right] - \frac{I_{SC,ref} R_{S,ref}}{R_{SH,ref}} \quad (9)$$

For open circuit voltage: $I = 0$, $V = V_{OC,ref}$

$$0 = I_{L,ref} - I_{0,ref} \left[e^{\frac{V_{OV,ref}}{a_{ref}}} - 1 \right] - \frac{V_{OV,ref}}{R_{SH,ref}} \quad (10)$$

At the maximum power point: $I = I_{mp,ref}$, $V = V_{mp,ref}$

$$I_{mp,ref} = I_{L,ref} - I_{0,ref} \left[e^{\frac{V_{mp,ref} + I_{mp,ref} R_{S,ref}}{a_{ref}}} - 1 \right] - \frac{V_{mp,ref} + I_{mp,ref} R_{S,ref}}{R_{SH,ref}} \quad (11)$$

The derivation at the maximum power point is zero:

$$\frac{d(IV)}{dV} \Big|_{mp} = I_{mp} - V_{mp} \frac{dI}{dV} \Big|_{mp} = 0 \quad (12)$$

Where dI/dV is given by:

$$\frac{dI}{dV} \Big|_{mp} = \frac{\frac{-I_0}{a} e^{\frac{V_{mp} + I_{mp} R_S}{a}} \frac{1}{R_{Sh}}}{1 + \frac{I_0 R_S}{a} e^{\frac{V_{mp} + I_{mp} R_S}{a}} \frac{R_S}{R_{Sh}}} \quad (13)$$

Finally the temperature coefficient of open circuit voltage is given by:

$$\mu_{Voc} = \frac{dV}{dT} \Big|_{I=0} \approx \frac{V_{OC,ref} - V_{OC,T_C}}{T_{ref} - T_C} \quad (14)$$

The numerical evaluation of $\mu_{V_{OC}}$ needs value of V_{OC} in some temperature around the reference temperature. Due to the fact that 1 to 10°C variation in cell temperature does not have notable impact on V_{OC} , reference condition value can be used for this purpose. It is necessary to find expressions for temperature dependency of a , I_L , I_O and R_{Sh} in order to obtain the value of V_{OC,T_c} from Eq. (10). A part from R_{Sh} which is assumed to be independent of temperature, the operation condition temperature dependence of three other parameters is known through the following equations:

As can be seen from Eq. (14) all the parameters are constant and n_1 is assumed independent of temperature consequently the modified ideality factor (a) is linear function of temperature:

$$\frac{a}{a_{ref}} = \frac{T_c}{T_{c,ref}} \quad (15)$$

Where a and $T_{c,ref}$ are represent of modified ideality factor and cell temperature for reference condition, while T_c and a refer to the same parameters for new operating condition.

The ratio of diode reverse saturation current (I_O) in new operating condition to reference condition can be expressed based on diode theory by the following equation [98]:

$$\frac{I_O}{I_{ref}} = \left[\frac{T_c}{T_{c,ref}} \right]^3 \exp \left[\frac{1}{K} \left(\frac{E_g}{T_{ref}} - \frac{E_g}{T_c} \right) \right] \quad (16)$$

Where K is the Boltzmann's constant and E_g refers to material band gap. Ven Aeghbroeck [99] presents an equation which shows the small temperature dependence of E_g for silicon cells:

$$\frac{E_g}{E_{g,T_{ref}}} = 1 - 0.0002677(T - T_{ref}) \quad (17)$$

Where E_g in reference condition is considered to be 1.121 eV for silicon cells.

The light current (I_L) is proportional to solar irradiation and normally used as an indicator in the process of measuring incident solar irradiance in pyranometers. The light current

depends on the absorbed solar irradiance (S), the cell temperature (T_C), the short circuit current temperature coefficient ($\alpha_{I_{sc}}$) and the air mass modifier. I_L can be obtained in various operating condition through the following equation:

$$I_L = \frac{S}{S_{ref}} \frac{M}{M_{ref}} [I_{l,ref} + \alpha_{I_{sc}}(T_C - T_{C,ref})] \quad (18)$$

Where the parameters with subscript *ref* represent the reference condition and the ones without subscript specify the new operating condition.

Air mass refers to the ratio of mass of air at any given time and location that beam radiation has to traverse to the situation sun directly is overhead. The air mass modifier can be defined as a function of the local zenith angle and cell material through the empirical equation developed by King et al. [92]:

$$\frac{M}{M_{ref}} = \sum_0^4 \alpha_i (AM)^i \quad (19)$$

Where

$$AM = \frac{1}{\cos(\theta_z) + 0.5057(96.080 - \theta_z)^{-1.634}} \quad (20)$$

The α_0 , α_1 , α_2 , α_3 and α_4 are constant for different type of materials used in PV panel fabrication and θ_z is the zenith angle (angle between directly overhead and geometric center of the sun).

As the last step it is necessary to discuss the impact of series resistance R_S , and the shunt resistance R_{Sh} on PV panel I-V curve. The change in series resistance has effect on I-V curve shape around the maximum power point. The (R_S) values can be identified for different operating conditions through the methods proposed by De Soto [94]. Since the change on the curve is small for different values of series resistance, it is assumed constant at its reference value for various operating conditions. The slope of I-V curve at short circuit condition depends on the value of R_{Sh} , increasing the amount of shunt resistance leads to horizontal slope. Absorbed radiation has notable impact on the amount of R_{Sh} , but developing relation between S and R_{Sh} would not be possible without having

experimental data in few operating conditions which is not normally available. Short-circuit current can be considered as a precious indicator for absorbed radiation. So inverse relation between short-circuit current and shunt resistance at very low irradiance condition [94] results in empirical equation which shows how R_{Sh} varies with absorbed radiation (S):

$$\frac{R_{Sh}}{R_{Sh,ref}} = \frac{S_{ref}}{S} \quad (21)$$

All five parameters can be identified using the aforementioned equations and I-V curve could be modeled at various operating conditions (different solar radiation and ambient temperature) in order to predict produced energy through the installed PV panels.

3.3.1 Validation of five-parameter model

It is necessary to validate the model in various operating conditions to ensure reliability and accuracy of PV output prediction, particularly in low irradiance condition. Research article by De Soto et al. [4] compares predicted current-Voltage curve with experimental data from a building integrated photovoltaic facility at the National Institute of Standards and Technology (NIST) for common PV technologies (single crystalline, poly crystalline, silicon thin film and triple junction amorphous) over a range of operating conditions. As it is shown in Figure 10 excellent agreement exists between prediction from five-parameter model and NIST measurements. The power at maximum power point for both data series are tabulated in Table 4.

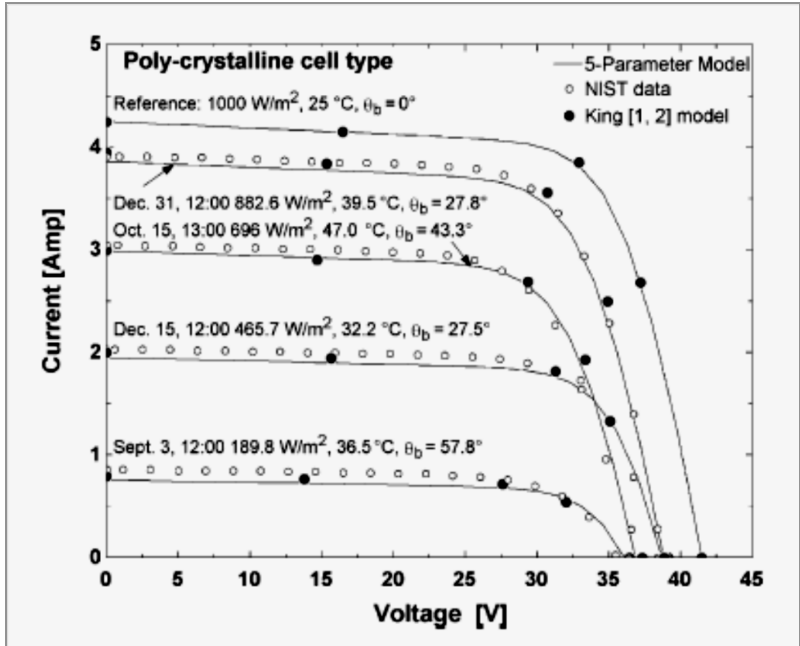


Figure 10: Current vs voltage predicted by the five parameter model, the king model and measured by NIST for the poly crystalline cell type [4]

Table 4: Maximum power values of the polycrystalline cell type from NIST measurements, King and five-parameter models [4]

Solar [W/m ²]	Temperature [°C]	Maximum power[W/m ²]		
		NIST	King	Five-parameter
1000.0	25.0	125.8	125.8	125.8
882.6	39.5	106.8	109.3	105.6
696.0	47.0	77.4	79.1	78.1
465.7	32.2	56.6	56.9	55.8
189.8	36.5	21.2	18.5	20.6

Contrary to other simulation software, the five-parameter model which is used in TRNSYS software applies conservative approach to predict PV output power. Consequently the model is powerful tool for energy prediction and simulation purposes through the small amount of data normally provided by manufacturer.

Table 5: PV input

	Name	Dimension	Unit
1	Total incident radiation on titled surface	Flux	kJ/hr
2	Ambient temperature	Temperature	C
3	Load voltage	Voltage	V
4	Array slope	Direction	deg
5	Beam radiation on titled surface	Flux	kJ/hr
6	Sky diffuse radiation on titled surface	Flux	kJ/hr
7	Ground diffuse radiation on titled surface	Flux	kJ/hr
8	Incidence angle on titled surface	Direction	deg
9	Solar zenith angle	Direction	deg
10	Wind speed	Velocity	m/s

Table 6: PV output

	Name	Dimension	Unit
1	Array voltage	Voltage	V
2	Array current	Current	amp
3	Array power	Power	W
4	Power at maximum power point	Power	W
5	Fraction of maximum power used	-	-
6	Voltage at MPP	Voltage	V
7	Current at MPP	Current	amp
8	Open circuit voltage	Voltage	V
9	Short circuit current	Electric	amp
10	Array fill factor	-	-
11	Array temperature	Temperature	K
12	Conversion efficiency	-	-

Table 7: PV parameters

	Name	Dimension	Unit
1	Mode	-	-
2	Module short-circuit current at reference conditions	Electric	amp
3	Module open-circuit voltage at reference conditions	Voltage	V
4	Reference temperature	Temper	K
5	Reference insolation	Flux	W/m
6	Module voltage at max power point and reference conditions	Voltage	V
7	Module current at max power point and reference conditions	Electric	amp
8	Temperature coefficient of Isc at (ref. cond)	any	any
9	Temperature coefficient of Voc at (ref. cond)	any	any
10	Number of cells wired in series	-	-
11	Number of modules in series	-	-
12	Number of modules in parallel	-	-
13	Module temperature at NOCT	Temperature	K
14	Ambient temperature at NOCT	Temperature	K
15	Insolation at NOCT	Flux	W/m
16	Module area	Area	m ²
17	tau-alpha product for nominal incidence	-	-
18	Semiconductor band gap	any	any
19	Value of parameter a at reference conditions	-	-
20	Value of parameter I _L at reference conditions	Electric	amp
21	Value of parameter I ₀ at reference conditions	Electric	amp
22	Module series resistance	-	-
23	Shunt resistance at reference conditions	-	-
24	Extinction coefficient-thickness product of cover	-	-

3.4 BATTERY

3.4.1 TRNSYS battery model

The present lead-acid battery model in TRNSYS electrical library is designed to operate in conjunction with solar array. Various parameters such as state of charge, rate of charge/discharge and total voltage will be controlled over time. The model utilizes Shepherd equations relating to battery voltage, current and state of charge in order to simulate battery operation in charge and discharge mode under real condition [3]. Different operating modes consider different assumptions including reference equations

(Shepherd or Hymen [5]) and input parameter (Power or current). The Shepherd model is simpler while Hymen model is more accurate and reliable at low current. In fact Hymen modified Shepherd equations based on developed model by Zimmerman and Peterson which takes into account the battery behavior at very low current.

Battery component is programmed in order to accept current or voltage as input to predict battery voltage and state of charge over the time.

Shepherd equations are originally developed to describe battery behavior during discharge however by considering few other parameters charging process also can be described through this model:

On discharge mode $I < 0$:

$$V(V) = e_{qd}(V) - g_d(V)H + I(A)r_{qd}(\Omega)\left(1 + \frac{m_d H}{\frac{Q_d}{Q_m} - H}\right) \quad (22)$$

And in charge mode $I > 0$

$$V(V) = e_{qc}(V) + g_c(V)H + I(A)r_{qc}(\Omega)\left(1 + \frac{m_c H}{\frac{Q_c}{Q_m} - H}\right) \quad (23)$$

Where V and I refer to voltage and current, e_{qd} and e_{qc} are representative of open circuit voltage at full charge on discharge and charge mode respectively, H shows fractional state of discharge, g_d and g_c are small-valued coefficients of H in volt unit in voltage-current-state of charge formulas, r_{qd} and r_{qc} illustrate Internal resistances at full charge when discharging/ charging, m is the cell type which determine the shape of I-V curve, Q_c , Q_d , are representative of capacity parameter in charge and discharge mode. As can be seen in above equations, temperature is not entered in above equations and does not have any effect on voltage or available capacity of battery during charge/discharge process. Due to experimental research on battery behavior at various operating conditions, (e.g. wet, dry, tropical) ambient temperature is known as notable parameter on battery functionality [100]. Regarding considered assumption for TRNSYS battery model, ambient temperature is supposed to be constant (25 °C) during operation consequently accuracy of predicted result would be decreased at higher or lower temperature than

reference temperature. The temperature directly impacts the available capacity and the final charge voltage. According to the fact that compatibility with various climate conditions is the most important purpose it is necessary to develop new model for estimating battery behavior at extended range of ambient temperature. TRNSYS battery model input, output and parameters are presented in Tables 8, 9, 10 respectively.

Copetti model has required features and selected to be utilized in this research that is explained in next section.

Table 8: Battery input

	Name	Dimension	Unit
1	Current/Power	Electric	Amp/W

Table 9: Battery output

	Name	Dimension	Unit
1	State of charge	Electric	Ah
2	Fractional state of charge	-	-
3	Power	Power	kJ/hr
4	Power lost during charge Total	Power	kJ/hr
5	Total current	Current	amp
6	Total voltage	Voltage	V
7	Max. Power of charge	Power	kJ/hr
8	Max. Power of discharge	Power	kJ/hr
9	Discharge cutoff voltage (DCV)	Voltage	V
10	Power corresponding to DCV	Power	kJ/hr
11	Charge cutoff voltage (CCV)	Voltage	V
12	Power corresponding to CCV	Power	kJ/hr

Table 10: Battery parameters

	Name	Dimension	Unit
1	Mode	-	-
2	Cell Energy Capacity	Electric	Ah
3	Cells in parallel	-	-
4	Cells in series	-	-
5	Charging efficiency	-	-
6	Max. current per cell charging	Current	amp
7	Max. current per cell discharging	Current	amp
8	Max. charge voltage per cell	Voltage	V

3.4.2 Copetti battery model

A comprehensive lead-acid battery model should illustrate relation among both external and internal parameters such as voltage, current, state of charge, temperature and internal resistance during charging and discharging process. Based on conducted literature review on the area of battery modeling it can be concluded that while many models have been developed to predict battery behavior; majority of these models are limited to the considered case study and does not have ability to be extended for other batteries with different features. Some models are developed to include wide range of battery types but they require numerous parameters which are not normally provided by manufacturers and should be investigated through particular experiments and equipment. The desired model should have capability to simulate battery behavior using commonly available parameters by battery specification sheets. The developed battery model by Copetti and Chenlo meets required features and considered as an appropriate model for predicting battery behavior during charge/discharge process. Copetti's model [53] has ability to represent battery's voltage trend during constant current charge or discharge. In fact Copetti model is the modified version of Shepherd's equation which including correction for temperature effects on main parameters. The normalized model with battery capacity would keep constant the value of effective parameters thereby stays valid for any size of battery. Based on equation (24) (The subscripts A and B represent different battery capacity) the resistance parameter value can be verified through battery capacity.

$$R_A \times C_A = R_B \times C_B \quad (24)$$

This assumption can be applied to other parameters and different manufactures which is helpful to generalize equations. Consequently all equations related to charge and discharge were rewritten as functions of C_{10} capacity rated. Discharge and charge equations are presented through Equation (25) to (30):

Discharge:

$$V_d = \left(2.085 - 0.12 \left(\frac{Q}{C} \right) \right) - \frac{I}{C_{10}} \left(\frac{4}{1 + I^{\frac{1}{3}}} + \right) + \frac{0.27}{\left(1 - \frac{Q}{C_T} \right)^{1.5}} + 0.02 \quad (1) \quad (25)$$

$$- 0.007 \times \Delta T)$$

$$C = \frac{C_T}{1 + 0.67 \left(\frac{I}{I_{10}}\right)^{0.9}} \quad (26)$$

$$C_T = 1.67 \times C_{10}(1 + 0.005 \Delta T) \quad (27)$$

Charge until $V < V_g$:

$$V_c = \left(2 + 0.16 \times \frac{Q}{C}\right) + \frac{I}{C_{10}} \left(\frac{6}{1 + I^{0.6}} + \frac{0.48}{\left(1 - \frac{Q}{C_T}\right)^{1.2}} + 0.036 \right) \quad (28)$$

$$\times (1 - 0.025 \Delta T)$$

Overcharge $V > V_g$:

$$V_{oc} = \left(2.45 + 2.011 \times \ln\left(1 + \frac{I}{C_{10}}\right)\right) (1 - 0.002\Delta T) \quad (29)$$

$$V_g = \left(2.24 + 1.97 \ln\left(1 + \frac{I}{C_{10}}\right)\right) (1 - 0.002\Delta T) \quad (30)$$

Despite less accuracy of normalized model, it can be utilized satisfactorily in photovoltaic system simulation program. Regardless of battery size or manufacturer, the model is valid for lead-acid batteries.

3.4.3 Developed Battery model (self-coded component)

The battery operating conditions in standalone PV systems are quite different in comparison with conventional applications thereby energy storage through batteries is one of the causes of failures and loss of reliability. Developing comprehensive theoretical model fitted to experimental data plays considerable role to understand batteries' behavior under realistic charge/discharge cycles. Comparison estimated and experimental results, shows less than 3 % error for constant current charging and discharging [48]. The model is so effective during the discharge but the results are therefore slightly

overestimated during charging. The battery component was coded in MATLAB based on Copetti equations in order to estimate battery voltage according to battery SOC, ambient temperature and charge/discharge current. As mentioned earlier charge controller allows PV panels to charges the battery based on MPPT mode until SOC reach to 70 percent. Then charging process continues accordance to preset specified voltage for 2 hours. The charge controller keeps battery at full charge by applying lower voltage to the battery component. During Float stage, charging current is limited to 0.2 Ampere. Certain limits were applied on charge equations to avoid sudden rise in battery voltage values as a result of fluctuation in input charge/discharge current. The self-coded battery component was connected to TRNSYS simulation studio to operate in charge and discharge cycles. During simulation at each time step charge controller (self-coded) component receives battery SOC and sends corresponding charge/discharge current to battery. MATLAB receives ambient temperature and input charge/discharge current as input data and estimates battery voltage according to Copetti equation. This cycles repeats at each time step. For accurate estimation of battery voltage in PV systems at various climatic conditions, it is necessary to determine ambient temperature during test period [48]. The new battery component can be coupled with other models in TRNSYS software. It is necessary to define the related M-file to corresponding component in TRNSYS component. Compatibility with various type of lead acid battery is major privilege for Copetti model. It is necessary to adjust the battery capacity corresponding to 10 hours discharge for different battery types. The component can be written in FORTRAN code to be utilized by TRNSYS without MATLAB software. Finally this model has capability to be added to TRNSYS library and be coupled with other components for more accurate results.

3.5 CHARGE CONTROLLER (SELF CODED)

TRNSYS charge controller component acts as on/off switch according to battery available capacity or cut-off voltage which is not appropriate for modeling the constant-power/constant-voltage of real charge controller operation. This component was coded in MATLAB in order to simulate three stages of charging (Bulk/Acceptance/Float) based on battery state of charge. Battery current and voltage profile are presented in Figure 11. The

first stage of charging process is bulk charge when charge controller use MPPT technique. During bulk charge maximum amount of current flows to the battery until battery voltage reaches the desired voltage set point. The charge controller component monitors battery state of charge in order to investigate end of bulk charge stage. Acceptance stage starts when Battery state of charge reaches to set threshold (70 percent of Ah capacity). This stage considered as the most important part of charging process since completes the charging by increasing battery bank level to maximum capacity. At this stage battery voltage remains constant while the current level start decreasing as the internal resistance in the battery increases. Two strategies are commonly used to determine the stage duration and avoid overcharging. Apart from current threshold, internal timer can be adjusted according to required time for returning battery to full charge. As can be seen in Figure 12, the flowchart illustrates how charge controller operates in various modes based on most common algorithms such as maximum power point tracking, constant voltage and float charging. The charge controller component equipped with timer to remain in acceptance stage continuously for the preset charge time period (typically two hours). Third stage is float charging which is necessary to avoid unwanted self-discharging in absence of load. When battery is fully charged somewhat lower float voltage is applied to maintain the battery in full state. The amount of current is drawn by lead-acid battery during float varies between 0.1 to 0.2 Ampere per 100 Ah of battery capacity. Some type of battery or system configuration requires two stage of charge, which eliminate Float charge mode. Self-coded charge controller component is capable of handling all three stage of charging process which enhances accuracy of simulation results.

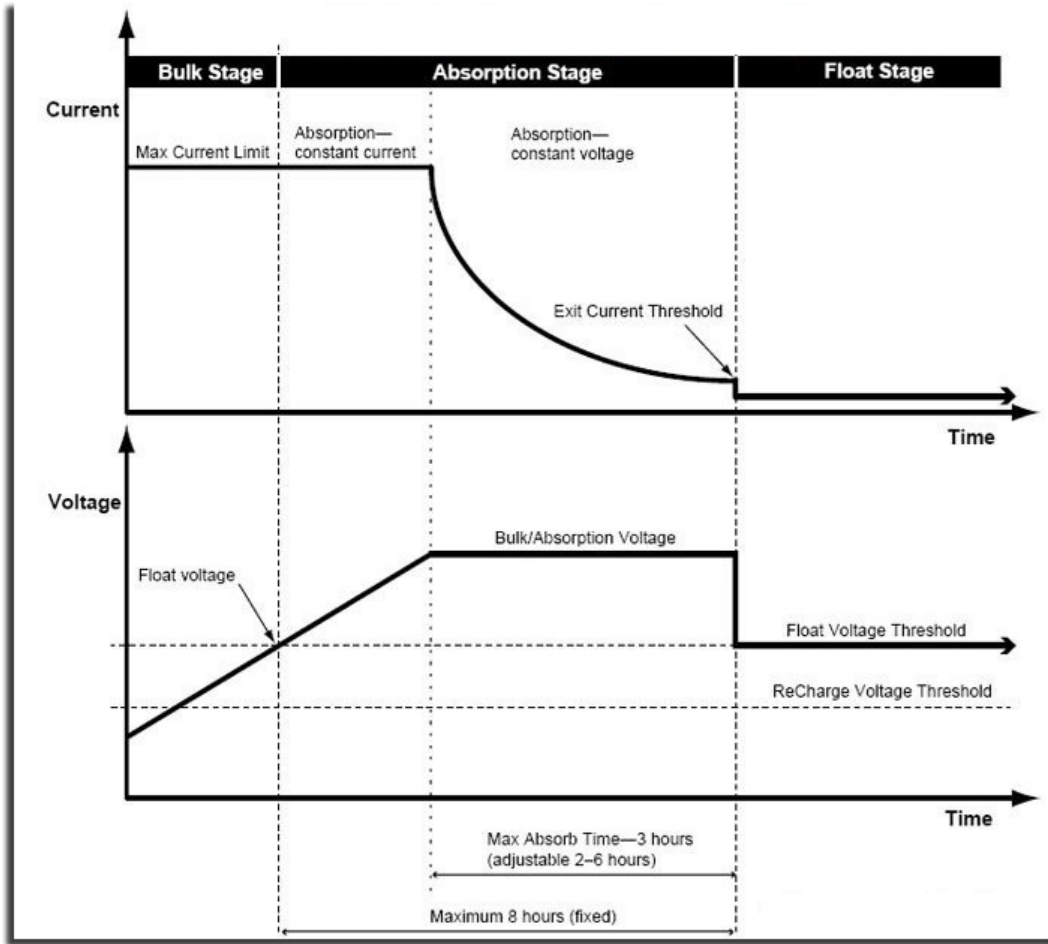


Figure 11: Current and voltage profiles for battery charging process [101]

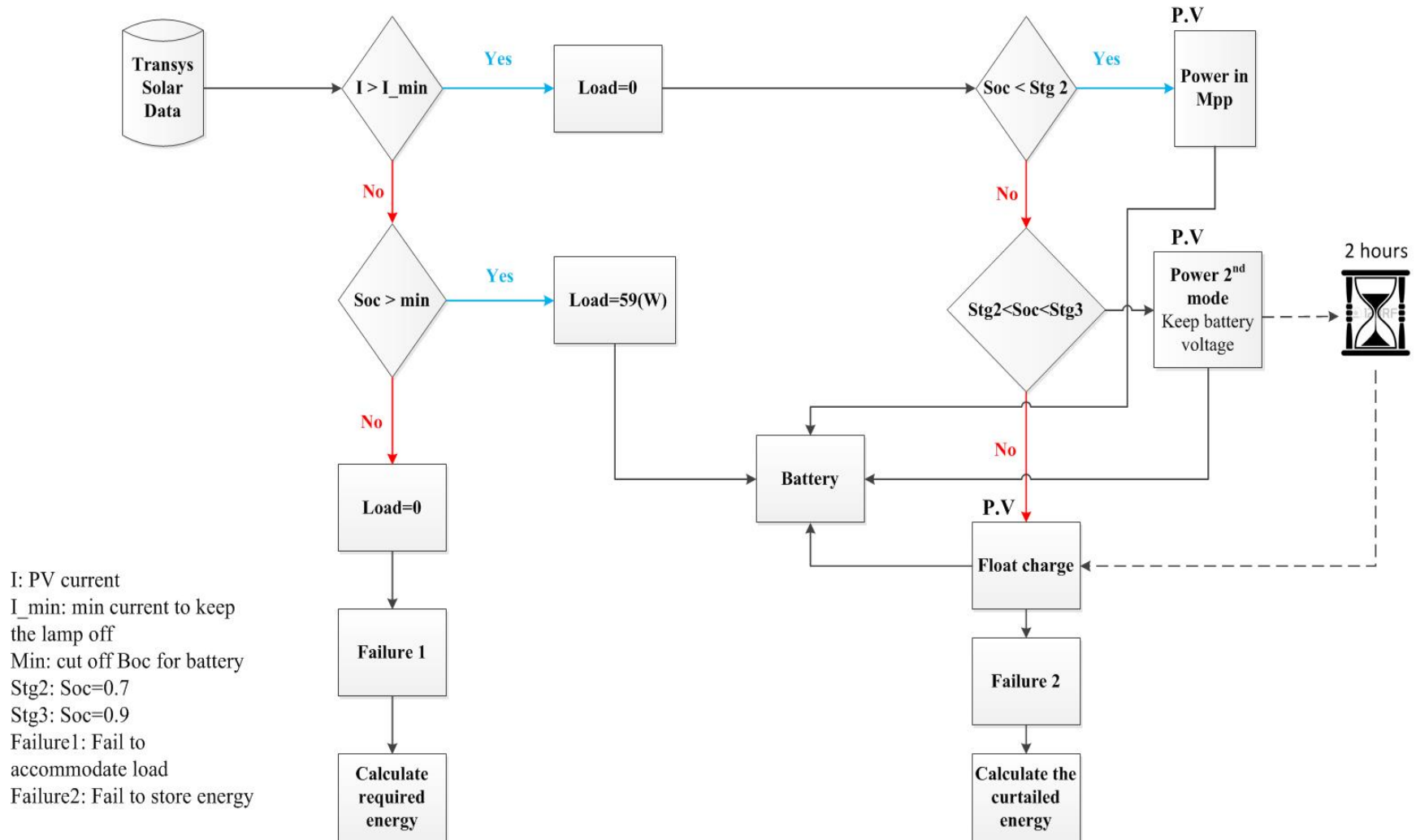


Figure 12: Simulation model flowchart

3.6 LIGHT CONTROLLER

In general, the length of a daytime varies throughout the year, and depends upon latitude. This variation is caused by the tilt of the Earth's axis of rotation with respect to Earth's elliptical orbit around the sun. Street light operating hours depends on length of day which varies continuously day to day. To increase reliability and efficiency of system it is necessary to use automatic lighting controller turns the lamp on at dusk and off at dawn. Modern charge controllers are equipped with lighting controller feature. Light controllers use different techniques to investigate where and when light is needed. Both luminance level and produced electricity (produced current) by PV panels can be considered as reliable parameters for light controlling. In TRNSYS model the controller component, simulates light controlling feature of charge controller through monitoring PV current. Light controller turns on the LED lamp when produced current by PV panels drops below 0.1 Ampere. The same strategy and current set point are applied for turning off the LED lamp when PV current reaches 0.1 Ampere.

As illustrated in Figures 13 and 14, TRNSYS 17 and MATLAB are linked together to model the typical off-grid street light. The system will be simulated at selected time step for the period of one year. At every time step each component will send to or/and receive data from its connected components. Failure occurs when stored energy in batteries is not sufficient to accommodate the lighting load during low solar-illumination hours (failure to provide) or when PV panels have to be shut down and battery capacity does not allow for more charging (i.e. too much PV or too little battery capacity).

It is worth mentioning discharge failure is more serious compared to charge failure. The charge failure is associated with inadequate battery capacity for storing produced electricity while discharge failure cause system unreliability. Optimized design could be achieved based on minimum number of failures.

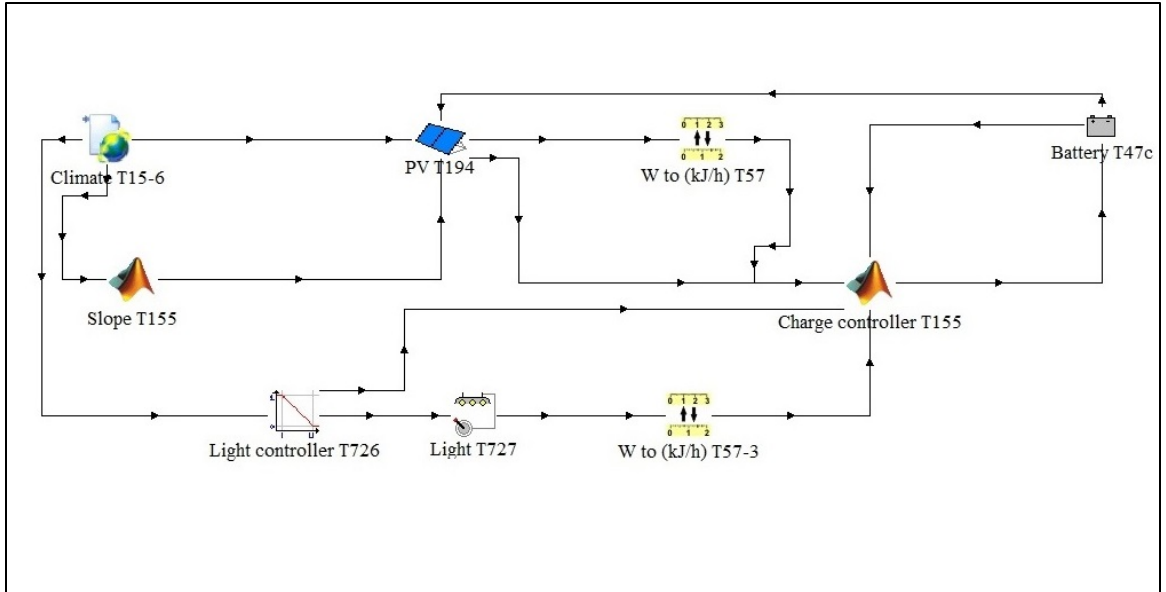


Figure 13: Simulation model (with TRNSYS battery component)

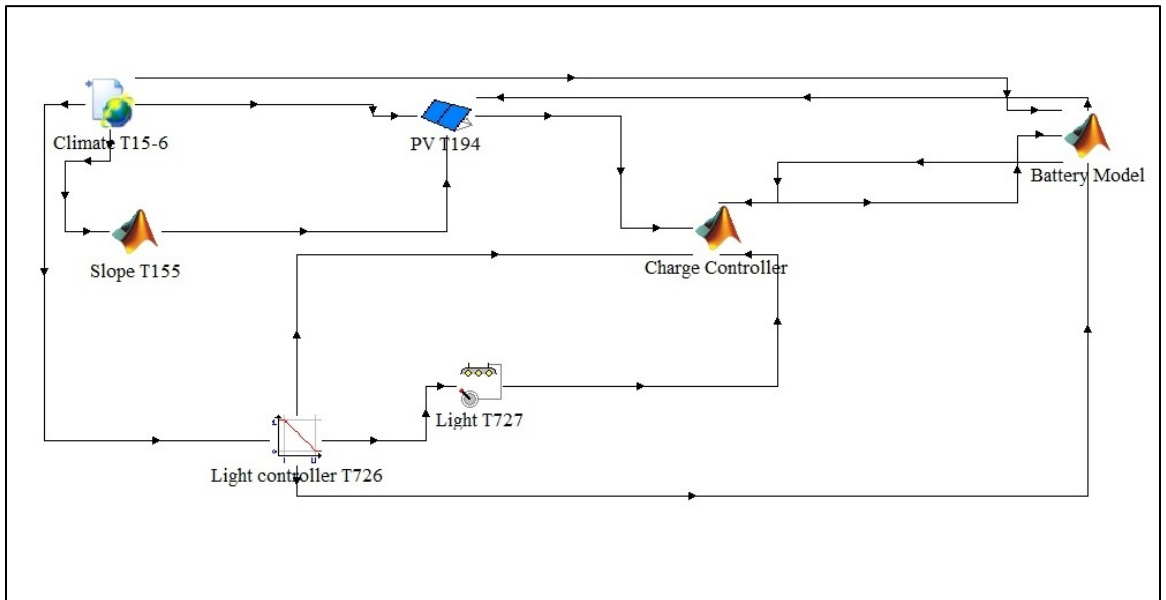
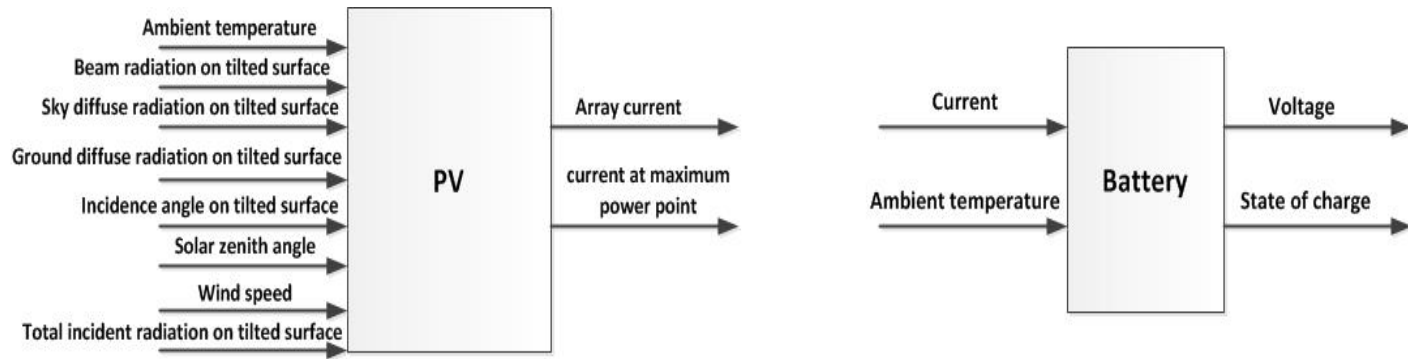


Figure 14: Simulation model (with self-coded battery component)

3.7 MODEL DESCRIPTION

Based on selected site, weather data component reads and processes data in order to calculate solar radiation properties on photovoltaic panels. A part from solar radiation data, few more parameters which are measured through Metronome database are sent to PV components. These parameters are including ambient temperature, wind velocity and solar angles such as azimuth, zenith and incidence angles. Then, according to received data photovoltaic components determines the electric performance of PV array. The model determines the current and power of the array at both specified voltage and maximum power point. Light controller component determines the LED lamp status (ON and OFF mode) by monitoring PV current and send controlling pulse to charge controller. Charge controller component discharge the battery continuously by sending negative current to the battery component until light controller turn off the LED lamp. Meanwhile battery component estimate battery voltage according to developed model which is coded based on Copetti's equation. Using a link between TRNSYS and MATLAB software in each time step battery model receive current data as input and calculate voltage and state of charge as outputs. Battery component utilizes MATLAB calculation engine in order to solve preset charge and discharge equations. Battery status like SOC and battery voltage is sent back to the charge controller at each time step during simulation. Charge controller determines charging mode (e.g. Bulk, Acceptance or Float) according to battery state of charge. System status including battery and charge controller components' performance, produced electricity and daily load are recorded and analyzed through MATLAB software. The developed model determines number of failures based on simulation results in order to achieve optimum sizing for system components.

Figure 15 shows inputs and outputs for every component which was used in simulation model.



53

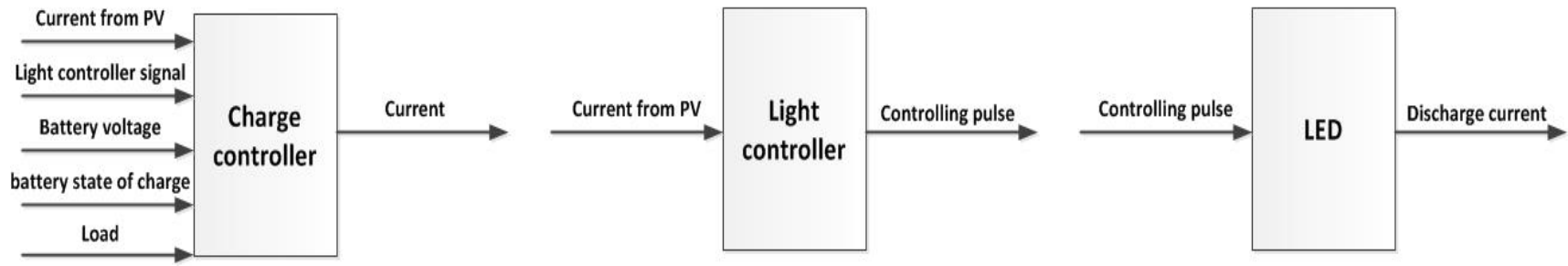


Figure 15: Simulation components' inputs and output

3.8 SIMULATION RESULTS

Simulation model results are presented in this section. For better data presenting, recorded data are transferred to Microsoft Excel file in order to use its feature for plotting required chart. Figures 16 and 17 show estimated solar irradiance during 14 to 31 May and 1 to 14 June respectively for Halifax. These days are corresponding to test period.

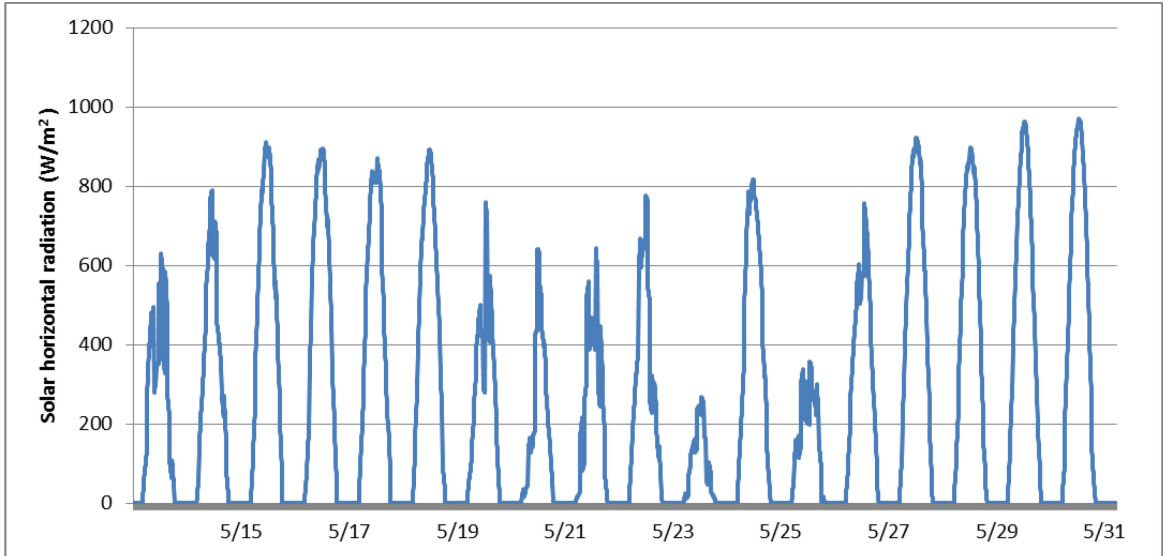


Figure 16: Halifax solar horizontal radiation (May 14-31)

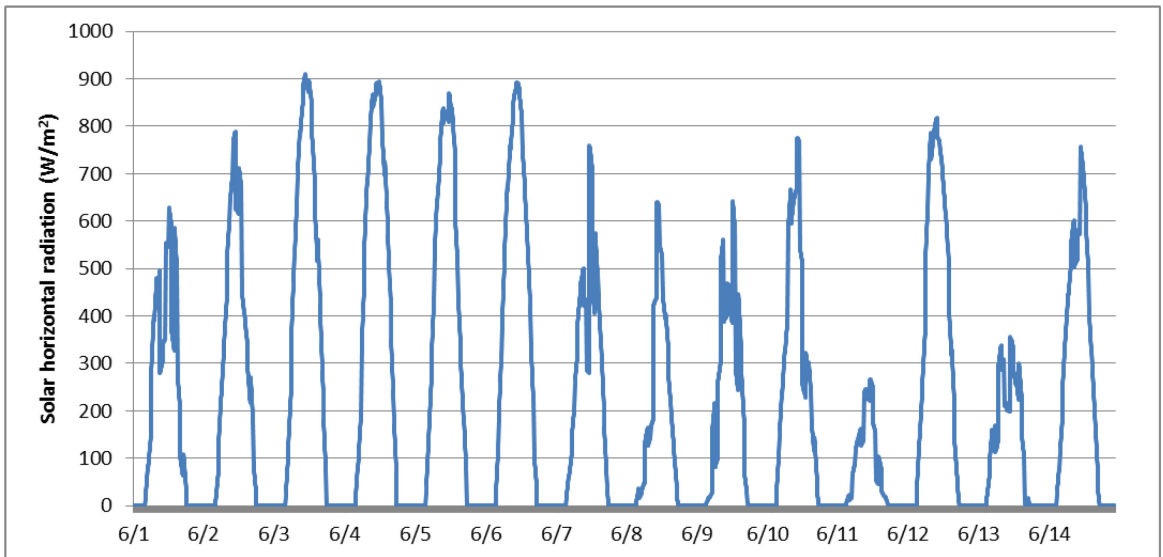


Figure 17: Halifax solar horizontal radiation (June 1-14)

3.8.1 PV

The installed PV arrays are modeled in TRNSYS through five parameters model. Estimated output voltage, current and power is presented in the Figure 18 and Figure 19.

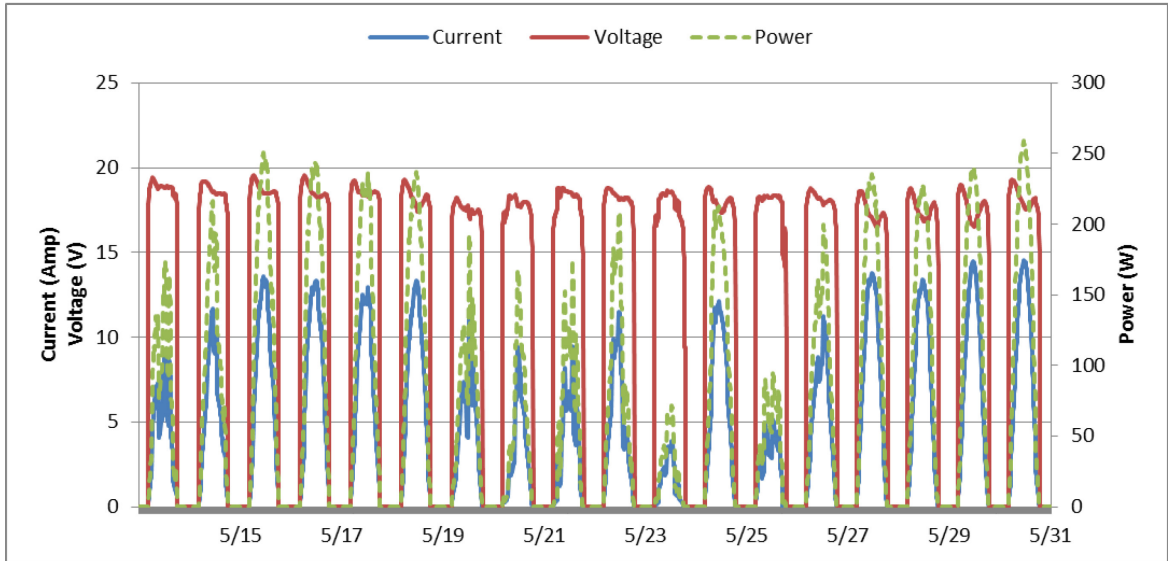


Figure 18: PV output current, voltage and power (May 14-31)

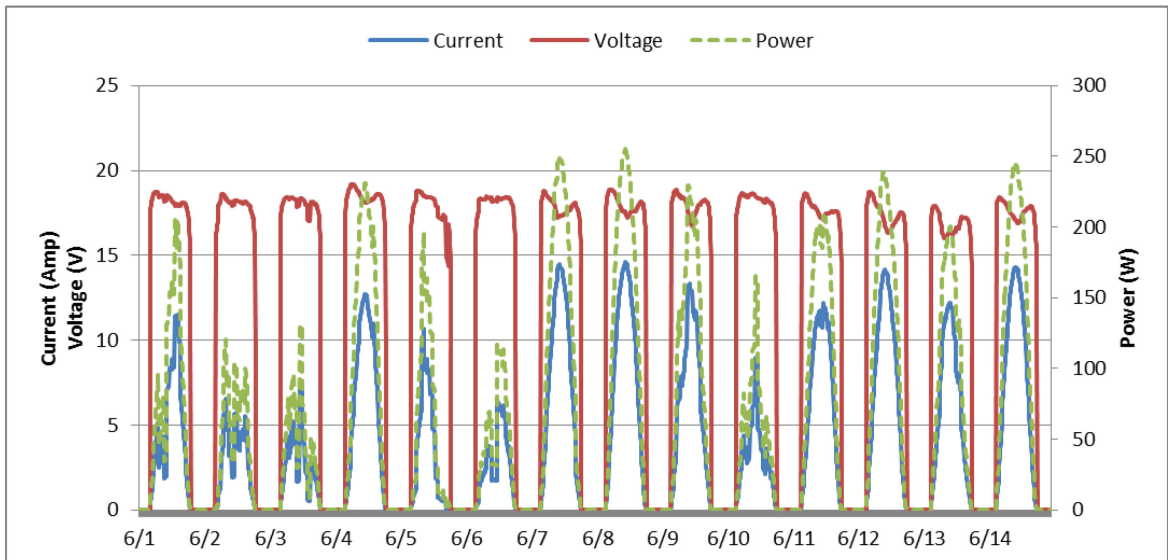


Figure 19: PV output current, voltage and power (Jun 1-14)

3.8.2 Battery

The charge controller component in TRNSYS model which is coded in MATLAB monitors the battery SOC in order to investigate charging mode. When battery SOC is less than 0.7, charge controller, charges the battery based on maximum power point mode. In second stage, charge controller keep charging the battery by switching to constant voltage mode. When battery SOC reaches to 0.9, charge controller reduce charging current to 0.2 A in order to avoid any over charging or unwanted self discharging. During discharge mode, light controller turning on the LED lamp based on PV output current. Consequently charge controller, discharge the battery according to received data. Battery current, voltage and power are presented in Figures 20 and 21.

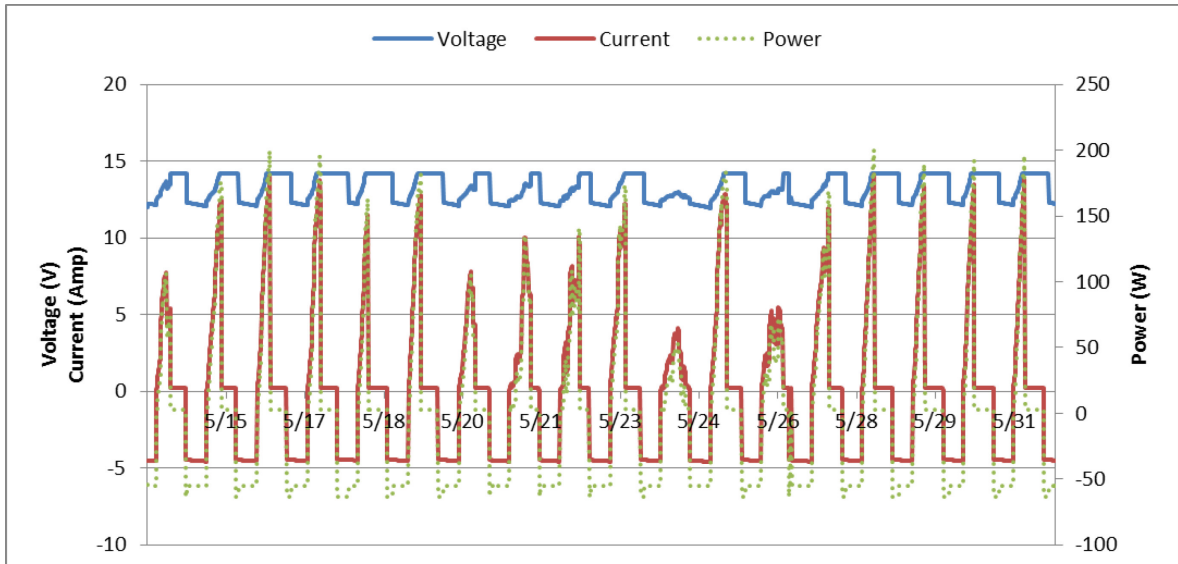


Figure 20: Battery current, voltage and power (May 14-31)

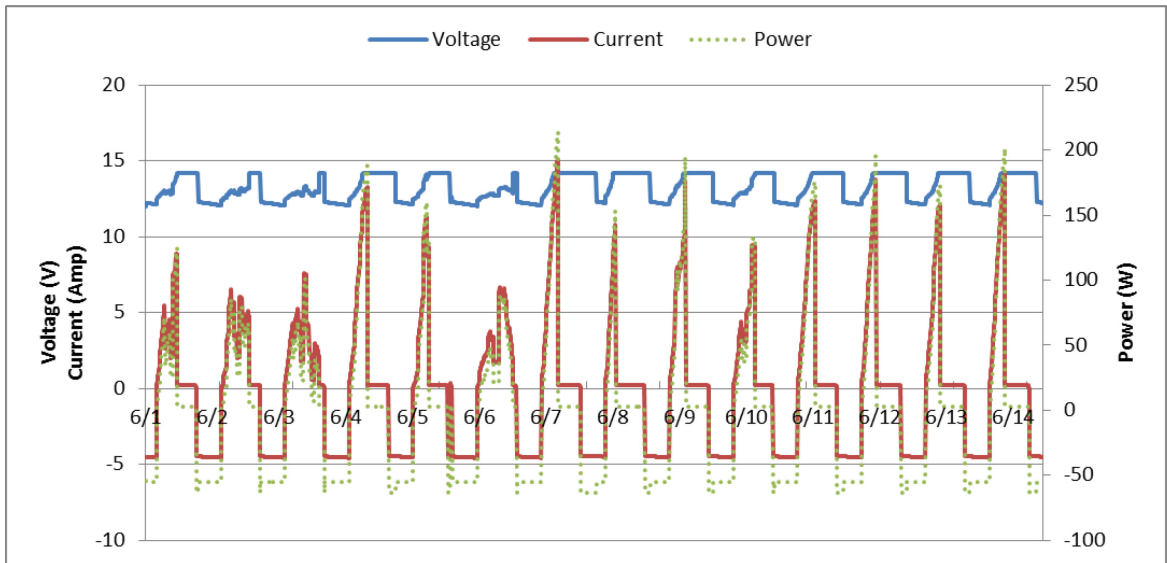


Figure 21: Battery current, voltage and power (Jun 1-14)

For better judgment about daily charging and discharging the ampere hour depletion diagram for the test period is presented in Figure 22. The overcharge is approximately 3 Ah during sunny days and cloudy days (e.g. May 25th) leads to incomplete charge.

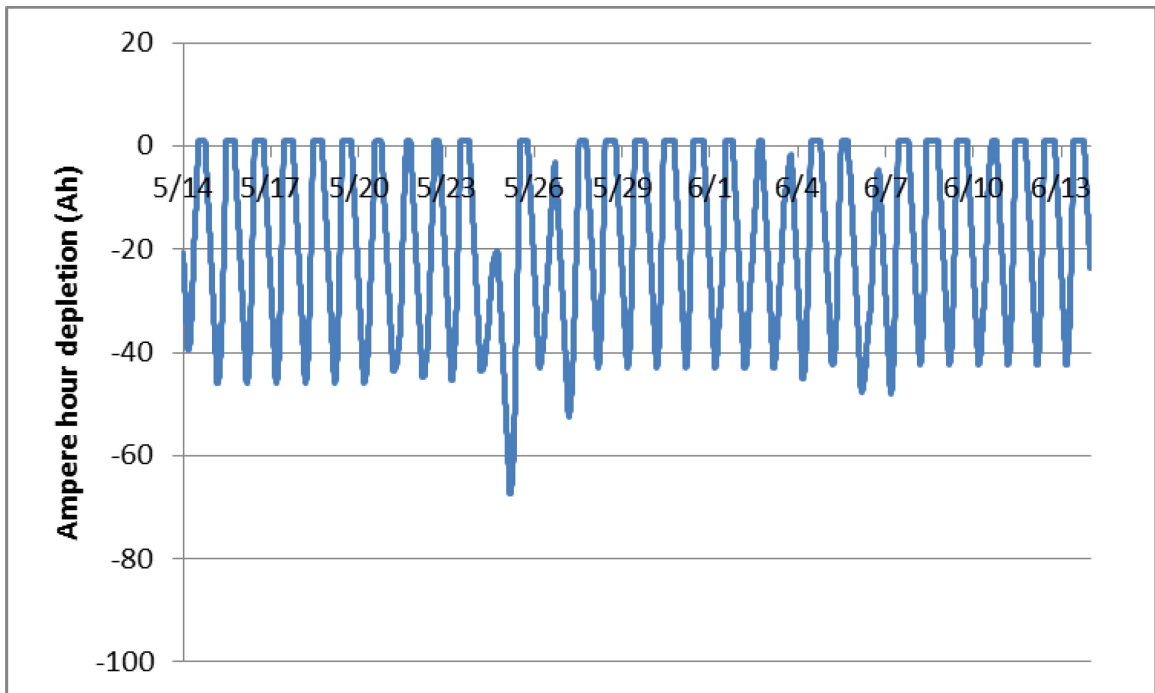


Figure 22: Ampere hour depletion (May 14-June 14)

Battery SOC is the other important parameter which should be consider for sizing the system. The model is capable of estimating monthly average and probability distribution of battery state of charge. Figure 23 shows the trend of battery SOC for the test period. Also, presented histogram in Figure 24 shows frequencies of different range of battery state of charge.

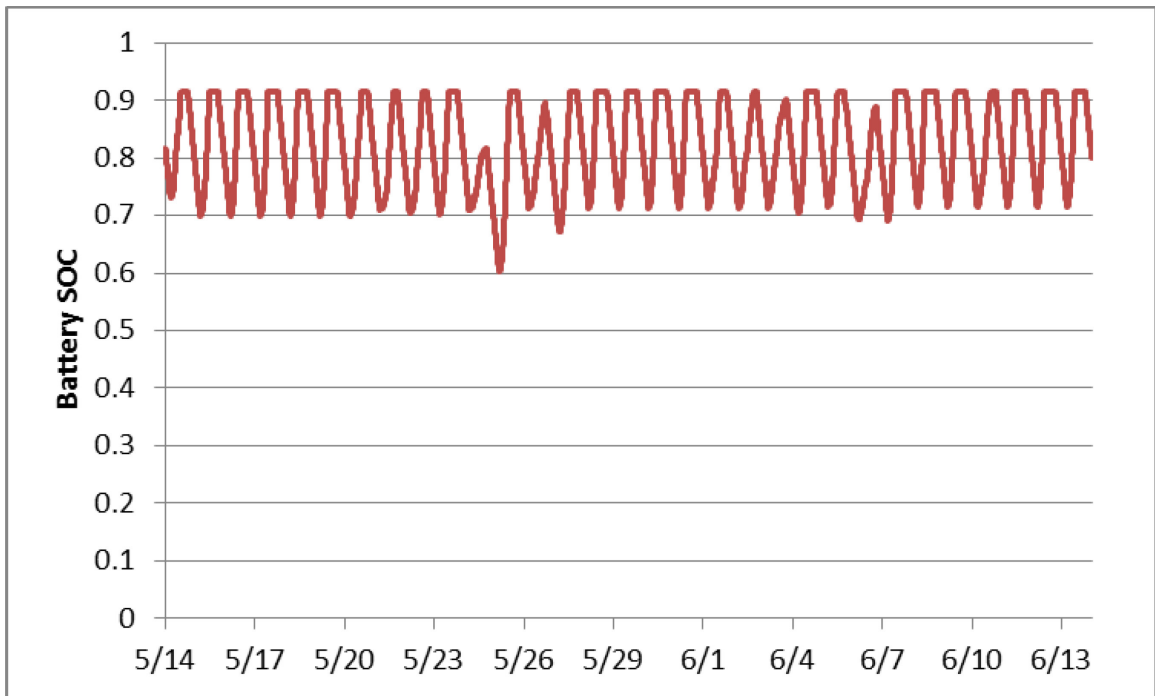


Figure 23: Battery state of charge (May 14-31)

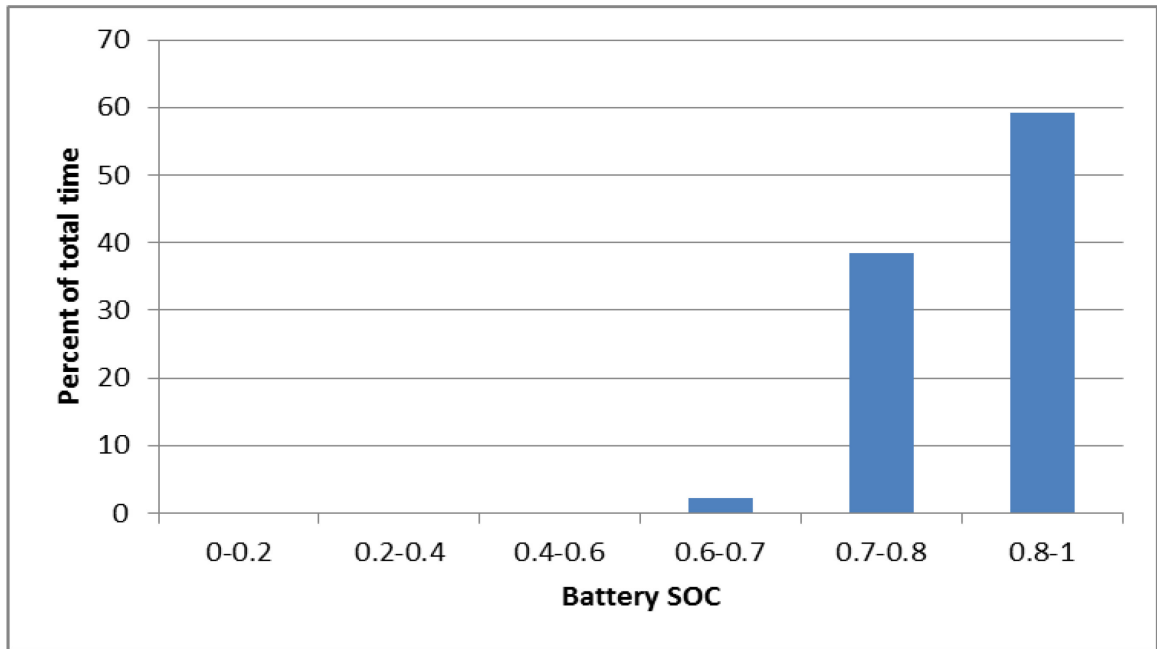


Figure 24: Probability distribution of battery state of charge (May 14-31)

Daily columbic capacity (Ah) of discharging and charging cycles almost is the most important indicator for evaluating system performance. Based on selected site, the model predicts the amount of produced and used electricity which are tabulated in the Table 11 to Table 14.

Table 11: Columbic capacity (Ah) of discharge and charge cycles (May14-22)

	14-May	15-May	16-May	17-May	18-May	19-May	20-May	21-May	22-May
Discharge (Ah)	45.09	45.05	44.75	44.93	44.93	44.94	43.48	45.76	45.14
Charge (Ah)	46.92	51.50	29.40	43.97	45.68	34.19	42.81	46.27	50.15
Columbic efficiency (%)	0.96	0.87	1.52	1.02	0.98	1.31	1.02	0.99	0.90

Table 12: Columbic capacity (Ah) of discharge and charge cycles (May23-31)

	23-May	24-May	25-May	26-May	27-May	28-May	29-May	30-May	31-May
Discharge (Ah)	44.45	45.49	42.72	48.58	42.78	42.68	42.64	42.10	42.13
Charge (Ah)	24.04	66.02	33.95	53.49	47.68	41.25	39.76	40.77	34.41
Columbic efficiency (%)	1.85	0.69	1.26	0.91	0.90	1.03	1.07	1.03	1.22

Table 13: Columbic capacity (Ah) of discharge and charge cycles (June 1-6)

	01-Jun	02-Jun	03-Jun	04-Jun	05-Jun	06-Jun
Discharge (Ah)	43.42	42.33	42.33	42.09	47.31	42.9
Charge (Ah)	41.13	41.32	53.49	31.01	44.39	54.49
Columbic efficiency (%)	1.06	1.02	0.79	1.36	1.07	0.79

Table 14: Columbic capacity (Ah) of discharge and charge cycles (June 6-12)

	07-Jun	08-Jun	09-Jun	10-Jun	11-Jun	12-Jun
Discharge (Ah)	41.38	41.53	42.19	41.73	41.58	41.57
Charge (Ah)	25.73	36.55	36.57	49.23	42.09	35.45
Columbic efficiency (%)	1.61	1.14	1.15	0.85	0.99	1.17

Daily amount of charge and discharge columbic capacity can be compared by presented bar chart in Figure 25. As can be seen the charge columbic capacity of May 24th is higher than average to make up the low charge at previous day.

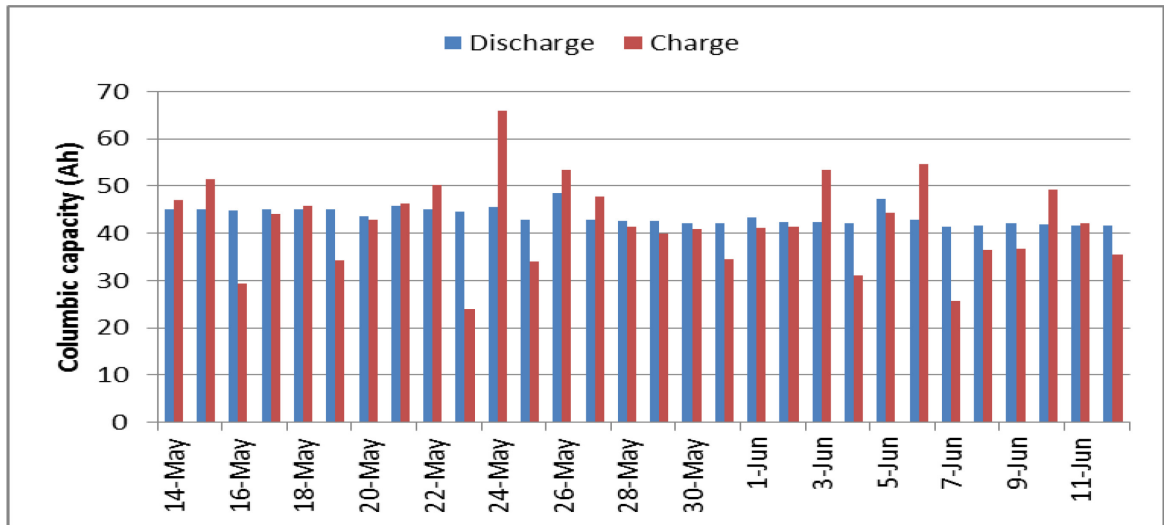


Figure 25: Columbic capacity (Ah) of discharge and charge cycles

As it can be seen, according to almost constant operation hours of LED and insignificant variation in discharge current discharge columbic capacity has not changed notable during the test period. On the other hand, charging columbic capacity is the function of various parameters such as solar irradiation, battery state of charge, wind velocity and ambient temperature and varies between 20 and 67 Ah. Apart from 6 full sunny days, charging columbic capacity is limited to 50 Ah. The detailed discussion about results is provided in chapter 5.

3.8.3 Temperature

As it mentioned in literature, ambient temperature has considerable impact on system performance. The five parameter model is capable of estimating PV array's temperature based on, ambient temperature, solar radiation and wind velocity which are available throughout TRNSYS weather database. Figures 26 and 27 show how ambient and PV temperature varies over the test period.

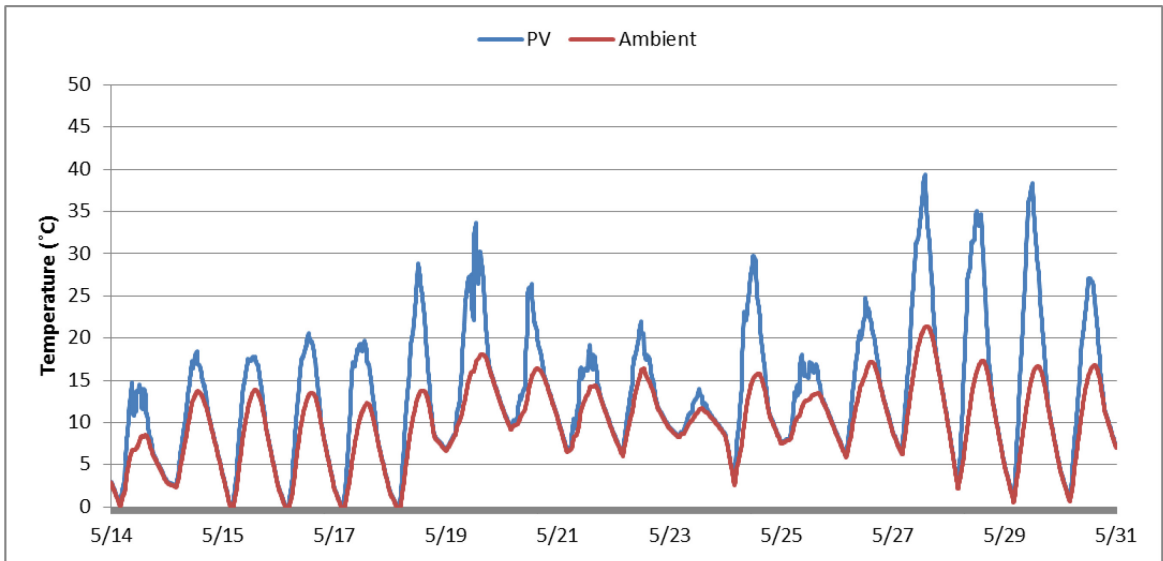


Figure 26: Ambient and PV temperature (May 14-31)

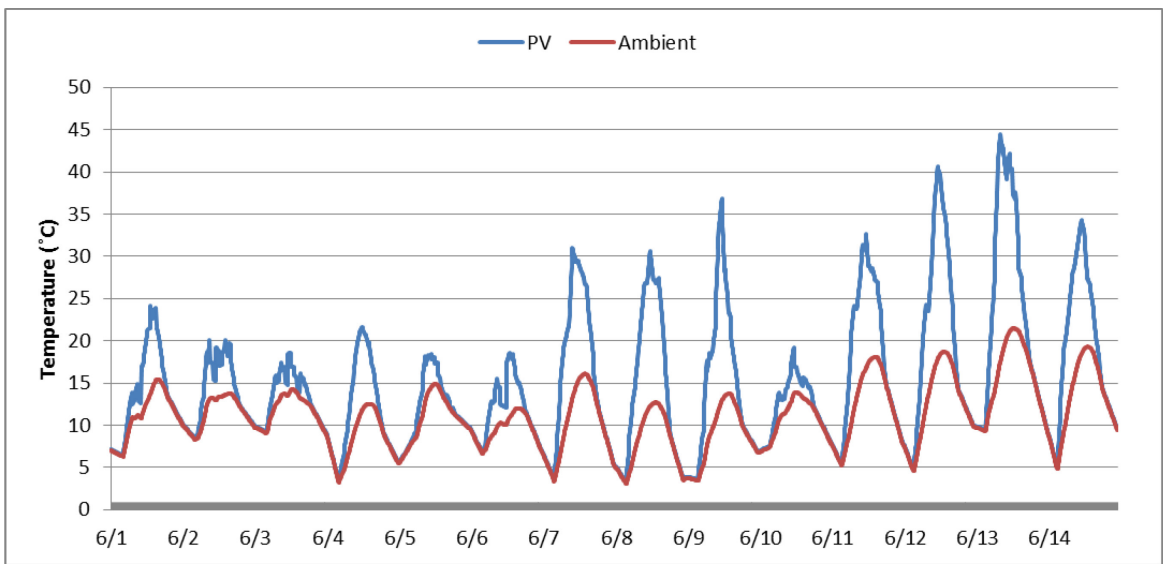


Figure 27: Ambient and PV temperature (June 1-14)

CHAPTER 4 EXPERIMENT

The test objective is to design and implement experimental setup for monitoring and recording actual data during operation of an off-grid solar street light. The recorded data would be used for system performance assessment as well as simulation validation. The list of modules has been used in experimental setup and measurement board is provided in Table 15.

Table 15: equipment list for main setup and measurement board

	Equipment	Quantity
Experiment setup	PV panel (135 W)	2
	Battery (250 Ah, 6 V)	2
	Charge controller	1
	LED lamp (55 W)	1
	Setup box	1
Measurement board	Electrical shunt	2
	Voltage divider (1:10)	2
	Data logger	1

The comprehensive explanation about each module can be found in following sections. In addition to required information about components operation, corresponding diagrams and photos are attached for more clarity.

The experimental setup was installed at Sexton Campus of Dalhousie University in Halifax, Canada which is at latitude 46.67°N , longitude 63.61°E . Installation conditions are tabulated in Table 16. It is worth mentioning that the PV panels with no labels are not related to this project. Only two upper PV panels which are labeled in Figure 28 are involved in test and provide required energy for LED lamp.

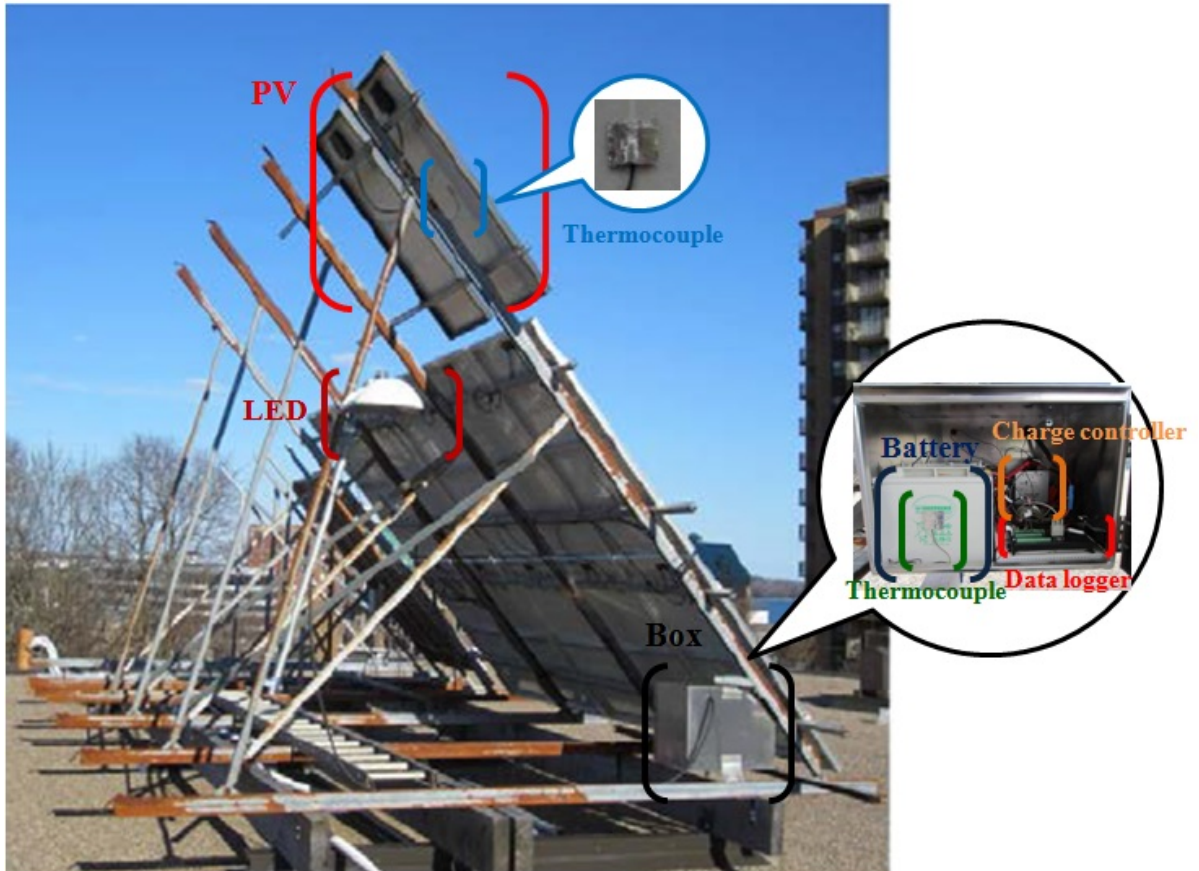


Figure 28: Experiment setup (Sexton Campus roof)

Table 16: Site features

Location	Sexton campus, Halifax, Canada
Latitude	46.67°N
Longitude	63.61°E
Elevation	145 m
PV tilt angle	45°
PV direction	South

4.1 LED LAMP

The LED lamp module, type SAT-48S [102], comprises of 48 LEDs which are placed in two separate rows on single piece die cast aluminum at 30 degree. This unique angled light engine provides maximum lumens to the target area which leads to notable rise in efficiency because of efficient light use. Fin based body configuration plays considerable role in maximum heat dissipation and prevent accumulation of debris and easily sheds water, snow and ice. As can be seen in Figure 29 the module dimensions are smaller than conventional street light while provides up to 80 % energy saving which substantially decrease life cycle cost. The detailed features of SAT-48S model are tabulated in Table 17.

Table 17: LED lamp feature

Power Consumption	55 W
Input Voltage	12 V
Mounting flange	42-60 mm
Weight	8.2 kg
Lens material	Acrylic
Power Factor	0.9
Fixture Efficiency	95 Lm/W
Fixture Output	5100 Lm
Life time	>100,000 hrs

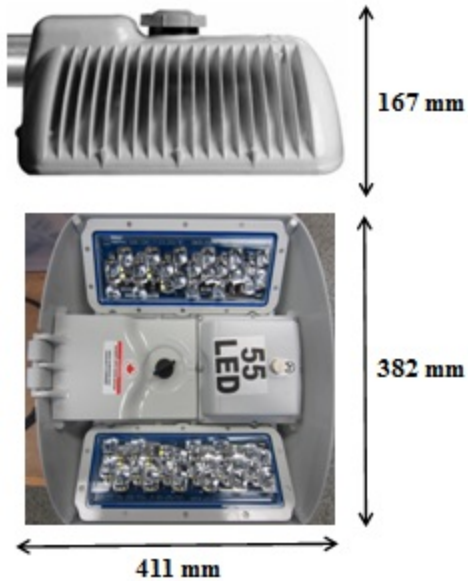


Figure 29: LED lamp dimensions

4.2 PV

The system components were sized to accommodate daily load for 55 W LED lamp during night hours. The PV array size was 135 W and two modules were connected in parallel. The detailed features of crystalline silicon type manufactured by Kyocera are tabulated in Table 18. As can be seen in Figure 30 each panel comprises of 36 cells which are placed in 9 columns and 4 rows.



Figure 30: Top and rear view of PV

Table 18: Photovoltaic panel key features

Manufacturer	Kyocera Co.
Model	KD135SX-UPU
Type	Silicone crystalline
Dimensions length/width/height	1500mm/668mm/46mm
Weight	12.5 kg
Characteristics at standard test condition (25°C 1000 W/m²)	
Power at maximum power point	135 W
Open circuit voltage	22.1 V
Short circuit current	8.37 A
Voltage at maximum power point	17.7 V
Current at maximum power point	7.63 A

4.3 BATTERY

Two sealed advanced glass mat (AGM) lead acid battery modules, type Hoppecke solar bloc 6V 250Ah (China), were connected in series mode. Each module has 3 internal cells and is rated nominal 6 V and 250 Ah. The modules were arbitrarily labelled module #1 and #2. Detailed values of size, mass, and volume based on manufacturer data sheet are given in Table 19. Battery bank is presented in Figure 31.

Table 19: Battery weight and dimensions

Mass (Kg)	Volume (L)	Dimensions L, W, H (mm)
41.4	9.1	308, 107, 275

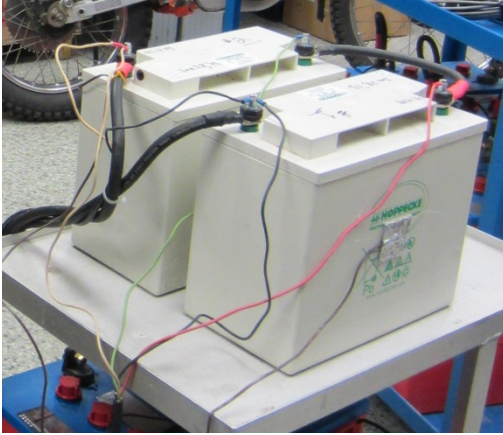


Figure 31: Battery bank connected in series (Type Hoppecke solar. bloc 6V)

4.4 CHARGE CONTROLLER

Charge controller is manufactured by Blue Sky Energy 1524 iX with three stages charging algorithms as well as maximum power point tracking and light controlling functionality.

4.4.1 Charge controller features

The charge controller is 12V or 24 V module and based on battery module and PV array capable of delivering up to 15 or 20 Amps. Regarding manufacturer data sheet SB-1524iX can surge current amount around 30% or even more compared to conventional charge controller using maximum power point tracking system. As it mentioned earlier three charging stages namely bulk, acceptance and float has been considered for charging process. This sophisticated charging algorithm has notable impact on improving battery performance and life while decreasing battery maintenance. The relation between charge modes and approximate charge level in addition to charge indicator status is illustrated in Table 20. Front plate and internal kit for charge controller is presented in Figure 32.

Table 20: Charge status indicator

Charge status indicator	Charge mode	Approximate charge level
Off	Charge off	-
Continuously on	Bulk	<70 % Full
Blinking. 1 sec on / 1 sec off	Acceptance	70 % - 95 Full
Blinking. 0.2 sec on / 1 sec off	Float	Fully charged
Rapid blinking. 0.2 sec on / 0.2 sec off	Equalize	-



Figure 32: Charge controller (Front plate and internal kit)

Open frame construction with conformal coated electronics mounted to rear of 5.3" x 5.3" (13.5cm x 13.5cm) clear anodized aluminum face plate. To avoid any harm or damage the whole system is mounted into standard (11.9cm) square electrical box. The vertical vents on the side of protector box enhance heat dissipation through natural ventilation so the charge controller should be mounted vertically.

4.4.1.1 Maximum power point tracking

MPPT is a technique to extract maximum possible power from photovoltaic array. Analyzing I-V curve is the typical way to interpret non-linear output efficiency of PV. When PV voltage is high enough to deliver constant power to the battery, because of

constant value of output power, decrease in voltage leads to boost in charge current about 30 percent. MPPT system applies appropriate resistance (load) in order to obtain maximum possible power at any environmental conditions.

4.4.1.2 Three stages of charge algorithm

During bulk charging, charge controller utilizes its maximum capacity using MPPT technique to deliver as much as charge current as possible in order to taper battery voltage to the pre-set acceptance voltage set point. When battery recovers sufficient charge and voltage rises up to threshold acceptance voltage, controller holds the battery voltage constant by reducing current as necessary during acceptance charging mode. Battery remains in acceptance mode and charging continues at a constant voltage till the battery becomes fully charged. There are two available options for avoiding over charging and determining fully charged battery.

- Setting time period for acceptance charge mode
- Set the threshold current for acceptance charging (Battery current reduce continuously during acceptance charging)

SB1524iX has capability to maintain the battery in fully charged states without water lost by applying float voltage when battery draws approximately 0.1 to 0.2 amps per each 100 Ah of battery capacity. Based on battery type, charge controller could be set for two stages charging by eliminating the floating stage.

4.4.1.3 Load operation on/off

Load operation can be controlled based on produced current by PV panels, when charge currents drops below certain amount, battery discharge start in order to accommodate required load and continue until battery voltage hit the pre-set threshold voltage set point. The load controller acts as high side switch from battery positive. To avoid probable errors in determining on/off condition over mentioned situations should be remain valid for 20 seconds.

4.4.1.4 Lighting control

The charge controller is programmed in order to control lighting automatically based on pre-set values. In Display menu post-dusk and pre-dawn timers can be set between 0 and

20 hours according to day length and required time period for lighting. Dusk or night time begins when the amount of produced electricity by PV arrays becomes negligible and insufficient to keep charge controller ON when current drops below 50 mA. In simulation model the solar radiation level corresponding to these current set points were calculated and set on light controller module. Day time or dawn starts with turning on the charge controller which occurs when PV current rises to 100 mA at battery voltage. In the case of full dusk to dawn lighting the post-dusk timer should be set to 20 hours. One of the unique features of the charge controller is the ability to daily update of dawn time by detecting night duration.

4.4.1.5 Temperature compensation

Battery temperature has impact on required set points voltage for batteries which are adjusted for reference temperature (25°C). To solve this problem temperature compensation of charge voltage is considered in order to enhance battery performance and minimize maintenance. Temperature sensor was connected to negative terminal of the battery in order to measure battery temperature and applies compensation factor of -5mV/ °C/cell that is suitable for most lead acid batteries.

4.4.2 Charge controller test

It was necessary to evaluate charge controller functionality before starting the real test in order to ensure controller operates based on anticipated charging modes and pre-set voltage set points. Regarding the Blue Sky manual for maximum heat transfer through natural convection it is necessary to mount the controller vertically to avoid over heat on the system. As it is shown in Figure 33 the controller mounted on prepared stand to stay in vertical position during experiment. An electrical power supply (Instek PSH-3620A) acts as PV module in order to control the delivering voltage/current to the charge controller. The output voltage and current was set to 25 V and 5 A respectively. As can be seen in Figure 33 two 50 Amp/50 mV shunts are necessary to monitor input/output current/voltage simultaneously through the four channels scope meter (Fluke Scope Meter 190 series II). After testing charge controller for 5 complete charge and full

discharged cycles it was investigated that charge controller works correctly based on adjusted voltage setpoints.

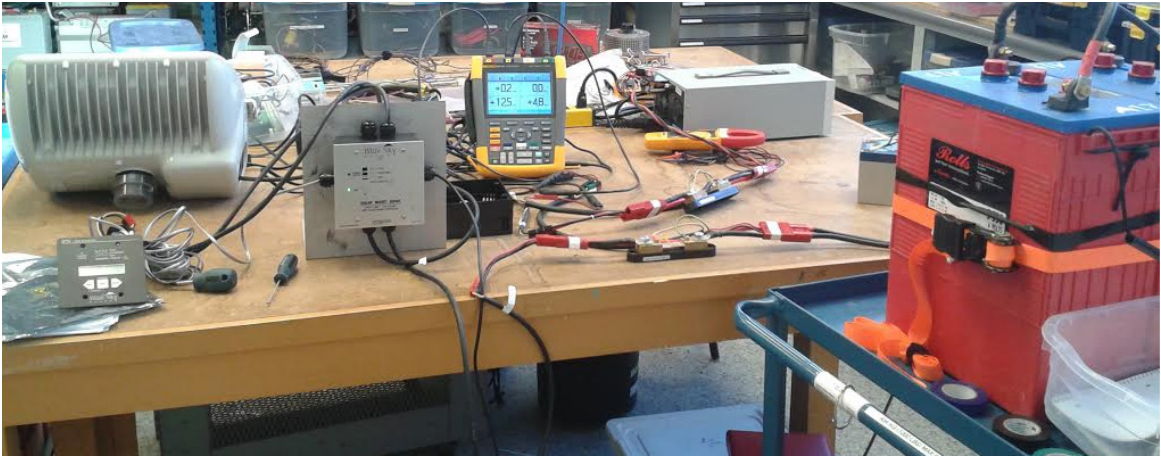


Figure 33: Pre-installation setup for testing charge controller operation

As mentioned earlier, SB1524iX can be programmed based on features of integrated battery components in order to improve system operation. Adjusting threshold voltage requires IPN-Pro Remote module which is used to setup voltage set point. The ProRemote not only used to adjust controller but also provides complete full featured battery monitoring system by measuring remained capacity of battery through voltage, net current and battery temperature.

4.4.3 IPN ProRemote

IPN ProRemote provides full featured remote monitoring of charge controller and battery components in single device. Required power and data for IPN ProRemote would be supplied through connecting to charge controller IPN DISPLAY connector. Standard 4-pin conductor RJ-11 voice telephone cable is the most appropriate option which can be used for data transferring between charge controller and IPN modules. Front LCD and three function keys provides enhanced setup monitoring by Accessing to different menus and adjusting charge controller setup parameters. Organized IPN ProRemote menus provide fast and easy access to certain type of information by entering the related menu. General information in associate with setup status which are typically of interest to the casual users such as battery voltage, net battery current and remained battery capacity are

gathered in the top menu. More technical information such as Battery charge parameters and load timer are available in the Advanced Display menu. Similar to charge controller, front panel LED indicator shows charge status by switching between solid, blinking and off modes. The various modes of charge status indicator are tabulated in Table 20. As mentioned earlier the various adjustable parameters of charge controller are categorized in four different menus:

- Top
- Advanced Display
- Setup
- Battery charge parameters



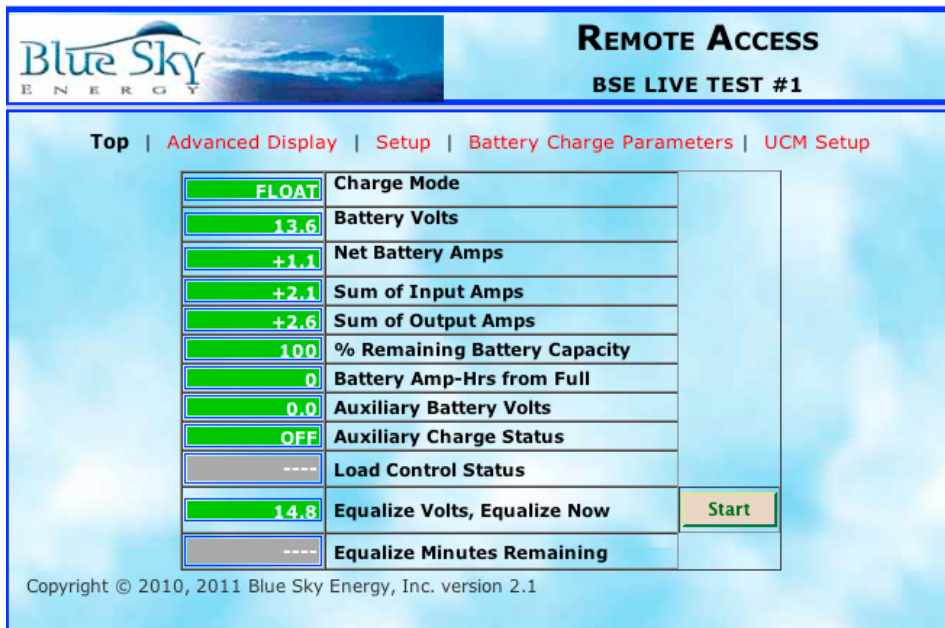
Figure 34: IPN Pro-Remote

Universal communication module is designed for programming and adjusting charge controller remotely through internet network. Apart from setting charge controller functions, UCM (universal communication module) is capable of monitoring and recording the system information (PV array and batteries status) and acts as data logger. Data transferring between UCM and charge controller required standard 4-pin telephone cable which also used in order to provide required power for UCM operation through charge controller. The universal communication module provides full featured communication bridge or gateway between charge controller and external set-up. This communication allows easy access to controller set-up parameters and recorded data. Ethernet connectivity includes a built in HTTP website server set-up parameters and

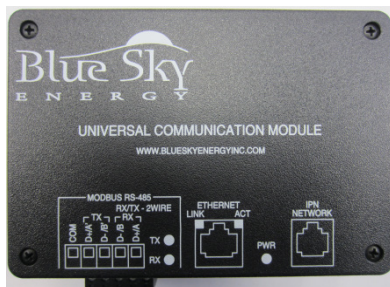
recorded data could be viewed or modified either locally or globally. Based on pre-set interval time, recorded data could be uploaded to remote server periodically as downloadable Microsoft Excel file. This file transferring required setting up an FTP server to host and store forwarded file.

As mentioned earlier, UCM built in website server provide easy access to all data and set-up parameters for both charge controller and UCM. Based on system application two options are available for connecting to UCM, direct computer connection and router based connection. The recorded data is presented as CSV in spreadsheet such as Excel file where organized into rows and columns. The information related to each datalog record is provided in the single row which contains variety of information that are presented in columns. It is necessary to consider that the internal memory has capacity to log up to 127 complete records. The detailed description of data log file can be found in

Figure 35. By accessing to prospective UCM HTTP website the following page appears which allows the users to select between different tabs including Top, Advanced Display, Setup, Battery Charge Parameters and UCM setup.



(a)



(b)

Figure 35: UCM device and website homepage (Start page)

As illustrated in Figure 35, all required parameters for adjusting the charge controller are organized through separate menus and comprehensive explanation for each parameter is provided in the IPN ProRemote section. UCM setup webpage has few sections for adjusting the location-name, password and prospective setting for FTP data file transferring and communicating.

Blue Sky ENERGY **REMOTE ACCESS**
MAC: 00 04 A3 35 FF A7

Top | Advanced Display | Setup | Battery Charge Parameters | **UCM Setup** |

UCM:

.....	UCM Password (14 max)	Set
BSE LIVE TEST #1	Location Name (20 max)	Set

FTP Data File Transfer:

ftp.website.com	FTP Server Address (29 max)	Set
ucm	User Name (14 max)	Set
.....	Password (14 max)	Set
0.1	Hours between uploads	Set

Increment file name
 Use same file name

Communications:

1	1	1	1	IPv4 IP Address	Set
255	255	255	0	Subnet Mask	Set
1	1	1	1	Gateway IP Address	Set

Copyright © 2010, 2011 Blue Sky Energy

UCM name and password should be set in this section which is used for logging to the device.

These parts should be filled based on prepared FTP server for periodic data uploading. The interval time shows hours between uploads.

Based on MAC ID of the UCM the allocated IP and router IP should be written in IPv4 IP and Gateway IP Address-bar.

Figure 36: UCM setup page for adjusting system communications

As can be seen in Figure 37 the recorded data includes crucial values which are required for accurate monitoring and interpreting the system status during operation are tabulated. In each data log record, the amount of time for acceptance and float charge mode is shown separately which can be used to evaluate the accuracy of TRNSYS model in terms of predicting charge modes. Unfortunately monitoring and recording the net discharge current depends on presence of ProRemote, and without ProRemote, UCM does not have ability to measure battery current.

SPREADSHEET COLUMN	COLUMN HEADING	DESCRIPTION / COMMENTS
A		Datalog record number, older records below newer records
B	MaxVbat	Maximum battery volts
C	MinVbat	Minimum battery volts
D	AccpTime	Total minutes in Acceptance charge mode
E	FloatTime	Total minutes in Float charge mode
F	MaxDscha	Maximum net battery discharge amps (negative) -- from IPN-ProRemote
G	MaxDschaAH	Maximum discharge amp-hours from full (negative) -- from IPN-ProRemote
H	MinDschaAH	Minimum discharge amp-hours from full (negative) -- from IPN-ProRemote
I	MaxTotChgA	Maximum total PV charge amps -- sum of all charge controllers on IPN network
J	RecdTime	Actual time period of this record in hours
K	#0MaxInV	Maximum PV volts from Master charge controller -- IPN address 0
L	#0MaxOutA	Maximum output amps from Master charge controller -- IPN address 0
M	#0ChgAH	Total output amp-hours from Master charge controller -- IPN address 0
N	#1MaxInV	Same charge controller voltage, current and amp-hour data as columns K, L & M above, but for charge controller Slave address #1. Additional columns to the right contain the same data for charge controller address #2 - #7.
O	#1MaxOutA	
P	#1ChgAH	

Figure 37: Data log file descriptions

However these data shows system status by recording maximum and minimum values of various parameters during preset interval time, FTP file forwarding feature of UCM provides instant data (collected value at the time the file was sent).

Recorded data could be uploaded to external FTP server at pre-set interval time for more precise system monitoring. To use aforementioned feature, the section related to FTP data transfer should be set up by providing required information about host IP address, username and password. The following sample shows FTP data log file contents and descriptions.

SPREADSHEET COLUMN	COLUMN HEADING	DESCRIPTION / COMMENTS
A	ChgMode	5 possible charge modes — <i>Off, Bulk, Acceptance, Float or Equalize</i>
B	BatVolts	Battery voltage
C	BatAmps	Net battery current in amps, positive is charging — from IPN-ProRemote
D	BatDschAH	Battery discharge amp-hours from full (negative) — from IPN-ProRemote
E	BatTemp	Battery Temperature in °C, or <i>Bad or No Sensor</i> if faulty or not installed
F	AuxOut	State of the Auxiliary output, <i>ON or OFF</i>
G	AuxVolts	Auxiliary output voltage, operates in both <i>Aux. Battery Charge and Load Control</i> modes
H	TotChgA	Maximum total PV charge amps — sum of all charge controllers on IPN network
I	#0InVolts	PV input voltage from Master charge controller — IPN address 0
J	#0InAmps	PV input amps from Master charge controller — IPN address 0
K	#0OutAmps	PV output amps from Master charge controller — IPN address 0
L	#1InVolts	Same charge controller voltage and current data as columns I, J & K above, but for charge controller Slave address #1. Additional data and columns to the right contain the same data for charge controller address #2 - #7.
M	#1InAmps	
N	#1OutAmps	

Figure 38: FTP file data description

4.5 DATA LOGGER

Data logging is considered as crucial part of each experiment which requires precise sensors as well as reliable data retrieval methods. Due to the fact that experimental setup and measurement equipment were installed on the roof and the whole system was working under real operating conditions, the data logger should be water resistance and rugged enough for probable extreme conditions, however water resistance stainless steel box was used to protect batteries and sensitive electrical equipment. Since the battery was the only power source for the system, it was required to select data logger with optimized power consumption to decrease impacts on battery performance (e.g. overall energy and voltage) during test period.

Based on inherent characteristic of parameters which should be measured (e.g. voltage, current and temperature), testing strategy and operating conditions the CR-1000 CAMPBELL SCIENTIFIC was selected as data acquisition system. CR-1000 has capability to record data accurately and can be used in a broad range of measurements.

The measurement error of the CR1000 is $\pm 0.06\%$ of the reading which corresponds to 0.015 V when measuring the PV voltage during peak times at sunny days (24V). Based on prepared specification sheet by Campbell scientific, CR-1000 is capable of measuring voltage to within $\pm 0.06\%$ error in the range of 0 to 40 °C. The input voltage range is ± 5 V DC consequently due to approximate range of PV and battery voltage (up to 15 and 20 respectively) it is necessary to use voltage divider in order to bring sensors with high output voltages into the data logger's common mode range. As it mentioned earlier system battery supply power for data logger therefore it is necessary to ensure the impacts on battery performance are negligible. According to provided data sheet, the range of drained current by data logger varies with respect to module status (active or sleep modes) and availability of RS-232 communication. Data logger energy consumption in various modes are presented in Table 21.

Table 21: Data logger energy consumption

Data logger status/communication mode	Typical Drain Current (mA)
Sleeping mode	~ 0.6
Active mode (without RS-232 communication)	1 – 16
Active mode (with RS-232 Communication-monitoring recorded data)	17–28

For more accurate results, the data logger was programmed for real test condition (4 differential voltage and 4 T type thermocouples) and the amount of drained current was measured for 5 minutes. The amount of current extracted by Data logger depends on the pre-set interval time for scanning and recording data which varies between 0.6 mA to 21mA; respect to 6 seconds interval, drained current remained constant at 0.6 mA for 5 seconds and just for 1 seconds increased up to 15 mA; so the required Ah for test duration is calculated according to:

$$\text{Average current per cycle} = = \frac{5 \text{ Sec} \times 0.6 \text{ mA} + 1 \text{ Sec} \times 15 \text{ mA}}{6} = 3 \text{ mA}$$

$$\text{Daily consumption} = = 3 \text{ mA} \times 24 \text{ h} = 72 \text{ mAh}$$

Test period (30 days) consumption = $30 \times 72 \text{ mAh} = 2.16 \text{ Ah}$

Compared to battery capacity (250 Ah) and daily charge/discharge average (45 Ah), the consumed amount of energy was negligible and did not have considerable effect on battery performance. Since the charge controller open circuit when battery voltage drops below adjusted voltage set point (10.8 V) in order to protect battery against over discharging; it was necessary to wire data logger in parallel with battery to avoid shut down and data loss during test.

The most important factor for accurate data interpretation depends on selecting appropriate interval time for scanning sensors and recording achieved data. By considering type and changing speed of measured parameters, 6 seconds interval seems adequate for precise system analyzing. Increasing sampling rate results in generating too much data which decrease the duration of periods the data logger's memory can store new values without overwriting former data. Based on 4MB capacity of data logger internal memory and size of daily data, recorded values should be transferred from CR-1000 to database once every three days to ensure integrity of recorded data and avoid any corruption. CR-1000 like most of data acquisition systems provide both a single ended and a differential input connection and has capability to handle 16 single ended or 8 differential individually inputs. A single ended input measures the voltage between the input channel high and low level ground common to all the inputs while a differential input, measures the voltage between two individual inputs. However using single ended configuration, allows for the DAQ system to support more channels it is susceptible to noise from the common ground connection. Differential inputs provide more stable reading and it is recommended to use whenever noise is generally a problem. It is recommended to use differential inputs for particular sensors such as thermocouple to avoid any noise due to their very small signals. Due to accuracy of differential channel compared to single ended, and number of parameters which should be measured, differential input configuration were used for measuring required values. Generated voltage and current by solar panel through photovoltaic effect were measured to investigate the solar potential of the site. A 50 amperes shunt was used in couple with data logger to record voltage and current of PV before entering to the charge controller. Another 50 amperes shunt was coupled with data logger in order to measure and log

battery voltage and current during charging and discharging process. Apart from battery performance, accuracy of lighting controller was investigated through battery current data. In addition to afore mentioned parameters, temperature plays crucial role in efficiency and system performance. Ambient temperature as well as battery, box and PV temperature was measured and logged through 4 T-type thermocouples. Information about wiring diagram and each channel specification were tabulate in the following diagram. Data logger unit is presented in Figure 39.

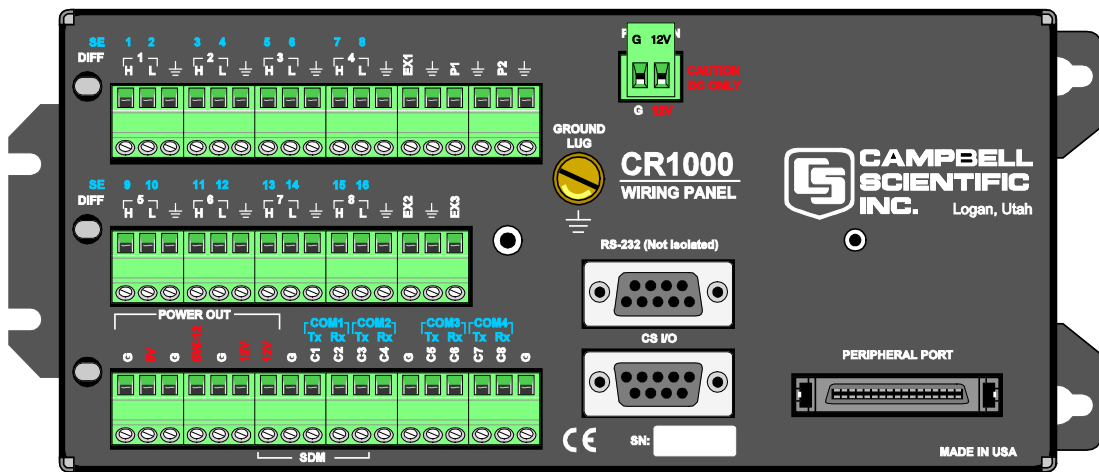



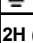




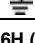
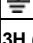




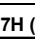





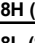
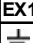



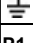
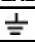
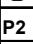
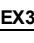




Figure 39: Data logger [103]

Table 22: Data logger channel wiring

Battery Positive +		12V	PV-Voltage +		1H (SE1)
Battery Negative -		G	PV-Voltage -		1L (SE2)
					
Battery Temperature-blue		5H (SE9)	PV-Current +		2H (SE3)
Battery Temperature-red		5L (SE10)	PV-Current -		2L (SE4)
					
Ambient Temperature-blue		6H (SE11)	Battery-voltage +		3H (SE5)
Ambient Temperature-red		6L (SE12)	Battery-voltage -		3L (SE6)
					
Box Temperature-blue		7H (SE13)	Battery-Current +		4H (SE7)
Box Temperature-red		7L (SE14)	Battery-Current -		4L (SE8)
					
PV Temperature-blue		8H (SE15)	NA		EX1
PV Temperature-red		8L (SE16)			
					
NA		EX2			P1
					
NA		EX3	NA		P2
					

It is worth mentioning that the data logger dimensions ((L, W, H) 25.2 x 10.2 x 7.1 cm) and weight (1 kg) were appropriate according to measurement board area. Aforementioned features made this module perfectly compatible with designed measuring system.

4.6 VOLTAGE DIVIDER

The 5 V maximum input limit on the analogue input channels on the CR1000 made a voltage divider necessary to lower the measurements which ranged from 0 volts to 24+ volts down to a 0-5 V range. Two resistors configuration is the most common type of voltage divider to turn high voltage into fraction of input voltage.

As can be seen in Figure 40, voltage divider has simple circuit and output voltage can be calculated based on Equation (31).

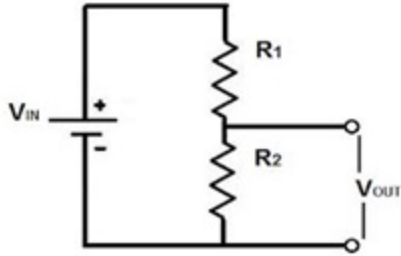


Figure 40: Voltage divider equivalent circuit

$$V_{out} = V_{in} \times \frac{R_2}{R_1 + R_2} \quad (31)$$

For safety reason and avoid any failure for data logger, two resistors were selected in order to satisfy ratio of 10 to 1 between output and input voltage. The resistors value, theoretical and experimental ratio are tabulated in Table 23. It is necessary to calculate realistic ratio through electrical measurement equipment such as power supplier and voltmeter to make the experiment results precise and accurate. Difference between calculated and experimental ratio is the result of in accuracy on resistor values.

Table 23: Voltage divider specification

R_1	680 k Ω
R_2	82 k Ω
V_2/V_1 (Theoretical)	0.107
V_2/V_1 (Experimental)	0.104

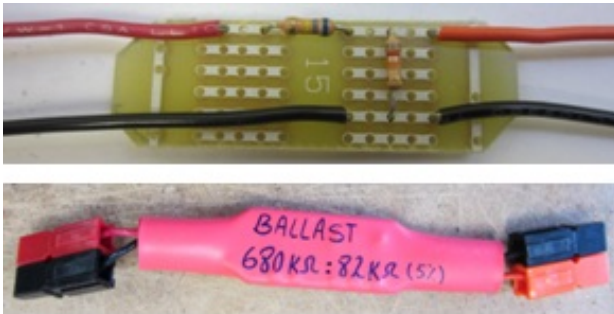


Figure 41: Voltage divider

4.7 ELECTRIC SHUNT

Due to maximum 5 mA limit on CR-1000 analog input channels, it is necessary to use appropriate shunt in order to turn high range of amperes to acceptable values for data logger. Shunt circuit comprises of accurate resistor which is placed in series with the load so all current to be measured will flow through it. The voltage drop is proportional to the current value and based on shunt resistance, output voltage can be scaled to show the amount of current. CR-1000 has feature which allows users to apply ratio or offset for each input channel. Based on shunts ratio, multiplier equal to 0.1 was selected for channels 2 and 4 which show PV and battery current respectively. As can be seen in Figure 42, two 50 Amp shunts (1 mV/A) were used in the experiment setup.

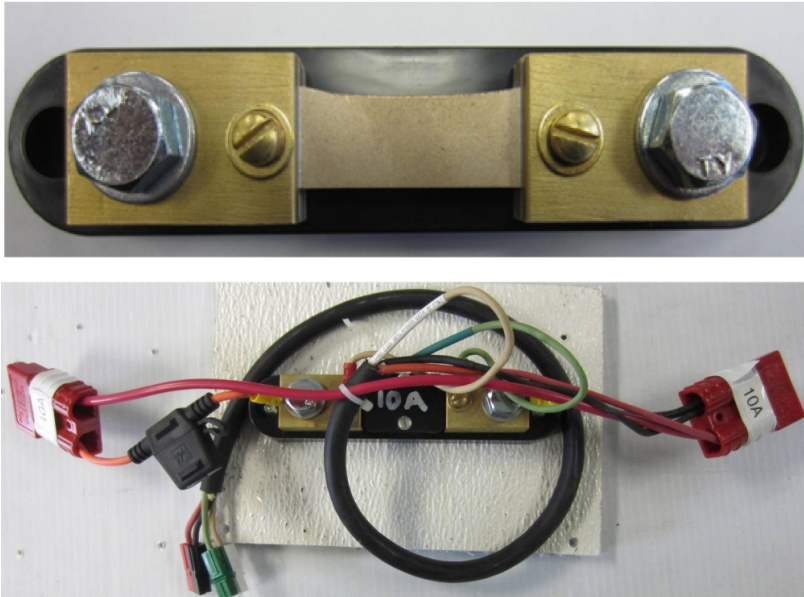


Figure 42: Electrical shunt for measuring voltage and current

4.8 BATTERY BOX

Appropriate enclosure can provide safe and reliable protection for battery bank and charge controller against rain, Sleet and snow. Based on system design various mounting options are available including underground and above ground. As it is illustrated in Figure 43 the enclosure which was used in this experiment capable of holding one up to four batteries and charge controller. According to considered design the battery bank comprised of two batteries which were placed on left side of box with adequate gap

between each module and around perimeter of batteries. The measurement board containing shunts, data logger and charge controller that was designed based on box dimensions, placed in vacant space on the right side of box. Body and doors fabricated from 16 gauge carbon steel and padlockable draw latch is made of carbon steel with a stainless steel hinge pin. Inside and outside surfaces are covered by ANSI-61 gray polyester powder over phosphatization process. Thanks to available external mounting plates on top and bottom of box, the enclosure was installed on the stack through two horizontal struts. Installed PV arrays acts as shelter and protect box against direct solar radiation, rain and snow. Two cable glands were installed on back side panel of the box to keep thermocouples and power cable. Cable glands closely hug wires and cable in order to securely seal available holes and provide watertight connector.

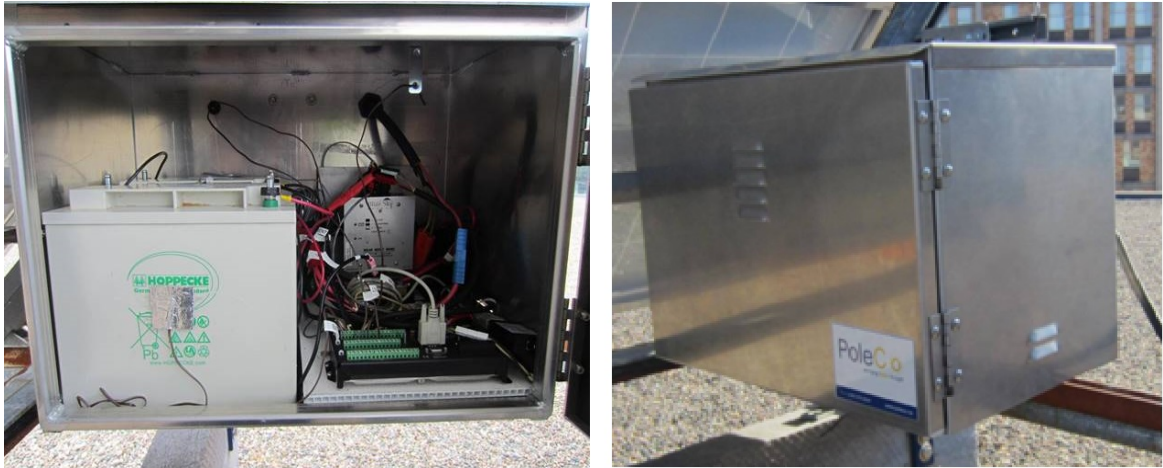


Figure 43: Battery box

4.9 THERMOCOUPLES

The simulation model is capable of predicting ambient temperature and PV arrays during selected periods. It is necessary to evaluate model accuracy by comparing actual and predicted data over measuring these two temperatures through thermocouples. In addition to aforementioned temperatures two thermocouples were utilized to record box and battery temperature trend during test periods. As can be seen in Figure 44 the T-type thermocouples correspond to PV and battery temperatures were adhered to the center side of PV array and battery module respectively. To ensure accuracy of measured

temperatures 3*3 cm piece of isolated foil tape were used to cover the attached thermocouples. The hovered thermocouples inside and outside the box were used to measure box and ambient temperature respectively. The thermocouple respective to ambient temperature was hanged under the box with adequate gap from enclosure surface to avoid direct solar irradiance. Comparing these fore recorded values might be useful to investigate how ambient temperature affects on battery and box inside temperature.

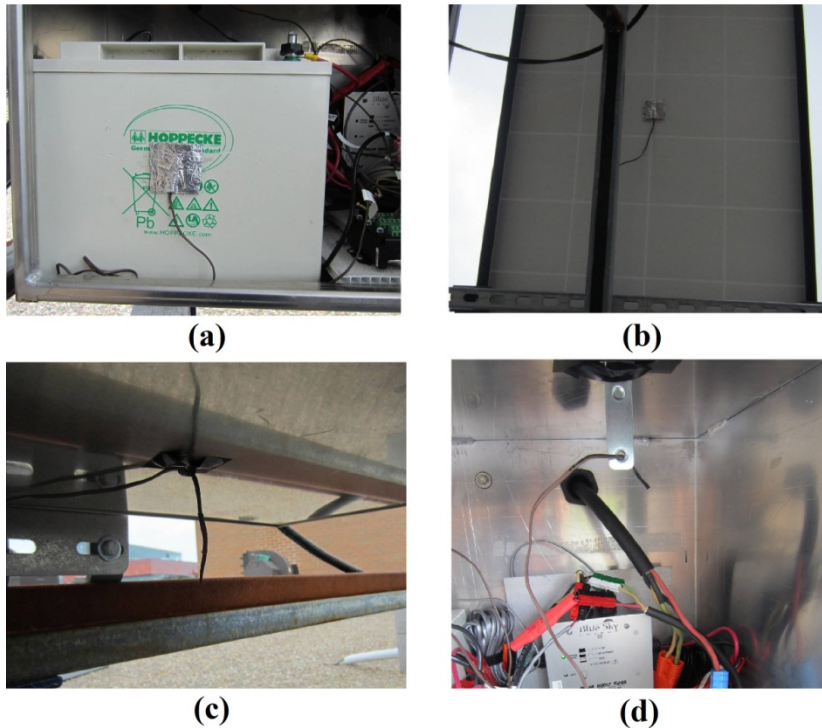


Figure 44: Installed thermocouples for (a) battery bank (b) PV panel (c) Ambient (d) box inside

4.10 WIRING AND CONNECTOR

According to considered design the battery modules were then assembled in series configuration (nominal pack voltage of 12 V; module #1 is most negative) and interconnected using custom cabling and PV panels were connected using parallel connectors. This setup includes high quality lugs (5/16”), cabling (12 AWG for battery connection and 10 AWG for LED and PV panels), and connectors (50 A continuous rated). The permitted type of solar cable is single conductor 8-14 AWG (2.5-10 mm²) with proper insulation to tolerate the maximum possible system open circuit voltage. The

conductor material should be copper only. Cable size was selected based on PV and battery manuals in order to achieve minimum voltage drop between modules and charge controller. LED lamp and PV panels were connected to charge controller through 10/4 (10AWG 4-Conductor) flexible water resistance cable.

4.11 EXPERIMENT BOARD

All measurement equipment and charge controller were installed on experiment board. Selection of board dimensions was based on enclosure and battery module size. As can be seen at Figure 45 two horizontal steel square tubes were installed on board bottom to keep all measurement equipment at higher latitude from enclosure surface. It is necessary to stand off the bottom of box in case water ingressed. The right angle stand that holding charge controller, was installed across the enclosure door to provide appropriate system monitoring through LED indicator. Figure 46 illustrates measurement equipment configuration on the board surface, including: charge controller stand, Two 50 A shunts, data logger and interface modem (which provides RS-232 signal).

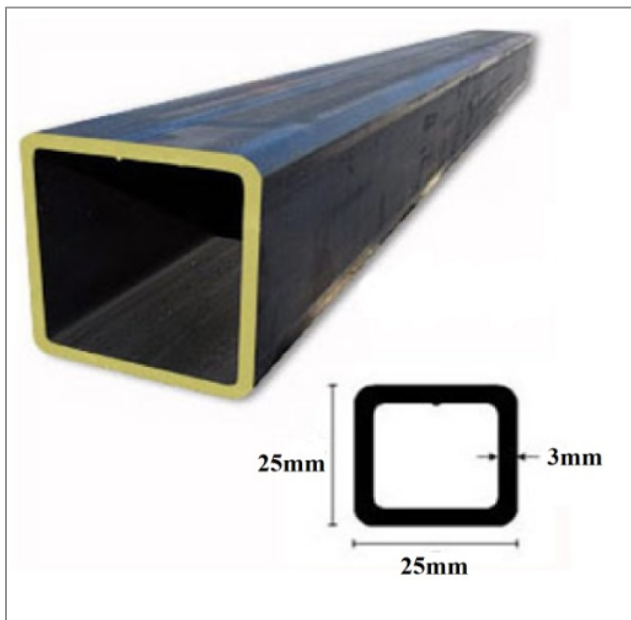


Figure 45: Experiment board stand dimensions



Figure 46: Experiment board (Including current shunt, charge controller and data logger)

As can be seen in Figure 47, the detailed wiring diagram shows how system components were connected together. The charge controller is located at the center and PV panels are connected to the corresponding terminal through 50 A shunt. Another identical shunt is placed between battery and charge controller in order to measure battery voltage and current during charge/discharge cycles. LED lamp is located at the top left corner of diagram and connected to controller through share negative terminal with battery. Four T-type thermocouples are used to measure ambient, battery, box and PV temperature and connected to data logger. Two 1:10 voltage dividers were used to decrease PV and battery voltage to the acceptable range of data logger. Data logger which is located at the bottom of diagram records aforementioned temperatures and PV/battery voltage/current. To avoid using external power source for data logger, battery bank is used to accommodate required energy for data logger operations.

4.12 SYSTEM INSTALLATION

Two struts (305.5 cm) were installed horizontally on stack according to distance between panel mounting holes. To avoid direct contact between panel frames and stack 8 mounting brackets were utilized to fix panels on top of stack. Bracket sketch and panel diagram is illustrated at Figures 48 and 49 respectively. Based on required gap between PV arrays and distance between mounting holes and panel's edge, bracket dimensions were selected to avoid any overlap between panels.

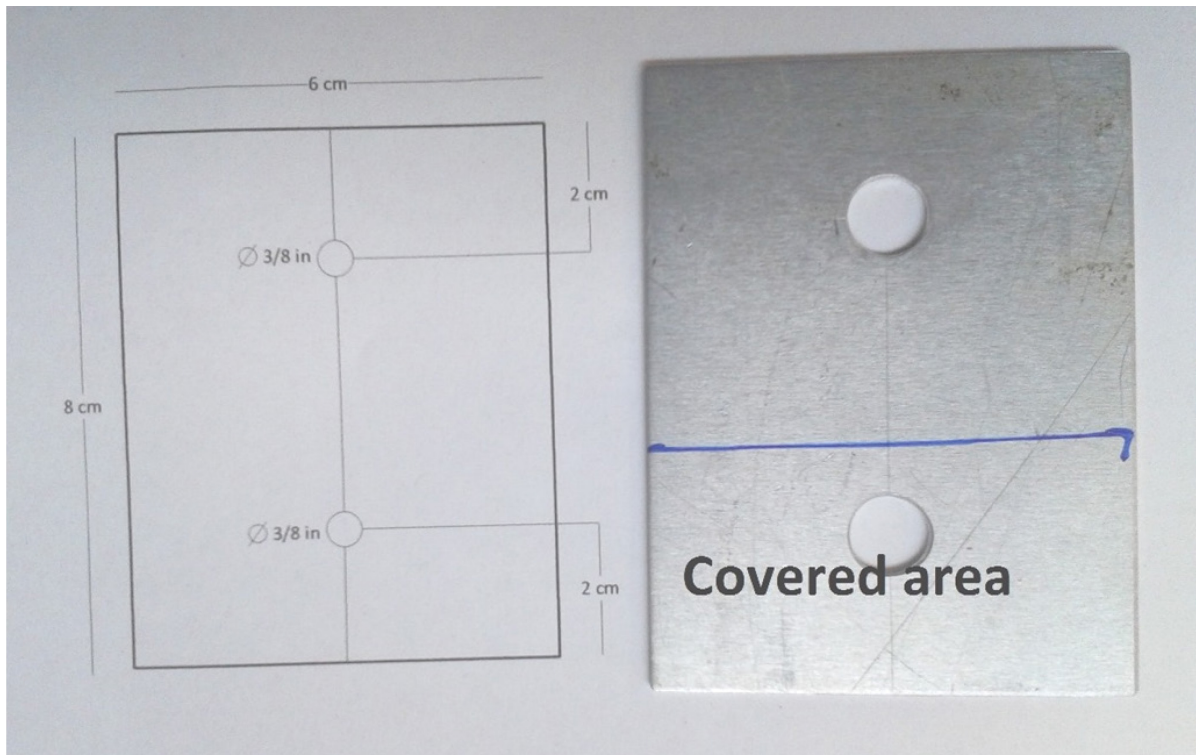


Figure 48: Bracket for installing PV array

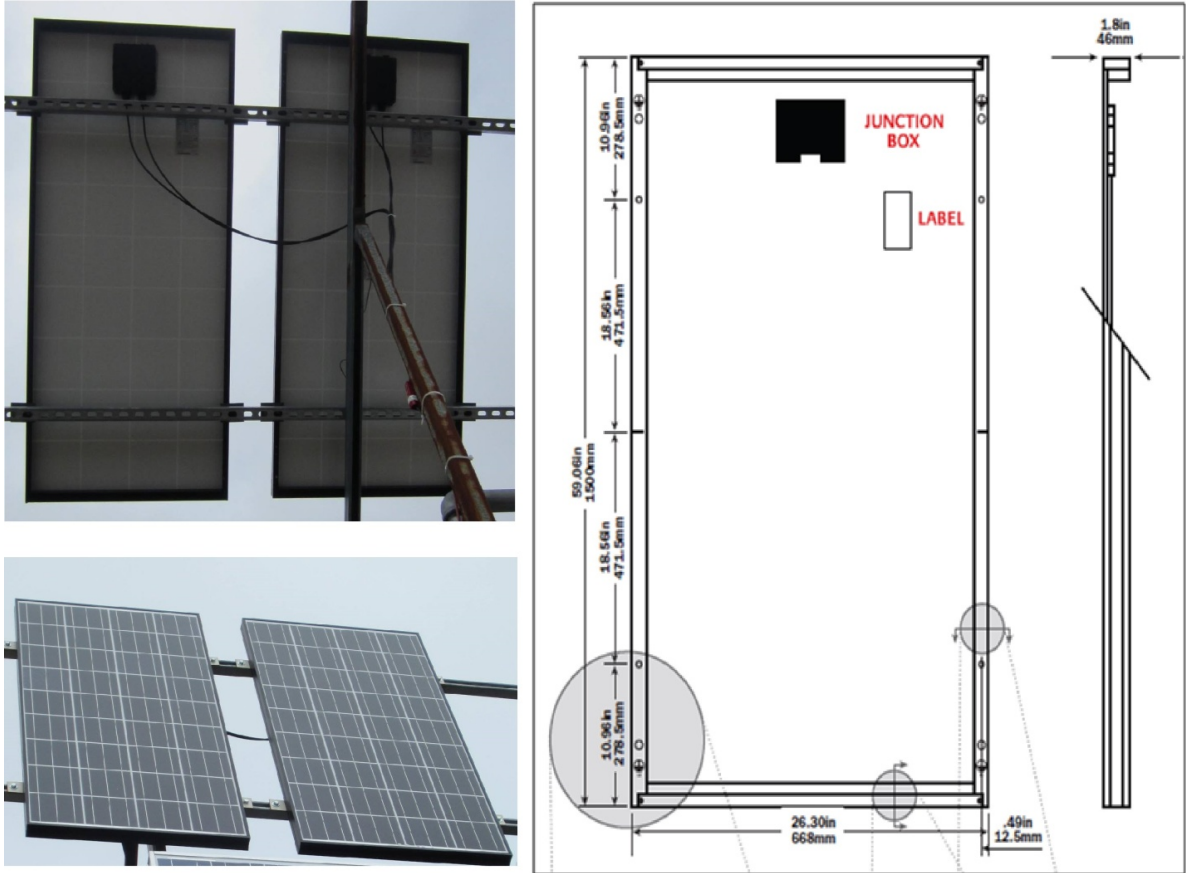


Figure 49: Front and rear view of installed PV panel & PV panel diagram

The provided detailed sketch at Figure 50 shows new installed struts and PV arrays position on stack.

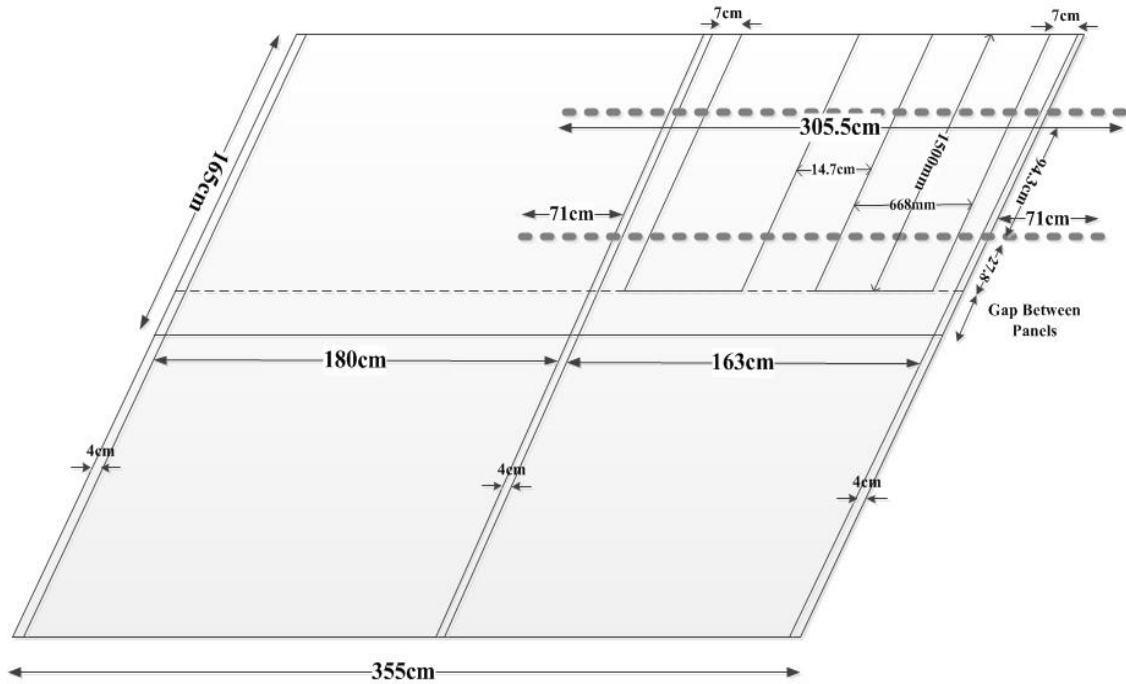


Figure 50: Dimensions and measurements for PV stack

As can be seen in Figure 51 both end threaded 1 ½" pipe and steel elbow were used as pole to hold LED lamp. The prepared pole was mounted on available oblique strut through two pipe clamps. LED lamp fixture was adjusted parallel to the ground in order to provide perpendicular luminance over surrounding area.

The day and night view of experiment setup is presented in Figure 51.



Figure 51: Installed street light (Day/Night)

Battery enclosure houses batteries and charge controller and protect them against rain, snow and direct solar radiation. In real street light system battery enclosure can be mounted on pole under PV arrays, or close to pole foundation on or underground. As can be seen in Figure 52 the battery box was installed under available PV arrays through available mounting plates. It is worth mentioning that battery bank weight is approximately 83 kg consequently it was necessary to fix box securely to tolerate this weight. It was necessary to add angle brackets and horizontal strut to fix box upper and lower plate on stack structure.

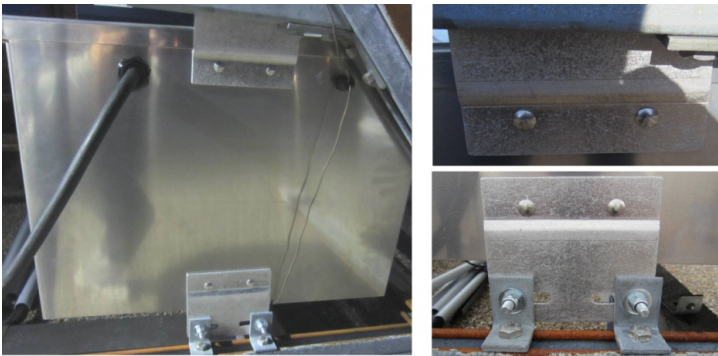


Figure 52: Enclosure mounting plates & box attachment angles



Figure 53: Solar street light setup (Day/Night)

Table 24: Setup and measurement equipments specification

Component	Dimension	Quantity	Type	Specification	Comment
PV	1500mm*668mm*46mm	2	Silicon Crystalline	Weight :12.5 kg Power at maximum power point: 135 W Open circuit voltage: 22.1 V Short circuit current: 8.37 A Voltage at maximum power point: 17.7 V Current at maximum power point: 7.63 A	Tilt angle: 45° Direction: South
Battery	308mm*275mm*107mm	2	AGM lead acid batteries Hoppeck Solar bloc	Weight: 41.4 kg Voltage= 6 V Capacity: 250 Ah	-
Voltage divider	-	1	Two resister configuration	$V_2/V_1=1:10$	-
Electric Shunt	-	2		Current: 50 A Ratio of voltage to current: 1 mV/A	
Data logger	252mm*102mm*71mm	1	CR-1000	Weight: 1kg Input voltage range: ± 5 V	Measured Values: PV current and voltage Battery current and voltage Ambient temperature, battery, PV and box temperature Interval time = 6 sec
LED	-	1	SAT- 485	Weight: 8.2 kg Power: 55w Voltage: 12 V	-
Charge controller	13.5*13.5*11.9	1	SB- 15240	Voltage: 12 or 24 V Current: 15-20 A	MPPT feature
Thermocouple	-	4	T type	-	Covered by 3cm*3cm isolated foil

4.13 EXPERIMENTAL RESULTS

The experimental data was acquired through data logger which is connected to PV arrays, battery, charge controller and thermocouples. The voltage divider was calibrated in place using a Fluke 87 multimeter capable of 0.05% of reading + 1 significant figure accuracy. The measurement error of the CR1000 is $\pm 0.06\%$ of the reading which corresponds to 0.0132 V when measuring the highest voltage in the PV output during charge (22 V). The thermocouples also measure temperature with 1°C error. Additionally the voltage dividers are associated with maximum uncertainty in this experiment. Measured data at 6 seconds interval time was recorded as excel file using PC-400 software. As can be seen in Figure 54 first column of each row indicates date and time of each scan by CR-1000. Scanned data including: battery voltage and current, PV voltage and current, ambient, inside box, PV and battery temperature which are presented at respected row.

1	Data & Time	RECORD NO	PV_Voltage V	PV_Current Amp	Battery_Voltage V	Battery_Current Amp	Battery_Temp Deg C	Ambient_Temp Deg C	Box_Temp Deg C	PV_Temp Deg C
2	5/13/2014 17:05	0	20.36	0.306	14.09	0.204	19.54	16.89	17.14	24.99
3	5/13/2014 17:05	1	20.37	0.306	14.09	0.204	19.53	16.74	17.01	24.72
4	5/13/2014 17:05	2	20.37	0.306	14.1	0.204	19.5	16.63	16.82	24.63
5	5/13/2014 17:05	3	20.37	0.306	14.1	0.204	19.55	16.78	16.89	24.7
6	5/13/2014 17:06	4	20.37	0.272	14.1	0.204	19.56	16.96	16.99	24.74
7	5/13/2014 17:06	5	20.37	0.306	14.1	0.17	19.59	17.35	17.3	24.79
8	5/13/2014 17:06	6	20.37	0.306	14.1	0.17	19.57	17.55	17.35	24.8
9	5/13/2014 17:06	7	20.37	0.272	14.09	0.17	19.6	17.51	17.33	24.9
10	5/13/2014 17:06	8	20.36	0.272	14.1	0.17	19.62	17.67	17.5	24.95

Figure 54: Experimental result sample

The experimental results which are presented in this chapter are divided into four sub sections. Information related to PV output current, voltage and power in addition to columbic potential (Ah) are presented in PV section. Battery section gives detailed data of charging and discharging cycles for each single day of test period. These data are supported by amp-hour depletion diagram and columbic capacity (Ah) bar chart, for each charging and discharging cycle. Load profile and wattage used by LED lamp are provided in LED section. Finally, last section presents data pertinent to minimum,

average and maximum temperature of system components. All data related to the period from 14/5/2014 to 14/6/2014. It was preferable to continue data recording for 12 months but components evaluation and system monitoring was limited to 2 months due to time limitation for this project. It is worth mentioning that since the system performance was evaluated for sunny, hazy and cloudy days, these 2 months period is enough for model assessment.

4.13.1 PV

As mentioned earlier output voltage and current of PV panel were measured through 50 A electrical shunt and achieved results including PV output voltage, current and power are illustrated in Figure 55.



Figure 55: PV output voltage, current and power

For better interpretation, the trend of maximum amount of current, voltage and power during test period are presented in Figure 56.

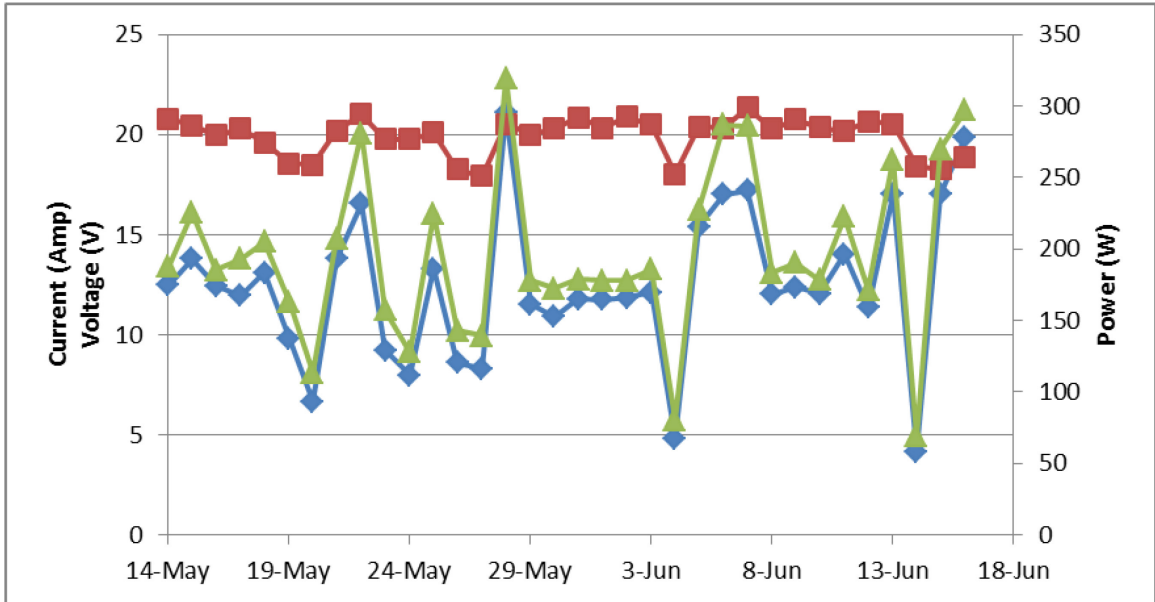


Figure 56: Maximum PV output current, voltage and power.

The amount of daily electricity production is an important parameter for evaluating site potential for accommodating required energy for the load. To achieve this purpose, PV current was measured before entering to the charge controller. The produced electricity by PV panels varies according to amount of absorbed irradiance. For better judgment on trend of this variation, Figure 57 shows daily and cumulative electricity production by PV panels over the test period.

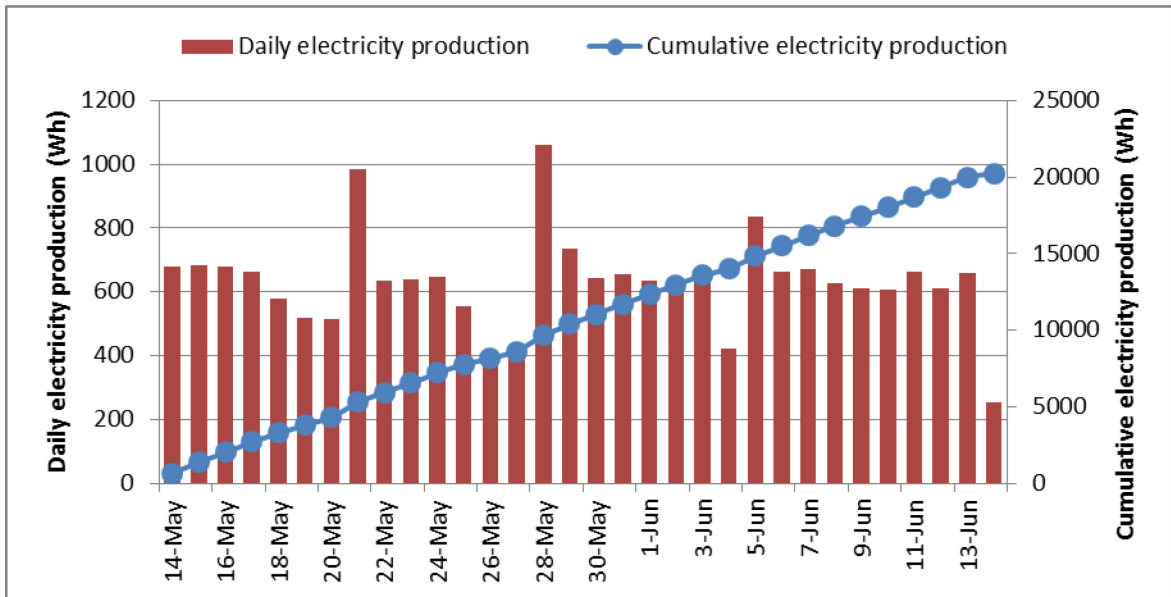


Figure 57: Daily and cumulative electricity production

Information related to daily produced electricity has crucial role in analyzing site potential for supporting off-grid applications. In addition to daily electricity production (Wh) data, it is necessary to investigate maximum values of output current, voltage and power in order to select appropriate components (e.g. battery bank, charge controller). Each component has certain limits which must be considered for increasing life cycle and efficiency of the system.

4.13.2 Battery

For interpreting the battery behavior under realistic condition, battery current, voltage and power profile are presented in Figure 58. Aforementioned data are measured through installed shunt between charge controller and battery bank.



Figure 58: Battery voltage, current and power profile

Figure 58 shows how battery current and voltage varies during test period. Cycles corresponding to LED lamp discharge and PV panel charge illustrate battery performance under real operating condition. The trend of maximum current and power for charge and discharge cycles are presented in the Figure 59. Fluctuations in maximum charge current and power values are caused by variation in the solar irradiance levels over test period. Contrary to the charge, during the discharge cycles, maximum current and power values show a constant trend.

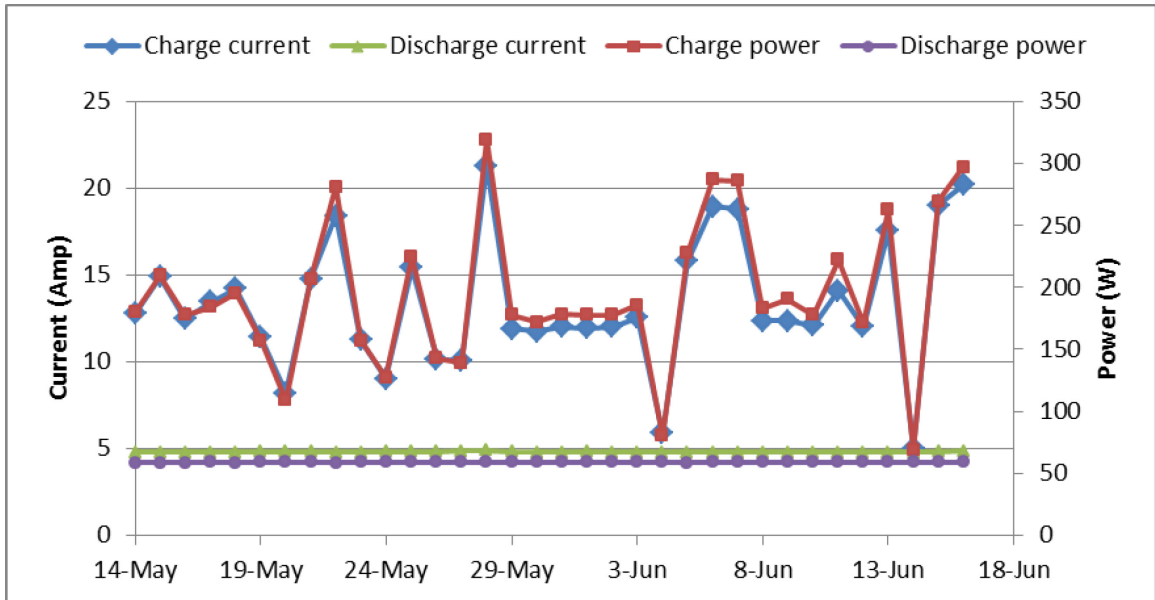


Figure 59: Maximum battery current and power for charging cycles.

In addition to maximum current and power in charging and discharging cycles, it is important to identify the range of battery voltage. Battery voltage at start and end point of each cycle are presented in Figures 60 and 61.

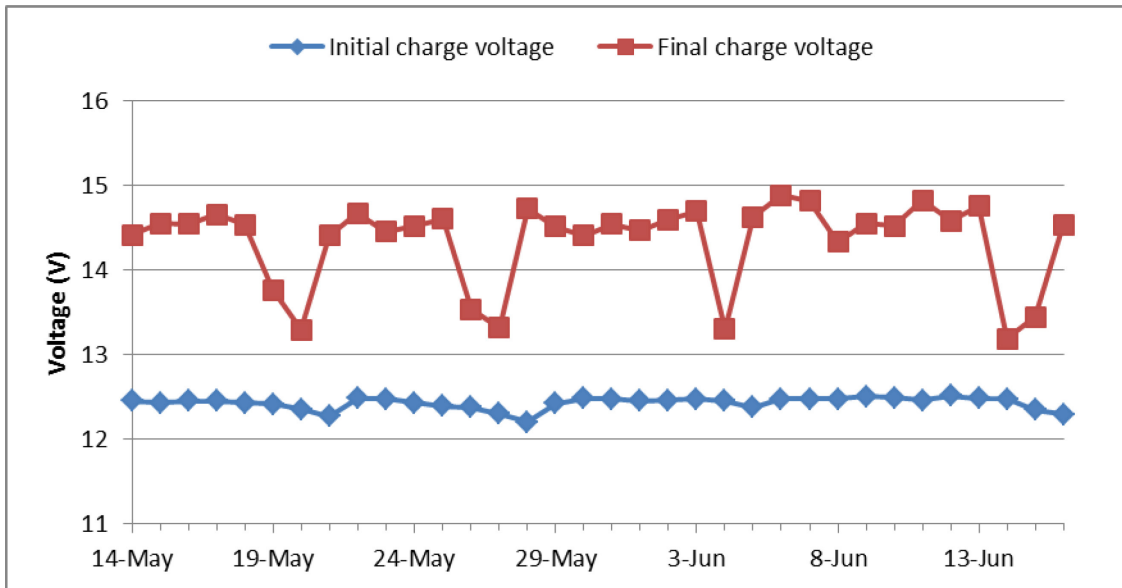


Figure 60: Initial and final battery voltage for charging cycles.

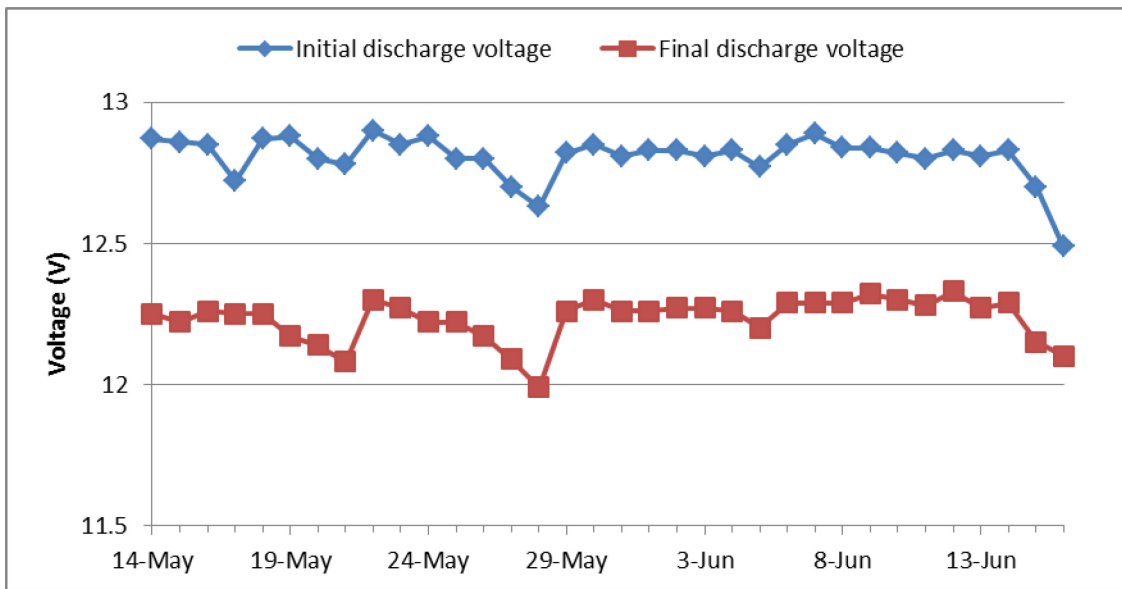


Figure 61: Initial and final battery voltage for discharging cycles.

During test period discharge and charge cycles were performed consecutively. Figure 62 gives columbic capacity (Ah) of discharging and charging cycles. Daily amount of charge and discharge columbic capacity can be compared by presented bar chart in Figure 62.

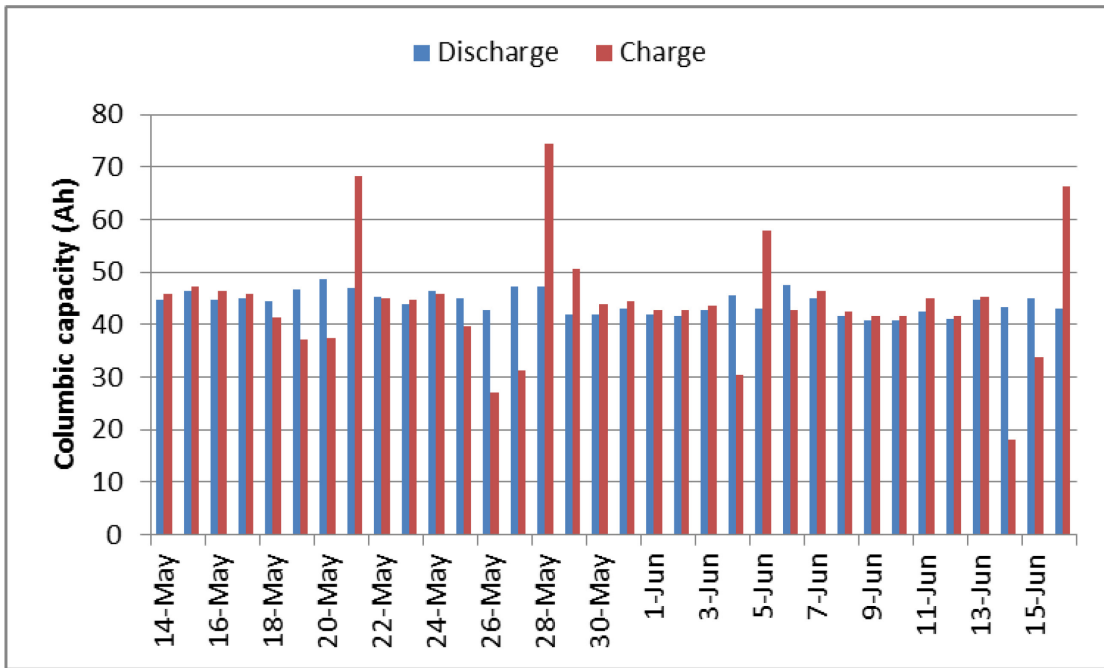


Figure 62: Columbic capacity (Ah) of discharge and charge cycles

As can be seen in Figure 62, charge columbic capacity of first sunny day after few continuous cloudy days is higher than average in order to compensates low state of charge of battery.

Ah depletion diagram as a function of test time for investigation of capacity performance is illustrated in Figures 63 and 64.

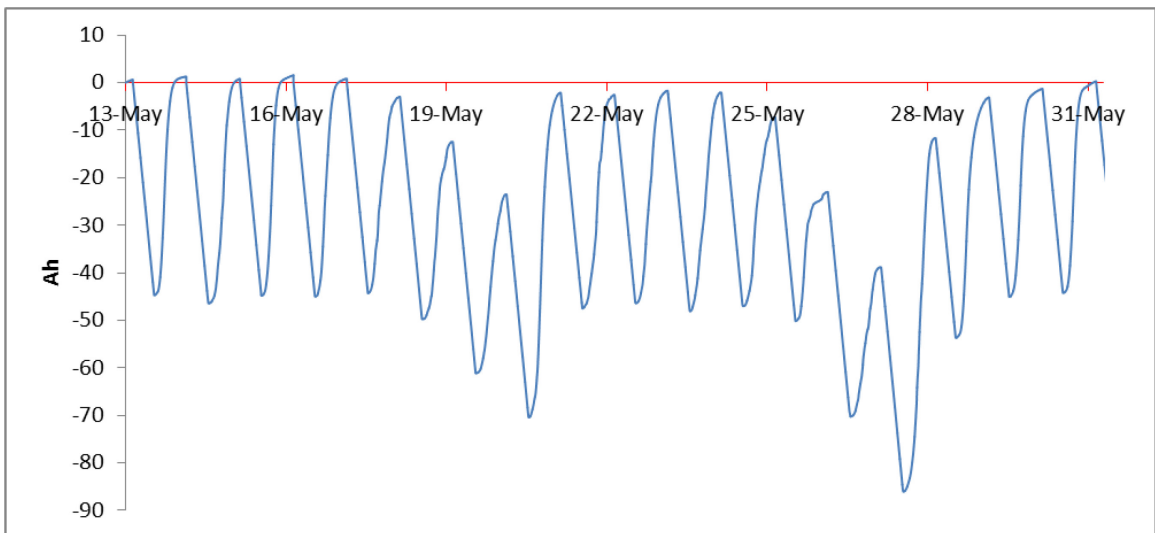


Figure 63: Battery Ah depletion (May 13-31)

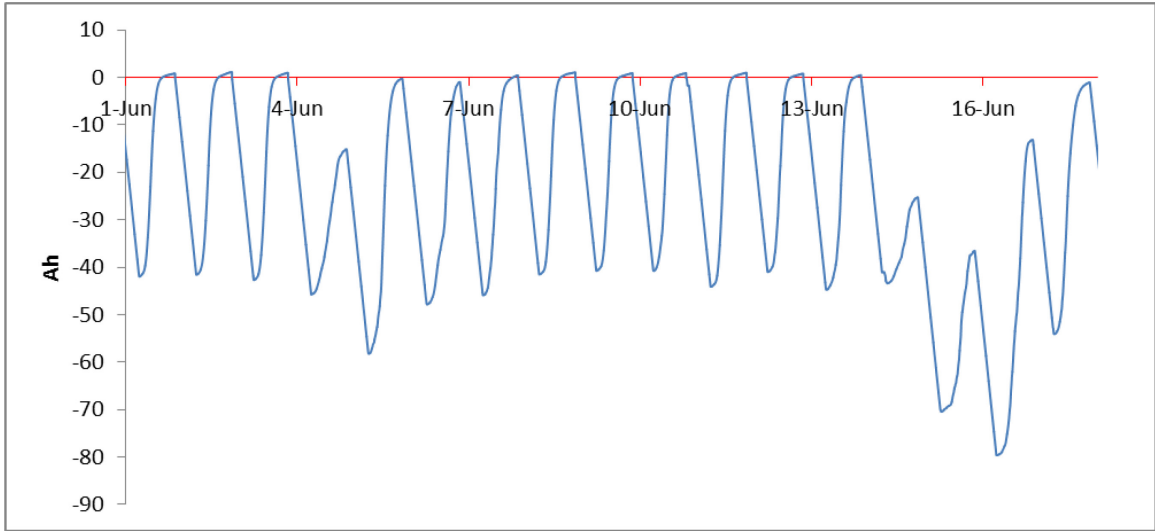


Figure 64: Battery Ah depletion (June 1-16)

As mentioned earlier charge controller has capability to control LED lamp. Consequently the start and end of LED operation are adjusted automatically through light controlling feature. The light controller performance in turning on/off the LED lamp is presented in Figure 65. As can be seen, normally charge controller turns on the LED lamp around 8:00 PM and turns off around 6:00 AM.

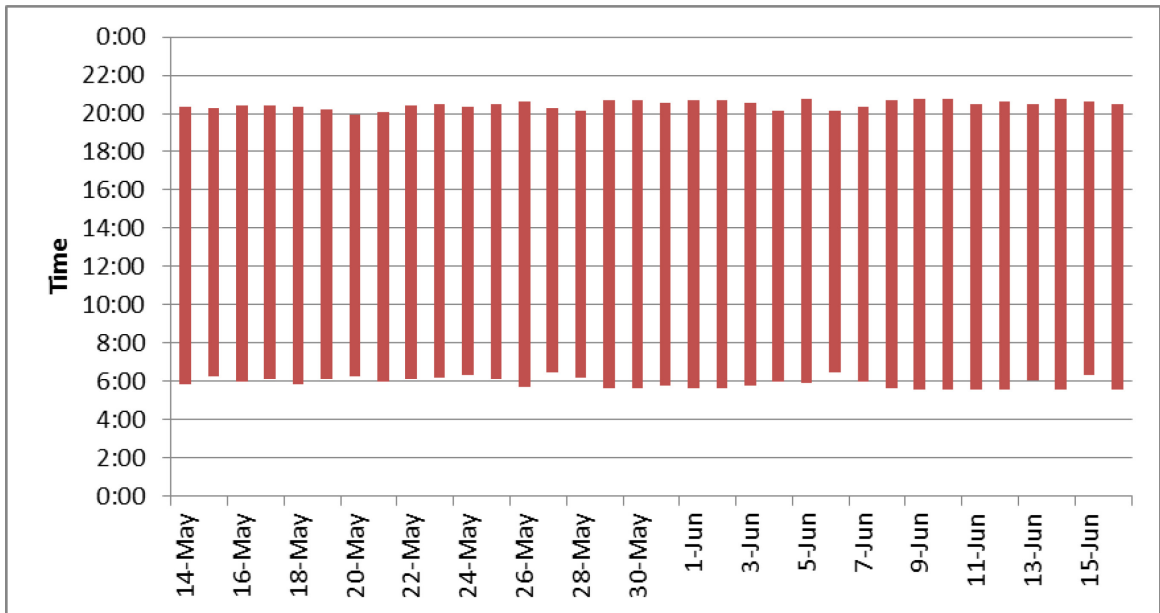


Figure 65: Daily operation of LED lamp

The summary of information related to wattage usage by LED including minimum average, maximum and standard deviation is tabulated in Table 25.

Table 25: Details of wattage usage by LED lamp

Minimum	Average	Maximum	Standard deviation
57.88 W	58.49 W	59.15 W	0.127

Based on measured data the average wattage usage of LED lamp is 58.49 W, which is higher than provided specification sheet by manufacturer.

Installed thermocouples accurately measured ambient temperature, box temperature, battery and PV temperature. For better interpretation, Figures 66 and 67 show the temperature trend for system components and ambient during May and June respectively.

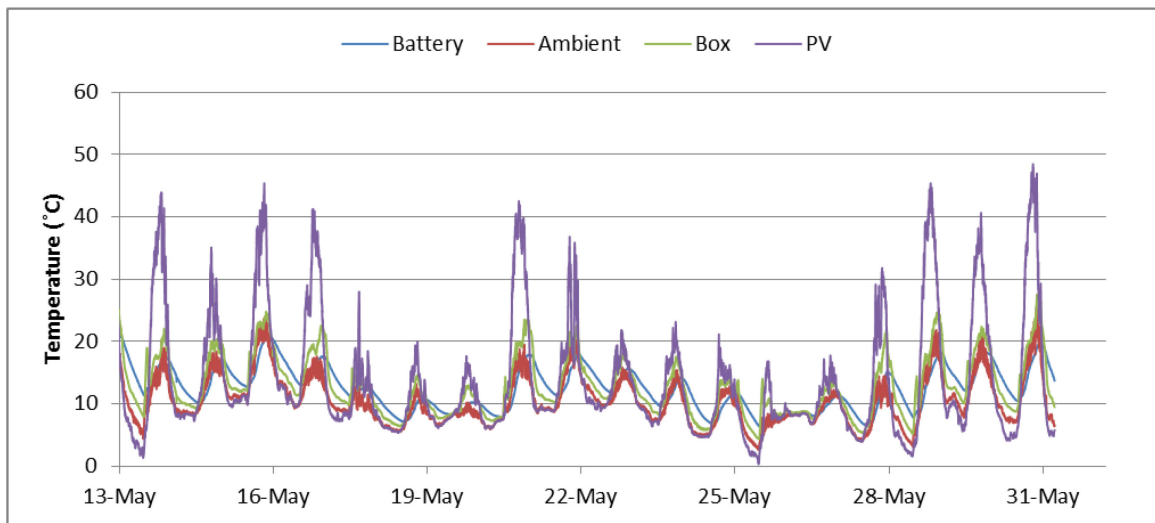


Figure 66: PV, ambient, box and battery temperature (May 13-31)

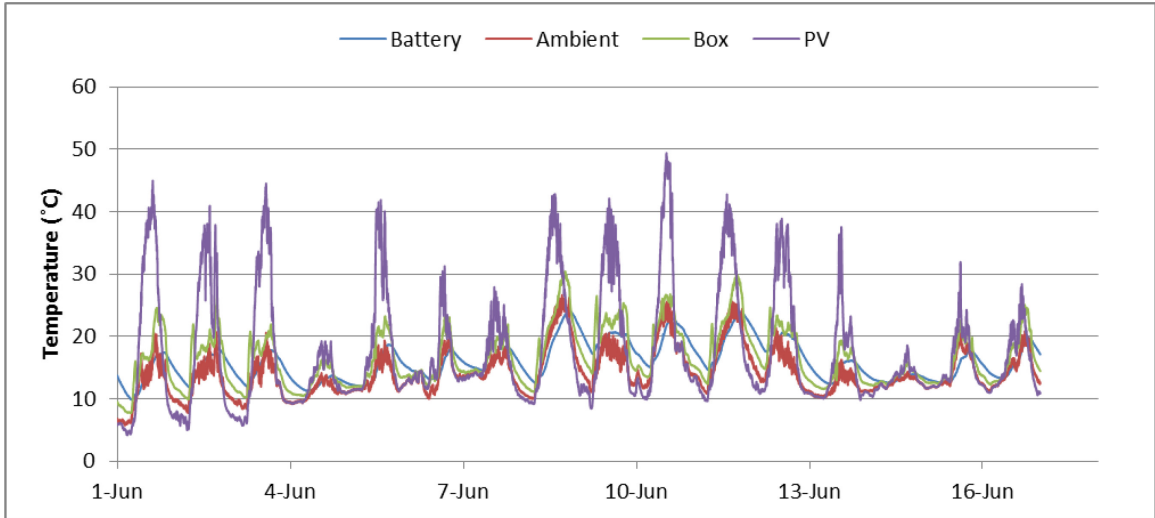


Figure 67: PV, ambient, box and battery temperature (June 1-16)

Summary of measured data including minimum, average, maximum and standard deviation for temperature of aforementioned components is tabulated in the Table 26.

Table 26: Detailed information for ambient and components temperature

Component	Minimum	Average	Maximum	Standard deviation
Battery	6.4 °C	14.1 °C	24.2 °C	3.7
PV	0.3 °C	15.5 °C	49.4 °C	9.5
Box	4.3 °C	14.5 °C	30.4 °C	4.9
Ambient	2.6 °C	12.2 °C	26.7 °C	4.2

CHAPTER 5 RESULTS AND DISCUSSION

This chapter gives comparison among experimental and simulation results to calibrate and evaluate the methods. TRNSYS model was tested using the Halifax weather data from TRNSYS weather database.

Figure 16 and Figure 17 show total horizontal solar irradiance in W/m^2 unit based on TRNSYS weather database (Metronome) which can be used as reliable indicator for evaluating site solar potential. For measuring realistic solar irradiance data, a pyranometers must be coupled with system. Based on installation position of pyranometers, recorded data is corresponding to solar irradiance on horizontal or tilted surfaces. TRNSYS solar radiation processor is capable of generating direct and diffuse radiation outputs for any surfaces with various ranges of orientation and inclination.

Due to the fact that input data (e.g. solar irradiance, ambient temperature and wind velocity) for simulation model and experimental setup are not completely identical, three different days were considered for evaluating the model. These three days were selected as representative of sunny, hazy and cloudy days in order to verify TRNSYS model performance in predicting PV output current and voltage. Two parameters including solar radiation level and amount of produced electricity were considered for this selection. The detailed information about selected days are tabulated in Table 27. However system assessment was conducted over May and June, it is reliable for whole year (e.g. winter) since various level of solar radiation (Sunny, hazy and cloudy days) were considered.

Table 27: Selected days for model verification

Climatic condition		Date	Electricity production (Ah)
Sunny	Simulation	May 24	66
	Experiment	May 21	68
Hazy	Simulation	June 10	49
	Experiment	May 24	45
Cloudy	Simulation	May 16	29
	Experiment	June 4	30

As can be seen in Figure 68 which shows PV output current and voltage during cloudy day, acceptable match exists between simulation and experimental results trend. It is worth mentioning that input data for experiment setup and simulation model are not identical so it is expected to get similar trend not same values. Consequently same trend for both data sets shows model simulation reliability.

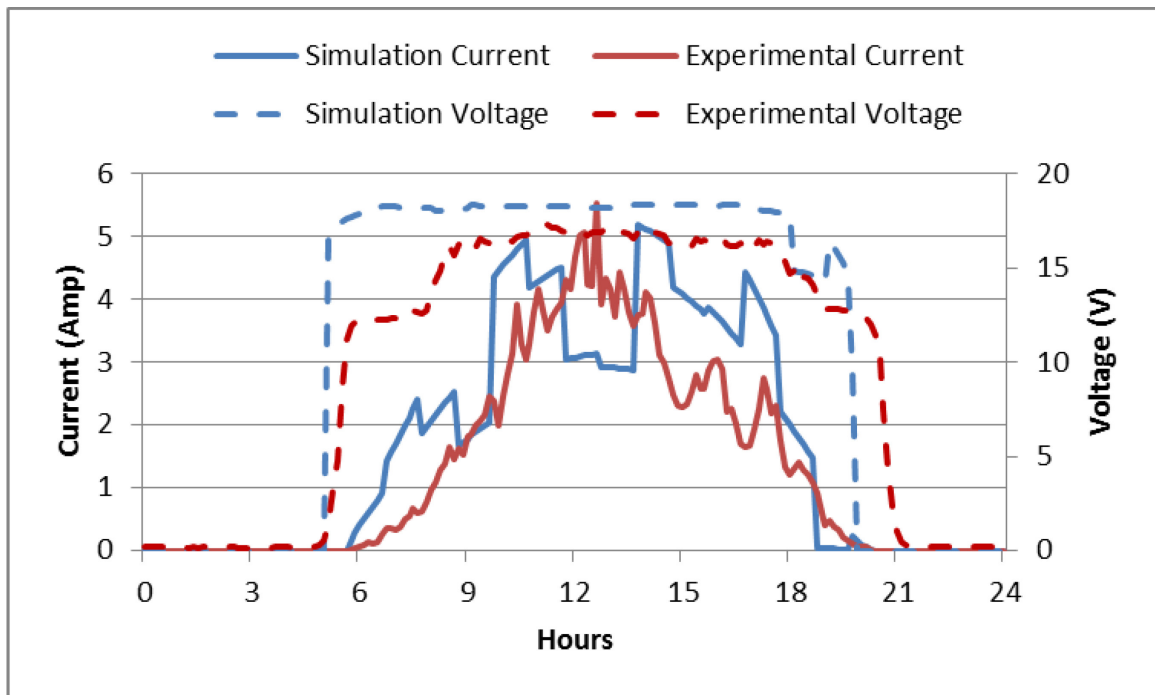


Figure 68: PV output current-voltage (Cloudy day)

During cloudy days, the average of columbic capacities (Ah) of charge cycles for simulation and experimental results were 29 Ah and 30 Ah respectively. In comparison to experimental data, model estimates higher PV output voltage particularly in first two hours. Both data sets show same peak output current around 5.1 A. As can be seen in Figure 68, Figure 69, Figure 70, experiment results show shoulder for PV output voltage which is caused by sudden surge in solar radiation level. According to short interval time for data recording (6 seconds) this increase in received solar irradiance illustrates shoulder in PV output voltage. Input data for simulation model is corresponding to

average of 30 years climatic data which leads to smooth output values with minimum fluctuation.

Figure 69 presents voltage and current profile corresponding to hazy days. As it is shown in Figure 69, time and amount of both peak output current are closely match with experimental results.

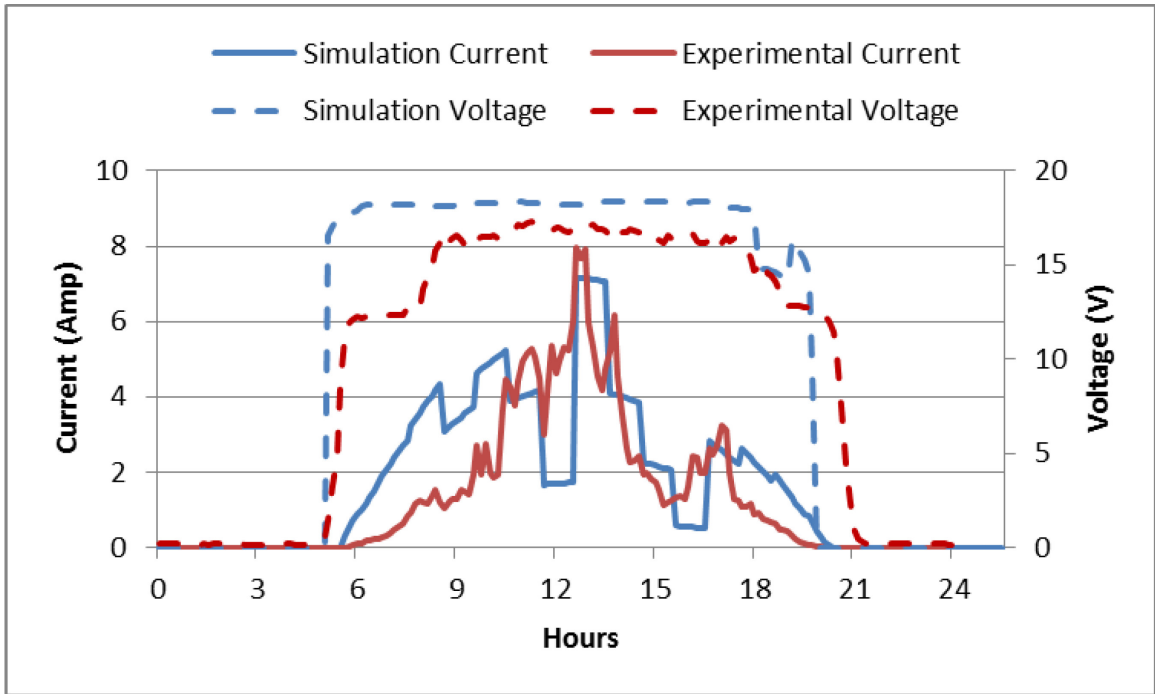


Figure 69: PV output current-voltage (Hazy day)

As it is shown in Figure 69, apart from gap in first two hours, a reasonable agreement exists between numerical and experimental results.

Finally the results for sunny day are presented in Figure 70. While the predicted peak output current by model is 12 A, experimental data recorded 13 A as maximum current.

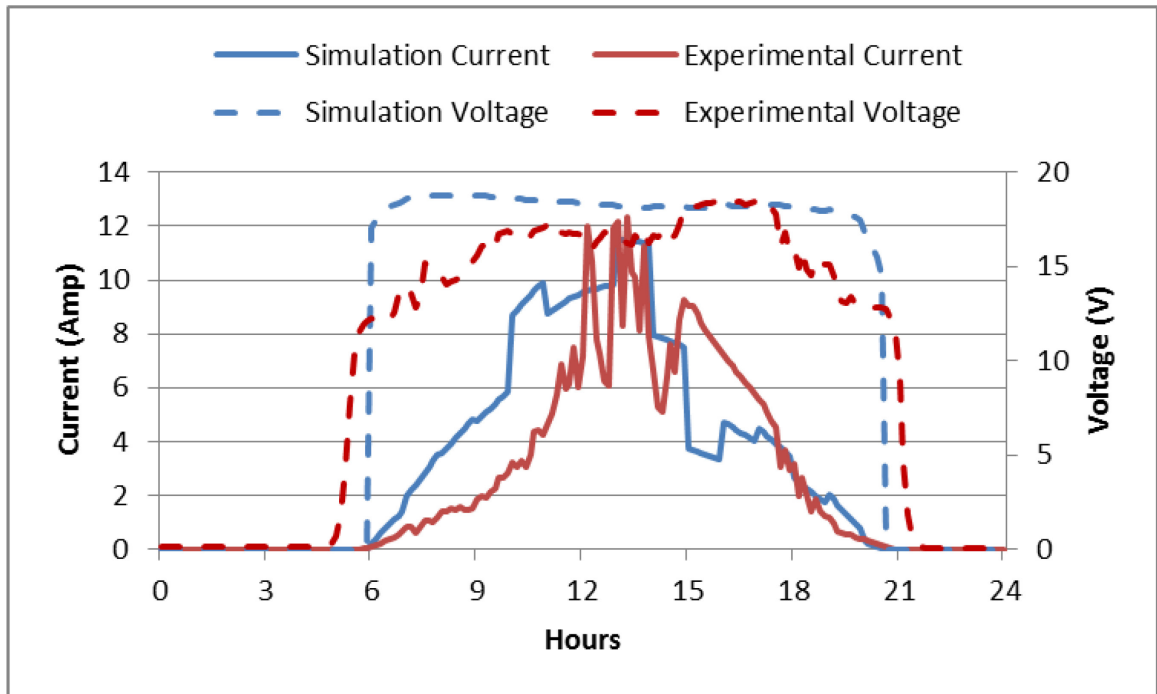


Figure 70: PV output current-voltage (Sunny day)

Figure 70 shows estimated and experimental PV output voltage profile. Although the model estimates constant voltage throughout the test time, experimental results exhibits steady incline during bulk charging stage and then stays constants. In simulation, during float stage, charge controller turn off the PV in order to measure amount of curtailed energy which results sharp drop in output voltage. The presented data in Figure 70 is corresponding to 24th of May in simulation and 21st of May in experimental data points.

As it expected and measured values are illustrated in Figure 71, Initial and final voltages of battery vary in discharge and charge cycles throughout test time. Battery performance in charging and discharging cycles depends not only on solar radiation, but also on battery state of charge. As it expected, after few cloudy or hazy days, the initial and final voltages of battery during charge and discharge cycles decrease to lower values. For better judgment, according to achieved data from experiment setup, Figure 71 presents real data in order to show how initial and final battery voltages vary with ampere hour depletion.

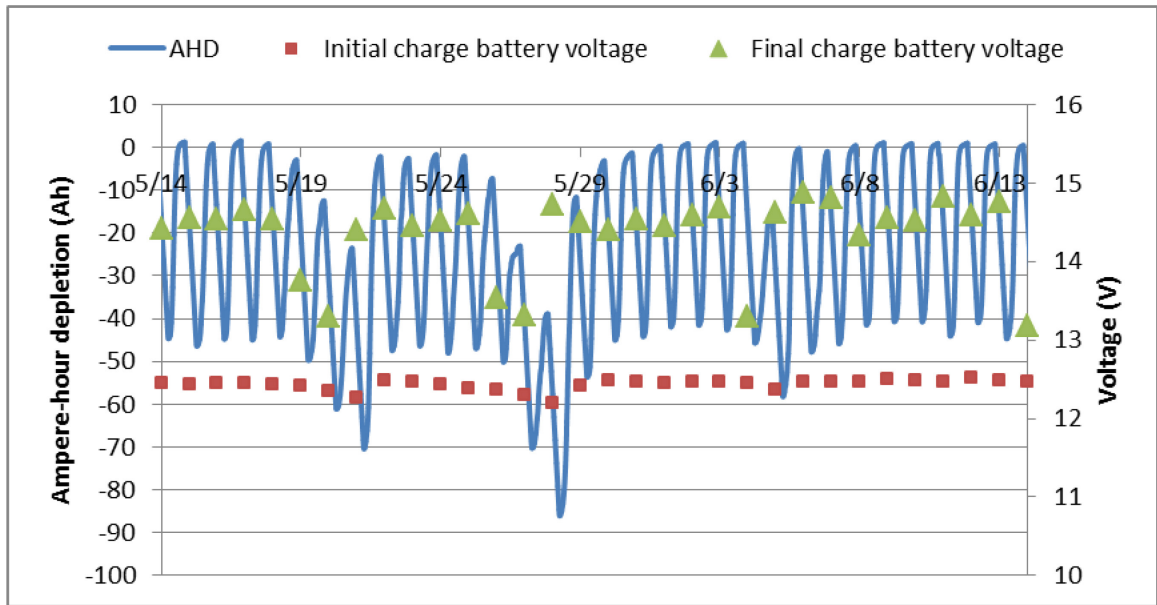


Figure 71: Measured initial and final battery voltage and AHD diagram

As it mentioned earlier since input data are not exactly identical for experiment setup and TRNSYS model, result are compared in hourly basis. In order to evaluate battery component behavior during solar cycles, two days were selected representing half and fully charged cycles. Comparison is conducted among days with same operating conditions (e.g. solar radiation and battery state of charge) and results are shown in Figures 72 and 74. Figure 72 shows battery current profile for simulation and experimental results in fully charged cycle.

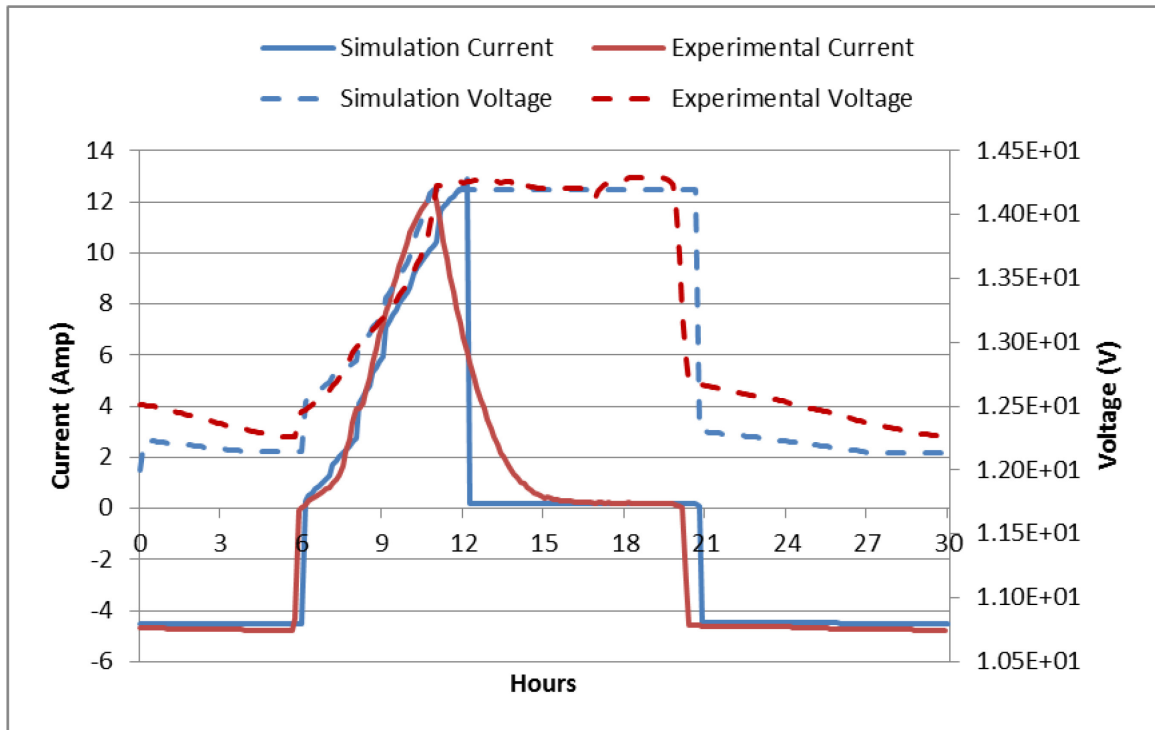


Figure 72: Battery current-voltage profile for fully charged cycle

As can be seen in Figure 72, apart from short period during float charging, acceptable agreement exists between both data sets during discharge and charge cycle. However experimental data exhibits logarithmic decay trend during float charging, instantaneous reduction is seen in simulation data. This sharp drop is the result of shutting down PV by charge controller according to fully charged battery. In real operating conditions charge controller requires more time to decrease the current to preset value while in simulation model charge controller component immediately stops charging. In addition, based on battery model's equations for charging mode, input current leads to rise in voltage, which is not match with realistic battery performance. According to low amount of current during float stage, the difference between simulation and experimental results is not significant. For better interpretation the ampere hour depletion diagram corresponding to fully charged cycle is presented in Figure 73.

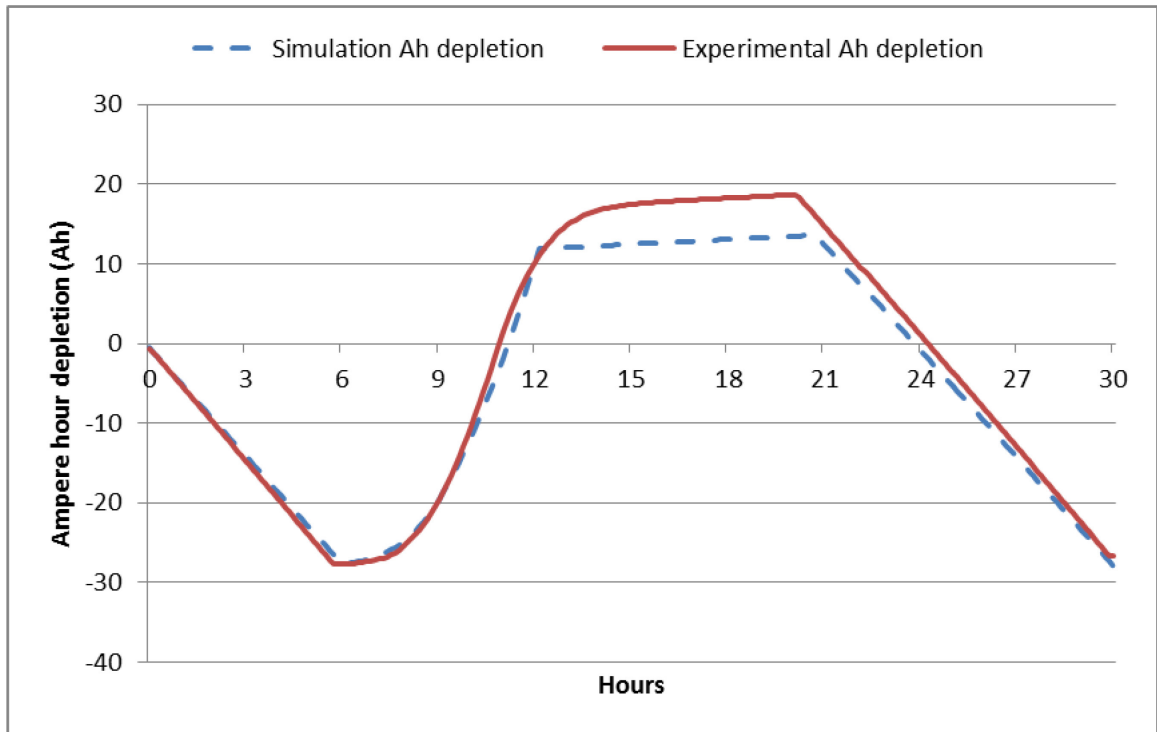


Figure 73: Ampere hour depletion diagram for fully charged cycle

As can be seen, simulation model well estimates the voltage throughout charging. Although both data sets show similar trend, less than 0.35 V offset exist between simulation and experimental results during discharging. Existing offset is related to battery state of charge at the end of previous cycle.

In cloudy or hazy days, due to insufficient solar radiation battery voltage does not reach to acceptance voltage setpoint. Figure 74 shows battery voltage and current profile of simulation model and experimental setup during cloudy day.

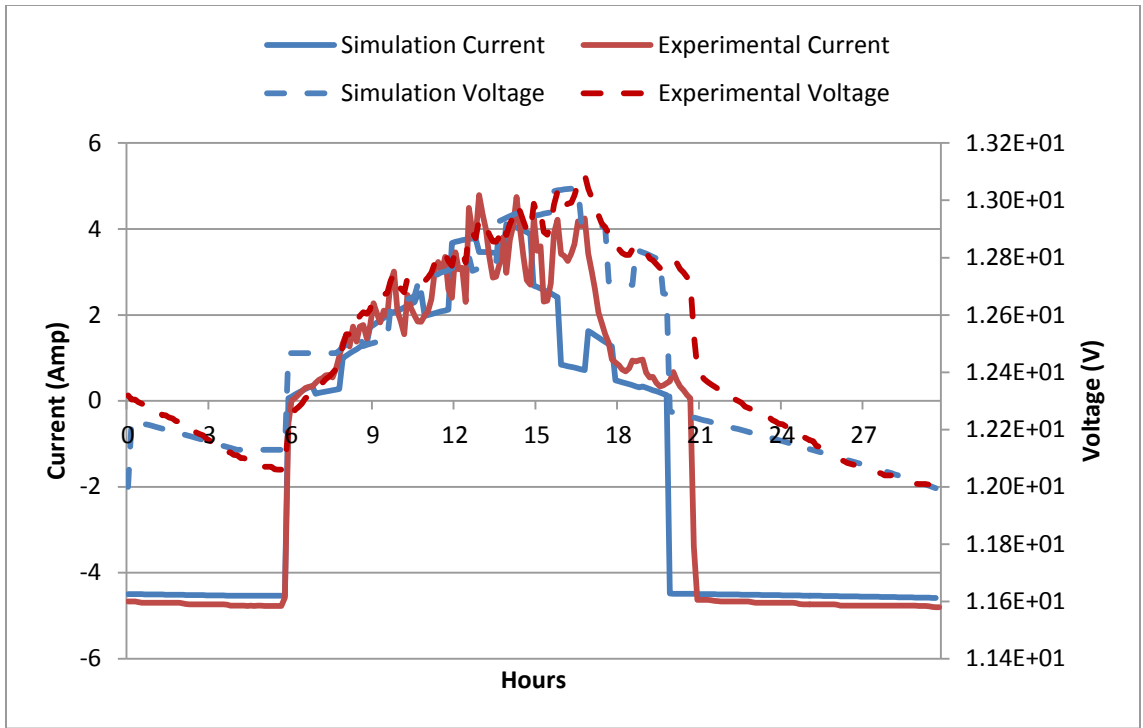


Figure 74: Battery current-voltage profile for half charged cycle

Experimental current in second half of day (after 2:00 PM) is slightly higher, which results insignificant offset among estimated and measured battery voltage. Similar to fully charged cycle, Figure 75 presents ampere hour depletion chart for half charged cycle.

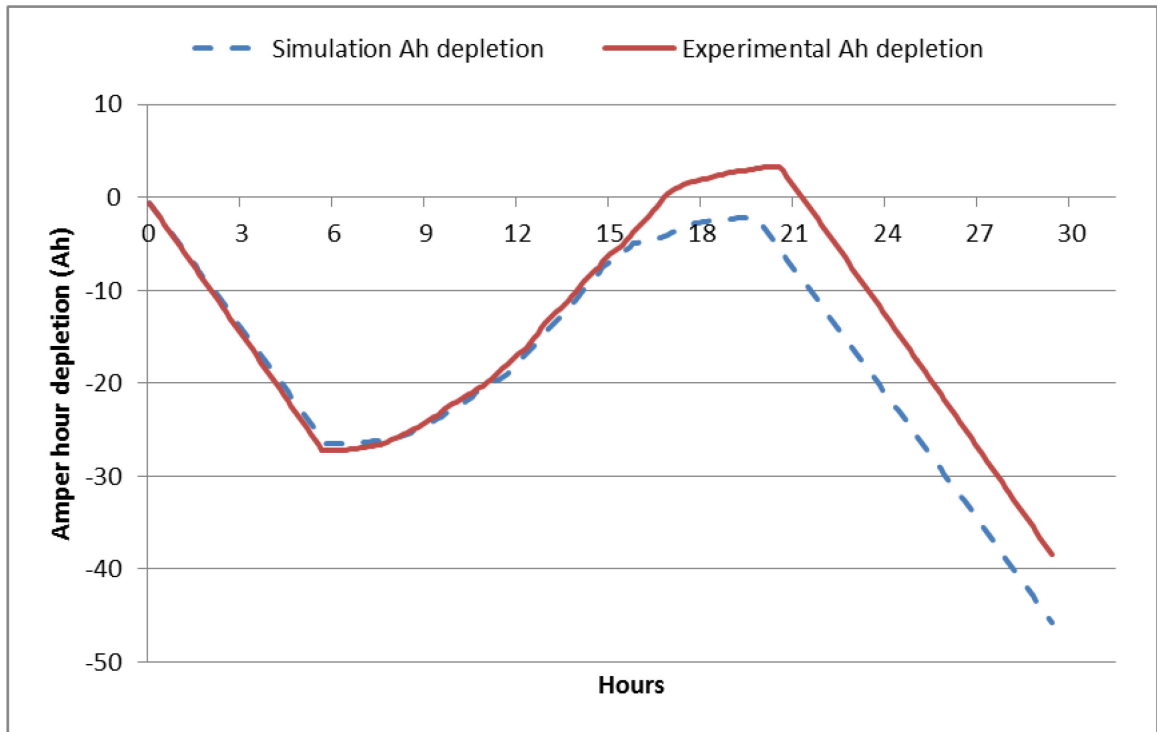


Figure 75: Ampere hour depletion diagram for half charged cycle

Based on these sample cycles, TRNSYS model well predicts amount of drawn current from battery bank during discharge cycles. Columbic capacity of discharge and charge cycles for simulated and measured results are presented in Figures 25 and 62 respectively. Comparison among aforementioned values shows average of estimated columbic capacity (Ah) by TRNSYS model for discharge cycles is very close to measured values. Current profile during charging cycles is function of solar radiation, ambient temperature and wind velocity. Since operating conditions are completely dynamic and aforementioned values fluctuate significantly, comparison between estimated and measured results were conducted in hourly basis. For better evaluation ampere hour depletion diagram for simulated and measured value during test period are presented in Figures 76 and 77, respectively.

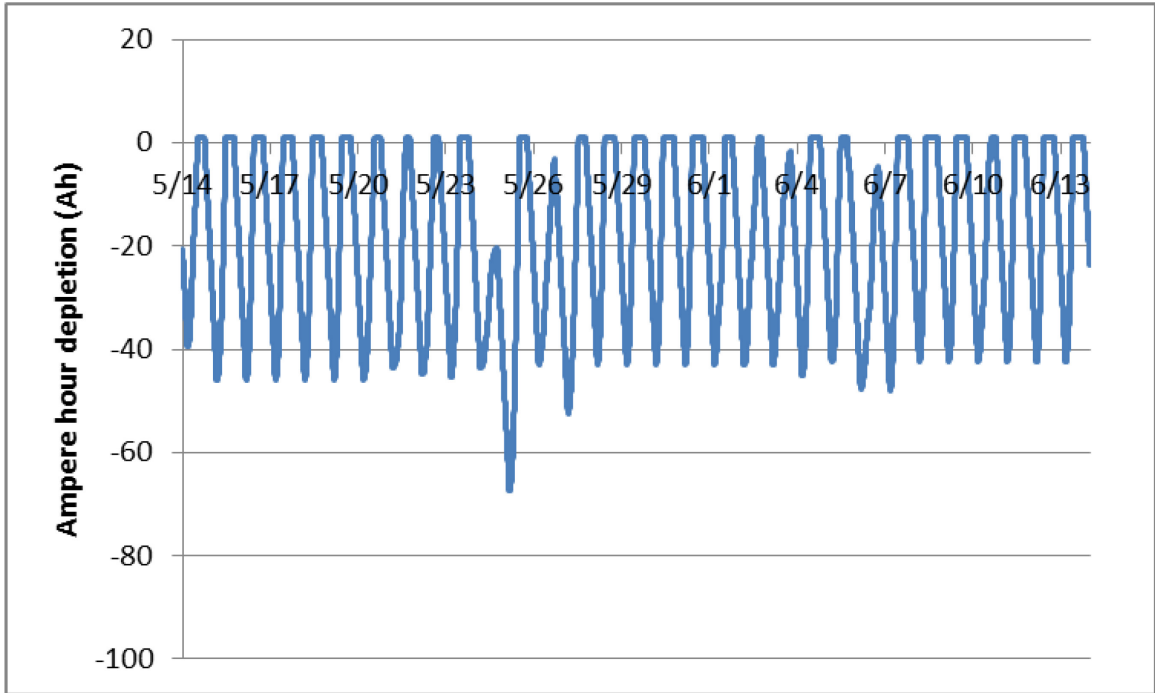


Figure 76: Simulated ampere hour depletion

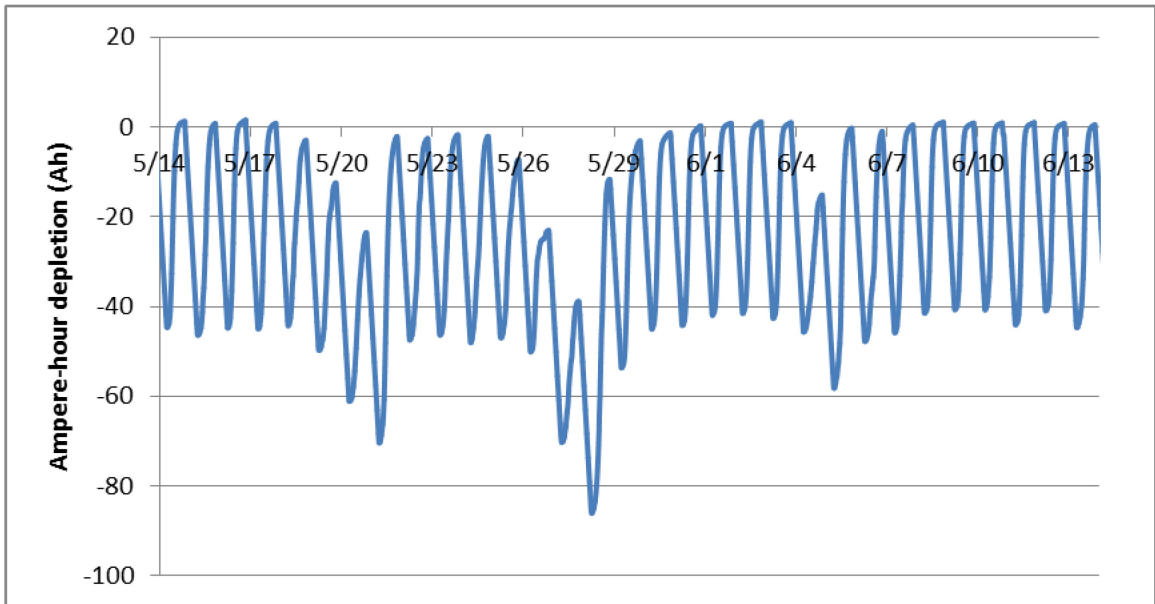


Figure 77: Experimental ampere hour depletion

For better comparison, average of charging and discharging cycles for both simulation and experimental data is tabulated in Table 28.

Table 28: Monthly average of columbic capacity (Ah)

	Simulation	Experimental
Charge (Ah)	42.13	44.12
Discharge		
Columbic capacity (Ah)	43.60	44.19

Additionally, frequency distribution of columbic capacity of each charging and discharging cycles for simulation and experimental data are presented in Figure 78.

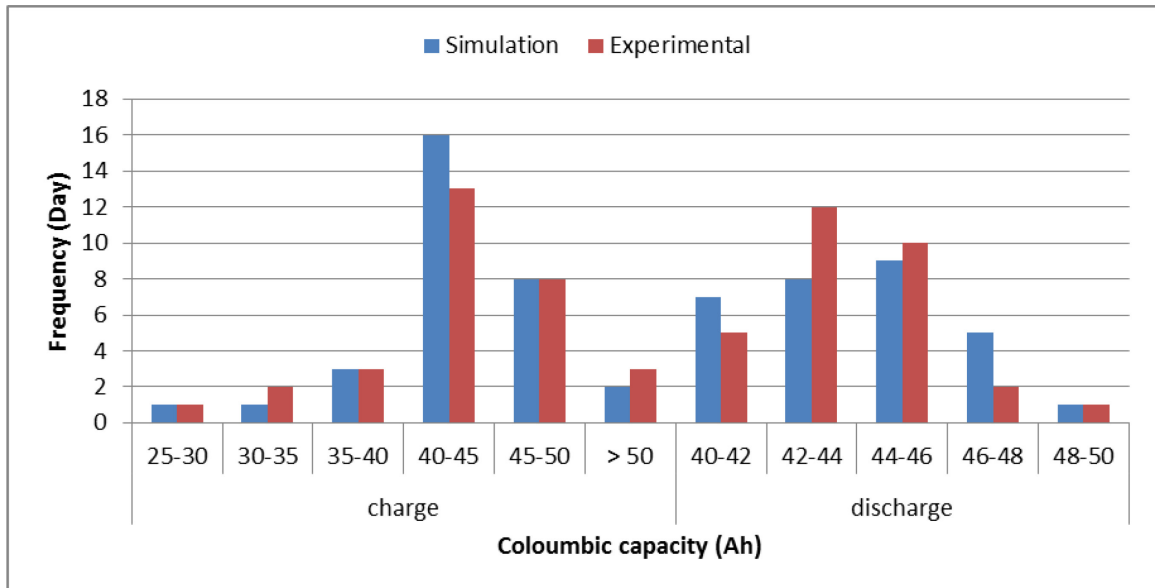


Figure 78: Frequency distribution for charging and discharging cycles

As it is presented in histogram, both data sets have almost similar frequency distribution during test period from May 14th to June 14th. Taking into account all these comparison, TRNSYS model is capable of accurately predicting system performance. TRNSYS database uses average values for estimating climatic conditions of selected site; Thereby error between simulated and measured values in similar dates is completely probable. The model has more reliable estimation for system performance in longer period of time (e.g. monthly average of columbic capacity for charge and discharge). As it mentioned

earlier, the model has capability to predict system behavior at any selected site by using TRNSYS weather database. So, for model evaluation instead of using measured value from pyranometer or installed thermocouples, TRNSYS weather database was used for providing input data.

5.1 SIMULATED PERFORMANCE FOR VARIOUS CONFIGURATIONS

According to achieved data from running the simulation for whole year, the selected configuration is not appropriate for Halifax. System works appropriately without any failure throughout April to the end of September. During November, December and January, produced electricity is insufficient to accommodate required load for night hours. In February and October, selected configuration is not capable of keeping light on until dawn time for 19 nights. And finally, simulation model estimates just 7 failures for March. The total number of hours that system is not capable of keeping light on during night hours is 1286 hours. Second type of failure occurs, when batteries are fully charged and charge controller does not allow for extra charging. Model accurately estimates the amount of curtailed energy by subtracting battery input current from maximum PV output current. October is a good example for exhibiting system failure; Figure 79 shows battery current and voltage profile for this month. After October 9th stored energy is not sufficient for feeding the LED during whole night, which results failure. The amount of stored energy during day hours provides required energy for 6 to 8 hours of LED operation while whole night is approximately 15 hours.

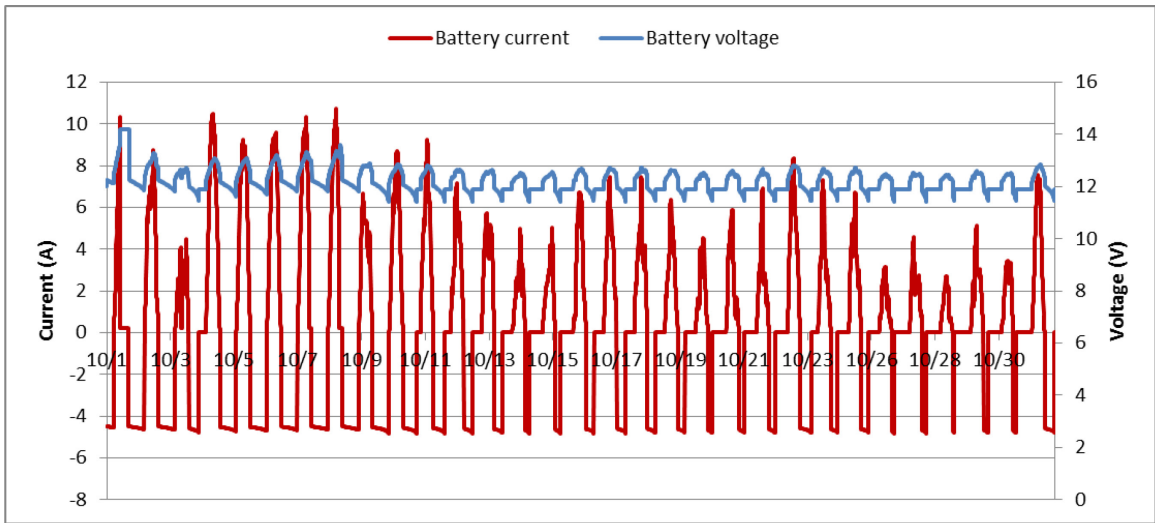


Figure 79: Simulated battery current-voltage profile (October 1-31)

For better judgment, the ampere hour depletion diagram for October is presented in Figure 80. As can be seen after October 15th, the discharged energy during night cannot be replaced completely which leads to failure.

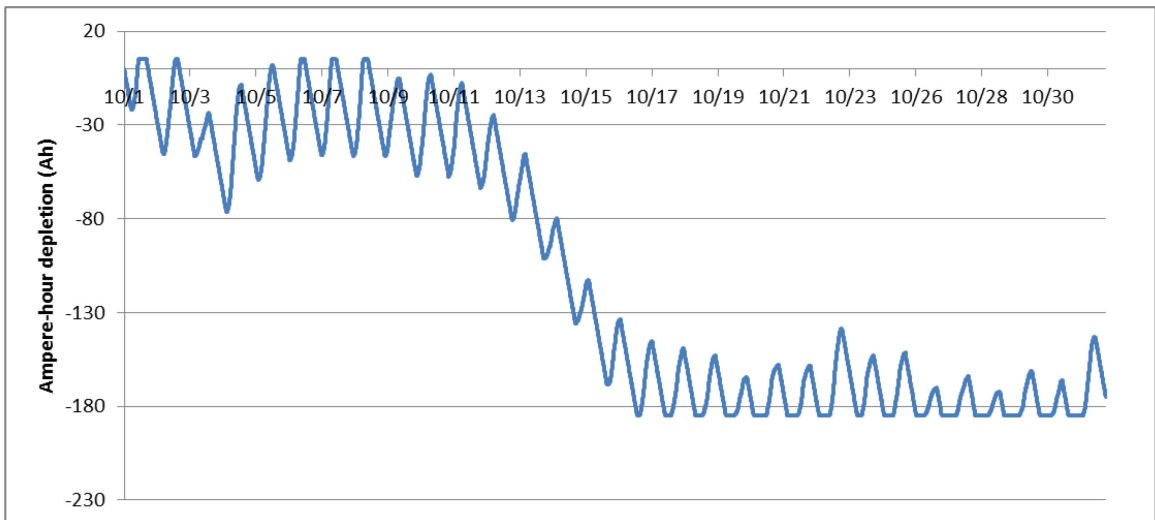


Figure 80: Simulated ampere-hour depletion (October 1-31)

As can be seen in Figure 80, selected configuration is not appropriate for October and during second half of the month, electricity production is not sufficient to keep the LED on over the night. To decrease the number of failures, two different configurations were simulated and the results are presented in Figure 81. Information related to these new configurations is tabulated in Table 29.

Table 29: PV and battery size for new configurations

System Number	PV size	Battery bank
1	405 W	250 Ah-12 V
2	405 W	375 Ah-12 V

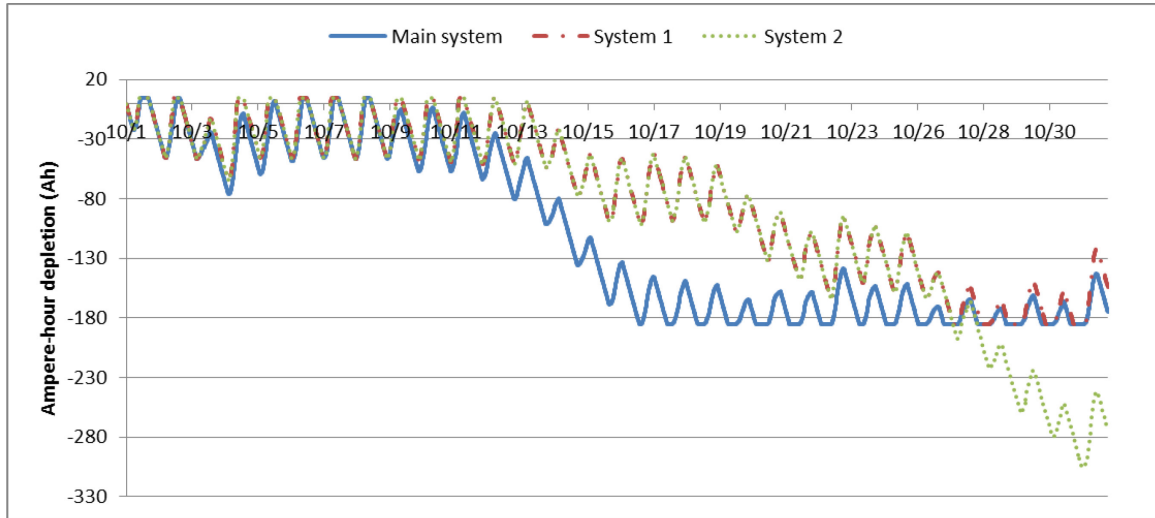


Figure 81: Comparison of simulated ampere-hour depletion (October 1-31)

As it is seen in Figure 81, system 1 reduces the number of failures from 19 to 6 with the same size of battery, by increasing the total power of PV panels, from 270 W to 405 W. Additionally, providing more back up energy for system through increasing the capacity of battery bank to 375 Ah, leads to 0 failure during October. Various configurations were simulated in order to investigate appropriate size for system components to minimize the number of failures. By increasing the capacity of battery bank to 375 Ah and total power of PV arrays to 675 W, number of failures decreases to 46. By adding another 135 W PV array, the number of failures reaches to 28 nights.

5.2 SIMULATED PERFORMANCE FOR VARIOUS LOCATIONS

As it mentioned before the model has capability to simulate solar street light performance with various size of PV and battery bank at different locations. Two sites with different climatic conditions and number of sunny days were selected for simulating system

performance with various configurations. Failure occurs when charge controller turns off the LED lamp due to low battery state of charge (SOC < 0.2). The first location is Doha, Qatar; the information related to this site is tabulated in Table 30 [104, 105].

Table 30: Site and weather information for Doha, Qatar [104, 105]

Location	Qatar
Latitude	25.2867° N
Longitude	51.5333° E
Elevation	13 m
Average high temperature	41 °C
Average low temperature	14 °C
Yearly PV potential (kWh/kW)	5223

For better judgment, the monthly maximum electricity production, required electricity for LED lamp and columbic capacity for charge and discharge of system with 270 W PV panel and 3000 Wh battery are presented in Figure 82.

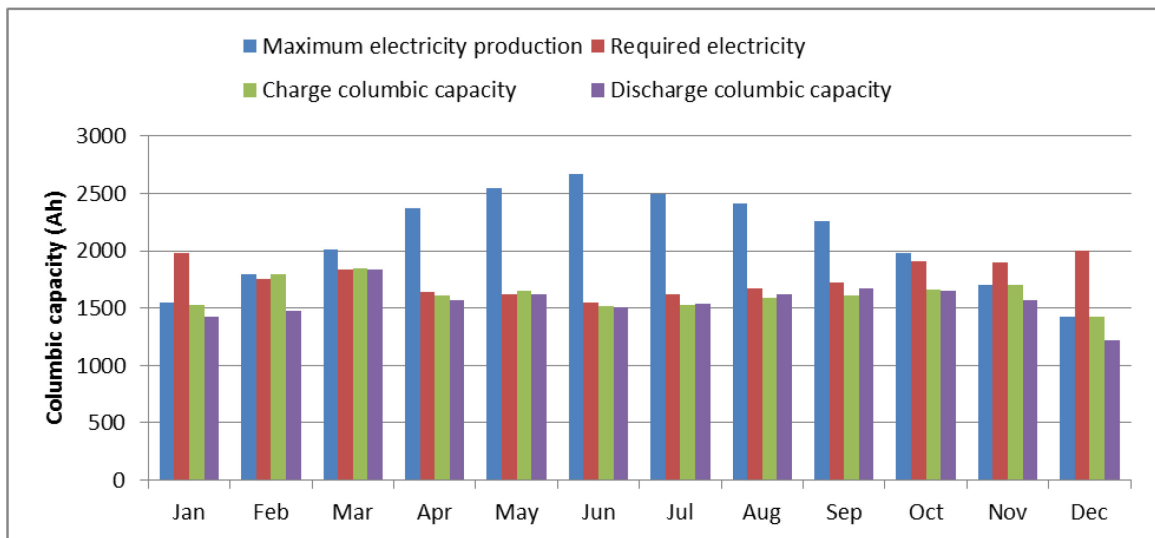


Figure 82: Monthly columbic capacity of charge-discharge (Qatar)

The second site as representative of cold weather with low number of sunny day is Montreal, Canada. For better judgment about this city, corresponding information are provided in Table 31 [104, 106].

Table 31: Site and weather information for Montreal, Canada [104, 106]

Location	Montreal
Latitude	45.5° N
Longitude	73.5667° W
Elevation	233 m
Average high temperature	26 °C
Average low temperature	-14 °C
Yearly PV potential (kWh/kW)	1185

The monthly maximum electricity production, required electricity for LED lamp and columbic capacity for charge and discharge of system with 405 W PV panel and 3000 Wh battery are presented in Figure 83.

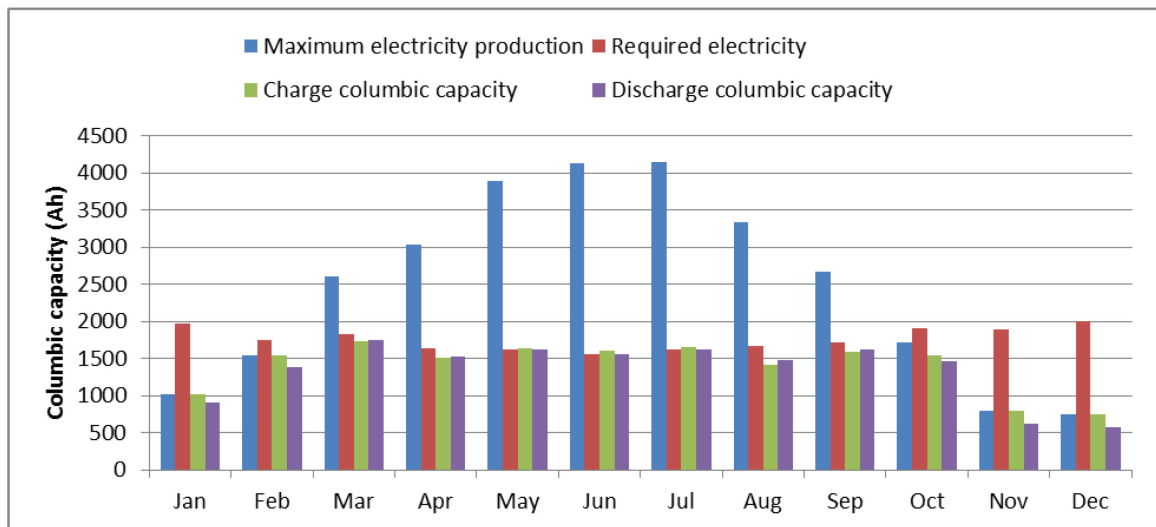


Figure 83: Monthly columbic capacity of charge-discharge (Montreal)

The estimated numbers of failures for different size of PV and battery bank for Montreal and Doha are tabulated in Tables 32 and 33 respectively. It is worth mentioning that for

increasing system efficiency and decreasing number of failures it is possible to turn on portion of LED lamps during certain night.

Table 32: Failure matrix for various configurations (Qatar)

PV Power	Battery Energy (Wh)			
	1500	3000	4500	6000
135 W	229	220	214	207
270 W	46	28	15	11
405 W	3	0	0	0
540 W	0	0	0	0
675 W	0	0	0	0
810 W	0	0	0	0
945 W	0	0	0	0

Table 33: Failure matrix for various configurations (Montreal)

PV Power	Battery Energy (Wh)			
	1500	3000	4500	6000
135 W	270	262	258	249
270 W	152	146	138	133
405 W	123	97	95	95
540 W	93	88	83	79
675 W	77	72	67	59
810 W	53	47	39	31
945 W	24	14	8	0

CHAPTER 6 CONCLUSION AND RECOMMENDATIONS

Due to unique features and availability of solar energy, PV technology has grown rapidly and become popular all over the world. Standalone (Off-grid) photovoltaic systems are appropriate solution for area with no access to national electricity grid. Off-grid PV solar street light can be specified for different purposes including: roadway, parking spot and portable lighting. Owing to site dependency feature of solar systems, modelling and simulation is necessary to investigate dynamic performance of components. Each system should be customized for the light, battery, PV and control parameters to certain lighting requirements, site location and weather conditions.

In this research an off-grid solar street light model was developed using TRNSYS 17 and MATLAB software. An off-grid solar street light comprised of PV arrays (2×135 W), lead acid batteries (2×250 Ah.6V), charge controller (MPPT system), LED lamp (55 W) was installed and monitored through a data acquisition system. The typical off-grid solar street light components were modeled in TRNSYS software using combination of existing TRNSYS libraries, modified or self-coded components. At every time step each component will send to or/and receive data from its connected components. TRNSYS weather database simulates climatic conditions for various locations through the world in order to estimates system performance under real operating conditions. Failure occurs when stored energy in batteries is not sufficient to accommodate the lighting load during low solar-illumination hours (failure to provide). Optimized design could be achieved based on minimum number of failure. Data logger was set to records 8 parameters including: voltage and current of PV and battery components, ambient temperature, PV, battery and box temperature every 6 seconds. Model verification was carried out by comparing simulation results against measured values.

6.1 CONCLUSION

This study developed the model for estimating the performance of off-grid solar street lighting system for different locations over the world. The model reliability was evaluated by comparing measured and simulated values of system performance for

installed setup at Halifax, NS during May 14th to June 14th. Following conclusions are drawn from this comparison:

- Selected sealed lead-acid battery type is appropriate for this application and performed well throughout the test however the battery capacity is not sufficient for accommodating required energy for the load at Halifax.
- Based on wattage used by LED lamp and battery columbic capacity, fully charged battery is sufficient for approximately 50 hours of autonomy in absence of any charge.
- The provided PV panels are capable of providing sufficient charge (42-70 Ah) to keep the LED on, over the night hours indefinitely given sunny and hazy solar days. Charging columbic capacity (Ah) on cloudy days limited to 20-25 Ah which is not adequate to replace the entire utilized energy on the previous night. But will be replaced in a subsequent sunny day.
- According to adjusted charging strategy, charge controller should end absorption (Acceptance charging stage) based on preset time limit (2 hours). As can be seen from battery voltage profile, apart from 4 cycles during test period, charge controller cannot start float charging stage after 2 hours. It happens since charge controller cannot sustain the preset voltage across the battery and controller converts to bulk mode and reset the timer. Consequently shunt/IPN pro remote should be coupled with charge controller for controlling the duration of absorption stage.
- Ambient, box and battery temperature have the same trend during test and the temperature inside the box always remains higher than ambient temperature in both charging and discharging cycles. However the maximum recorded ambient temperature is 26.7 °C, the temperature of PV panels reach to 50 °C.
- Light controlling function of charge controller, which is working based on PV output current performed well in switching the light on/off as required.
- Similar to other battery models, in the Copetti equations, input current is the most effective parameter which affects battery voltage. Due to notable fluctuation in PV output current during noon, difference exists between simulation and

experimental results for battery voltage. The battery component MATLAB code was modified to avoid sudden surge and rise in battery voltage. Due to almost constant discharge current, acceptable match exists between estimated and measured battery voltage during discharging cycles.

- Comparing between monthly average results for PV output ampere hours, shows up to 5 % differences among simulation and experimental results. The simulation model estimates the amount of discharge ampere hour with less than 2 % error compared to measured values.
- Based on simulation results, selected configuration is not appropriate for Halifax locations during the period of October-February. Apart from seven nights in March when the LED street light would only be lit for the first half of the night, selected configuration performs well in the rest of the year.

6.2 SUMMARY OF CONTRIBUTION

No evidence exists in literature about comprehensive model for performance analyses of off-grid solar street light at difference locations over the world. Following are the key contributions this research has made.

- The TRNSYS model has capability to predict system performance with selected configurations (size and number of PV and battery module) throughout the world.
- A new measurement board was designed and built with capability to monitor and record performance of any battery based off-grid street light system.
- A new battery component based on Copetti equations was developed in MATLAB which is compatible with any TRNSYS modeling. The new model considers ambient temperature of battery as effective parameter in estimating battery available capacity and voltage.
- The new solar charge controller component was coded in MATLAB in order to operate according to three stage charging algorithms. Present charge controller components in TRNSYS library act as on/off switches which are not appropriate for modeling the constant-power/constant-voltage of real charge controller operation.

6.3 RECOMMENDATIONS

From the outcomes of the study, it is suggested that the following recommendations would help to improve the model:

- The battery model can be calibrated for specific type of battery in order to achieve more accurate results.
- Model should be evaluated for longer period in order to investigate its reliability for estimating system performance during winter.
- Improving the simulation model to incorporate battery aging and degradation of other component to analyze system cost and predict system life span for different configurations.

6.4 FUTURE RESEARCH

- Performance analyses of charge controller in order to identify appropriate voltage set points for charging process.
- Collect the solar radiation data by installing pyranometers for evaluating the simulation model with realistic data.
- Generating world map for optimized configuration of off-grid solar street light
- Developing new standard for designing and selecting appropriate components for selected location throughout the world.

Reference

- [1] M. Mutmansky, T. Givler, J. Garcia and N. Clanton, "Advanced Street Lighting Technologies Assessment Project," San Diego Gas & Electric, San Diego, 2010.
- [2] "<http://www.savcosolar.com/lighting.html>," [Online]. [Accessed 21 March 2014].
- [3] TRNSYS, "<http://sel.me.wisc.edu/trnsys/user17-resources/index.html>," TRNSYS 17 manual, Solar Energy Lab, Madison, 2009. [Online]. [Accessed 17 June 2014].
- [4] W. De Soto, S. Klein and W. Beckman, "Improvement and validation of a model for photovoltaic array performance," *Solar Energy*, vol. 80, p. 78–88, 2006.
- [5] C. Shepherd, "Design of Primary and Secondary Cells II. An Equation Describing Battery Discharge," *Electrochemical Society*, vol. 112, p. 657, 1965.
- [6] P. R. Boyce, "Road Lighting Standards," in *Lighting for driving*, Boca Raton, FL, CRC Press, 2009, pp. 91-96.
- [7] R. Williams, "Becquerel Photovoltaic Effect in Binary Compounds," *Chemical Physics*, vol. 32, no. 5, pp. 1505-1514, 1960.
- [8] E. Becquerel, "Mémoire sur les effets électriques produits sous l'influence des rayons solaires," *Comptes Rendus*, vol. 9, pp. 561-567, 1839.
- [9] W. Smith, "Effect of Light on Selenium During the Passage of an Electric Current," *Nature*, vol. 7, no. 173, p. 303, 1873.
- [10] W. Adams and R. Day, "The action of light on selenium," *Proceedings of the Royal Society*, vol. A25, p. 115, 1877.
- [11] "According to Marius Paulescu and others Weather Modeling and Forecasting of PV System Operations," *Springer Verlag*, no. 1, 2013.

- [12] A. Einstein, "Über einen die Erzeugung und Verwandlung des Lichtes betreffenden heuristischen Gesichtspunkt (On a Heuristic Viewpoint Concerning the Production and Transformation of Light)," *Annalen der Physik*, vol. 17, no. 6, p. 132–148, 1905.
- [13] "The Nobel Prize in Physics 1921," 5 October 2008.
- [14] "April 25, 1954: Bell Labs Demonstrates the First Practical Silicon Solar Cell," *APS News (American Physical Society)*, vol. 18, no. 4, April 2009.
- [15] D. Chapin, C. Fuller and G. Pearson, "A New Silicon p-n Junction Photocell for Converting Solar Radiation into Electrical Power," *Applied Physics*, vol. 25, no. 5, p. 676–677, May 1954.
- [16] "http://en.wikipedia.org/wiki/Timeline_of_solar_cells," 05 June 2014. [Online].
- [17] "1962-ALPHA EPSILON 1," US Space Objects Registry.
- [18] "<http://www.fsec.ucf.edu/>," [Online]. [Accessed 07 June 2014].
- [19] "http://www.vintagecalculators.com/html/calculator_time-line.html," [Online]. [Accessed 07 June 2014].
- [20] J. Eilperin, "White House goes solar," Washington Post, 2010.
- [21] B. Plumer, "Are we wildly underestimating solar and wind power?," The Washington Post.
- [22] "http://en.wikipedia.org/wiki/Growth_of_photovoltaics," [Online]. [Accessed 09 June 2014].
- [23] I. Kaminska, "The exponential growth in solar consumption," The financial Times Ltd., 2012.

- [24] R. Kurzweil, "Climate change no problem, says futurist Ray Kurzweil," *The Guardian*, 2011.
- [25] "http://en.wikipedia.org/wiki/Photovoltaic_system," [Online]. [Accessed 12 June 2014].
- [26] U. Jahn, D. Mayer, M. D. R. Heidenreich, S. Castello, L. Clavadetscher, A. Frolich, B. Grimmig, W. Nasse, K. Sakyta, T. Sugiura, N. van der Brog and K. van Otterdijk, "Analysis of the operational performance of the IEA database PV systems," in *16th European Photovoltaic Solar Energy Conference and Exhibition*, Glasgow, United Kingdom, 2000.
- [27] A. Celik, T. Muneer and P. Clarke, "Optimal sizing and life cycle assessment of residential photovoltaic energy systems with battery storage," *Progress in Photovoltaics*, vol. 16, no. 1, pp. 69-85, 2008.
- [28] K. Bucher, "Site dependence of the energy collection of PV modules," *Solar Energy Materials and Solar Cells*, vol. 47, pp. 85-94, 1997.
- [29] V. Svoboda, H. Wenzl, R. Kaiser, A. Josse, I. Baring-Gould, J. Manwell, P. Lundsager, H. Bindner, T. Cronin, P. Norgard, A. Ruddell, A. Perujo, K. Douglass, C. Rodrigues, A. Joyce, S. Tselepsi, N. van der Borg, F. Nieuwenhout and N. Wilmot, "Operating conditions of batteries in off-grid renewable energy systems," *Solar Energy*, vol. 81, no. 11, pp. 1409-1425, 2007.
- [30] M. Gustavsson and D. and Mtonga, "Lead-acid battery capacity in solar home systems - Field tests and experiences in Lundazi, Zambia," *Solar Energy*, vol. 79, no. 5, pp. 551-558, 2005.
- [31] J. Munoz and E. Lorenzo, "On the specification and testing of inverters for standalone PV systems," *Progress in Photovoltaics*, vol. 13, no. 5, pp. 393-408, 2005.

- [32] M. Egido, P. Vega and M. and Horn, "Field evaluation of PV rural electrification project," in *19th European Photovoltaic Solar Energy Conference*, Paris, 2004.
- [33] S. Harrington and J. Dunlop, "Battery Charge Controller Characteristics in Photovoltaic Systems," in *7th Annual Battery Conference on Applications and Advancer*, California, 1992.
- [34] G. W. Vinal, *Storage Batteries*, Fourth Edition ed., John Wiley & Son, 1965.
- [35] H. Kiehne, *Battery Technology Handbook*, First Edition ed., Marcel Dekkar, Inc., 1989.
- [36] D. Linden, *Handbook of Batteries and Fuel Cells*, McGraw-Hil, 1984.
- [37] W. Allen, J. S. Ryba and S. E. Trenchard, "Evaluation of Solar Photovoltaic Energy Storage for Aids," Springfield, VA, 1981.
- [38] "Solar-LED streetlight controller with 25 W LED lamp driver and 85 W battery charger based on the STM32F101Rx," STMicroelectronics on Solar lighting application, 2010.
- [39] "http://batteryuniversity.com/learn/article/charging_the_lead_acid_battery," [Online]. [Accessed 15 May 2014].
- [40] P. Diaz and A. M. Egido, "Experimental analysis of battery charge regulation in photovoltaic systems," *Progress in Photovoltaics*, vol. 11, no. 7, pp. 481-493, 2003.
- [41] J. Stevens, J. Kratochvil and S. Harrington, "Field Investigation of the relationship between battery size and PV system performance," in *Photovoltaic Specialists Conference, Conference Record of the Twenty Third IEEE*, Louisville, KY, 1993.
- [42] "<http://www.morningstarcorp.com/en/support/library/8.%20Why%20PWM1.pdf>," Morningstar Corporation, 2000. [Online]. [Accessed 25 June 2014].

- [43] L. Sanidad, R. Parsons, Y. Baghzouz and R. and Boehm, "Effect of ON/OFF charge controllers on stand-alone PV system performance," in *Energy Conversion Engineering Conference and Exhibit, (IECEC) 35th Intersociety*, Las Vegas, NV, 2000.
- [44] M. Lujano-Rojas, J. R. Dufo-López and L. J. Bernal-Agustín, "Optimal sizing of small wind/battery systems considering the DC bus voltage stability effect on energy capture, wind speed variability, and load uncertainty," *Applied Energy*, vol. 93, pp. 404-412, 2012.
- [45] D. Corbus, C. Newcomb, E. I. Baring-Gould and F. S., "Battery voltage stability effects on small wind turbine energy capture," US National Renewable Energy, 2002.
- [46] W. I. Bower, J. P. Dunlop and C. W. Maytrott, "PERFORMNCE OF BATTERY CHARGE CONTROLLERS: AN INTERIM TEST REPORT," in *Proceedings of the 21st IEEE Photovoltaics Specialists Conference 1990*, Kissimmee, Florida, May 21-25, 1990.
- [47] W. Li, Y. Zheng, W. Li, Y. zhao and Xiangning, "A Smart and Simple PV Charger for Portable Applications," in *Applied Power Electronics Conference and Exposition (APEC), 2010 Twenty-Fifth Annual IEEE*, Palm Springs, CA, 2010.
- [48] N. Achaiboua, M. Haddadib and A. Maleka, "Modeling of lead acid batteries in PV systems," *Energy Procedia*, vol. 18, p. 538 – 544, 2012.
- [49] "http://www.intechopen.com/source/html/42271/media/image6_w.jpg," [Online]. [Accessed 19 August 2014].
- [50] D. Linden and T. Reddy, *Handbook of Batteries*, McGraw-Hill Professional, 2010.
- [51] P. Ruetschi, "Aging mechanisms and service life of lead-acid batteries," in *Presented at Eight Ulmer Electrochemische Tage*, June 20, 2002 - June 21. 2004.

- [52] D. U. Sauer and H. Wenzl, "Batteries lifetime prediction," in *Encyclopedia of electrochemical power sources*, 2009.
- [53] D. Sauer and H. Wenzl, "Comparison of different approaches for lifetime prediction of electrochemical systems-using lead-acid batteries as example," *Power Sources*, vol. 176, no. 2, pp. 534-546, 2008.
- [54] J. B. Copetti, L. Lorenzo and F. Chenlo, "A general Battery Model for PV System Simulation," *Progress in Photovoltaic Research and Application*, vol. 1, pp. 283-292, 1993.
- [55] J. F. Manwell and J. G. McGowan, "Lead acid battery storage model for hybrid energy systems," *Solar Energy*, vol. 50, no. 5, p. 399-405, 1993.
- [56] J. F. Manwell, A. Rogers, G. Hayman, C. T. Avelar, J. G. McGowan and U. Abdulwahid, "Hybrid2 – a hybrid system simulation model. Theory manual," University of Massachusetts and US National Renewable Energy Laboratory, 2006.
- [57] T. Lambert, P. Gilman and P. Lilienthal, "Micropower system modeling with HOMER," in *Integration of alternative sources of energy*, S. M. Farret FA, Ed., John Wiley & Sons, Inc, 2006, p. 379-418.
- [58] R. Dufo-López, J. L. Bernal-Agustín, J. M. Yusta-Loyo, J. A. Domínguez-Navarro, I. J. Ramírez-Rosado and J. Lujano, "Multi-objective optimization minimizing cost and life cycle emissions of stand-alone PV-wind-diesel systems with batteries storage.," *Appl Energy*, vol. 88, no. 11, p. 4033-4041, 2011.
- [59] S. CM, "Design of primary and secondary cells II. An equation describing battery discharge," *Electrochem Soc*, vol. 112, no. 7, p. 657-664, 1965.
- [60] C. Protopoulos, R. Marshall and B. J. Brinkworth, "Battery state of voltage modelling and an algorithm describing dynamic conditions for long-term storage simulation in a renewable system," *Solar Energy*, vol. 53, no. 6, p. 517-527, 1994.

- [61] J. N. Ross, T. Markvart and W. He, "Modelling battery charge regulation for a stand-alone photovoltaic system," *Solar Energ*, vol. 69, no. 3, p. 181–190, 2000.
- [62] J. Schiffer, D. U. Sauer, H. Bindner, T. Cronin, P. Lundsager and R. Kaiser, "Model prediction for ranking lead–acid batteries according to expected lifetime in renewable energy systems and autonomous power-supply systems.," *Power Sources*, vol. 168, no. 1, p. 66–78, 2007.
- [63] J. B. Copetti and F. Chenlo, "Lead/acid batteries for photovoltaic applications. Test results and modeling," *Power Sources*, vol. 47, no. 1-2, p. 109–118, 1994.
- [64] "<http://www.eskimo.com/~jrterry/lampspage.html>," [Online]. [Accessed 07 July 2014].
- [65] "<http://ecostreetlighting.com/types-of-lamps-used-in-street-lights.html>," [Online]. [Accessed 07 July 2014].
- [66] "<http://www.konarka.com>," Konarka Power Plastic, 2011. [Online]. [Accessed 08 July 2014].
- [67] K. Webdesign, "<http://citace.com/generator.php>," Citace 2.0 : vše o citování literatury a dokumentů, 2009. [Online]. [Accessed 08 July 2014].
- [68] "http://en.wikipedia.org/wiki/LED_lamp," [Online]. [Accessed 09 July 2014].
- [69] "<http://www.grahlighting.eu/learning-centre/street-lighting-technology-comparison>," [Online]. Available: 10. [Accessed July 2014].
- [70] J. D. Bollinger, *APPLICATIONS OF SOLAR ENERGY TO POWER STAND-ALONE AREA AND STREET LIGHTING*, UNIVERSITY OF MISSOURI-ROLLA, 2007.
- [71] S. Harrington and T. Hund, "Photovoltaic Lighting System Performance," in *Twenty fifth IEEE Photovoltaic Specialists Conference*, May 1996.

- [72] "http://en.wikipedia.org/wiki/Leadacid_battery," Wikipedia : the free encyclopedia, 2010. [Online]. [Accessed 23 May 2014].
- [73] P. Boldis, "<http://www.boldis.cz/citace/citace.html>," Bibliografické citace dokumentů podle ČSN ISO 690 a ČSN ISO 690-2, 2001. [Online]. [Accessed 23 May 2014].
- [74] "<http://www.nalanda.nitc.ac.in/industry/appnotes/Texas/analog/slua017.pdf>," Using the bq2031 to Charge Lead-Acid Batteries, 19 7 2011. [Online]. [Accessed 25 May 2014].
- [75] A. Mellita, M. Benghanemb, A. Hadj Arab and A. Guessoum, "An adaptive artificial neural network model for sizing stand-alone photovoltaic systems: application for isolated sites in Algeria," *Renewable Energy*, vol. 30, p. 1501–1524, 2005.
- [76] A. Mellita, M. Benghanemb and S. A. Kalogirou, "Modeling and simulation of a stand-alone photovoltaic system using an adaptive artificial neural network: Proposition for a new sizing procedure," *Renewable Energy*, vol. 32, p. 285–313, 2007.
- [77] A. Mellita and M. Benghanemb, "Sizing of stand-alone photovoltaic systems using neural network adaptive model," *Desalination*, vol. 209, p. 64–72, 2007.
- [78] J. Lagorse, S. Giurgea, D. Paire, M. Cirrincione and M. G. a. M. A. Simoes, "Optimal Design Analysis of a Stand-Alone Photovoltaic Hybrid System," in *Industry Applications Society Annual Meeting, 2008. IAS '08. IEEE*, Edmonton, Alta. , 2008.
- [79] J. Lagorse, D. Paire and A. Miraoui, "Sizing optimization of a stand-alone street lighting system powered by a hybrid system using fuel cell, PV and battery," *Renewable Energy*, vol. 34, p. 683–691, 2009.

- [80] A. Mellita, S. A. Kalogiroub and M. Drif, "Application of neural networks and genetic algorithms for sizing of photovoltaic systems," *Renewable Energy*, vol. 35, pp. 2881-2893, 2010.
- [81] M. A. D. Costa, G. H. Costa, A. S. Santos, I. Schuch and J. R. Pinheiro, "A HIGH EFFICIENCY AUTONOMOUS STREET LIGHTING SYSTEM BASED ON SOLAR ENERGY AND LEDES," in *Power Electronics Conference, 2009. COBEP '09. Brazilian*, Bonito-Mato Grosso do Sul , Sept. 27 2009-Oct. 1 2009 .
- [82] S. Nunoo, J. C. Attachie and C. K. Abraham, "Using Solar Power as an Alternative Source of Electrical Energy for Street Lighting in Ghana," in *Innovative Technologies for an Efficient and Reliable Electricity Supply (CITRES), 2010 IEEE Conference on*, Waltham, MA, 2010.
- [83] "Photovoltaics: Design and Installation Manual," New Society Publishers, Gabriola Island, BC, 2007.
- [84] "Stand-alone Power Systems Part 2: System Design Guidelines," AS 4509.2, 2002.
- [85] R. N. Chapman, "A simplified technique for designing least cost stand-alone PV/storage systems," in *19th IEEE Photovoltaic Specialists Conference*, New Orleans, 1987.
- [86] "Battery-Based Solar Photovoltaics Systems-code of Practice," Malawi Standards Board, Blantyre, 2004.
- [87] "<http://meteonorm.com/en/site/downloads?/download/maps/>," [Online]. [Accessed 12 April 2014].
- [88] "http://www.iac.ethz.ch/groups/schaer/research/rad_and_hydro_cycle_global/geba/," [Online]. [Accessed 12 April 2014].
- [89] "http://www.wmo.int/pages/index_en.html," [Online]. [Accessed 14 April 2014].

- [90] "<http://www.meteoswiss.admin.ch/web/en.html>," [Online]. [Accessed 15 April 2014].
- [91] P. G. Loutzenhiser, H. Manz, C. Felsmann, P. A. Strachan, T. Frank and G. M. Maxwell, "Empirical validation of models to compute solar irradiance on inclined surfaces for building energy simulation," *Solar Energy*, vol. 81, p. 254–267, 2007.
- [92] D. King, J. Kratochvil, W. Boyson and W. Bower, "Field Experience with a New Performance Characterization Procedure for Photovoltaic Arrays," in *The 2nd World Conference and Exhibition on Photovoltaic Solar energy Conversion*, Vienna, Austria, 1998 July 6–10.
- [93] D. King, "Sandia's PV Module Electrical Performance Model (Version, 2000)," in *Sandia National Laboratories*, Albuquerque, NM, 2000 September 5.
- [94] W. De Soto, *Improvement and validation of a model for photovoltaic array performance*, Mechanical Engineering, University of Wisconsin-Madison, 2004.
- [95] "<http://www.sandia.gov/pv/docs/Database.htm>," Sandia National Laboratories, 2002. [Online]. [Accessed 27 April 2014].
- [96] J. Duffie and W. Beckman, *Solar Engineering of Thermal Processes*, second ed., New York: John Wiley & Sons Inc., 1991.
- [97] J. Nelson, *The Physics of Solar Cells*, London: Imperial College Press, 2003.
- [98] R. Messenger and J. Ventre, *Photovoltaic Systems Engineering*, second ed., Boca Raton, FL: CRC Press LLC, 2004.
- [99] "http://ece-www.colorado.edu/~bart/book/book/chapter2/ch2_3.htm," *Principles of Semiconductor Devices*, 2004. [Online]. [Accessed 14 March 2014].
- [100] A. L. Bishop, "The effect of temperature on battery life," CALIFORNIA STATE SCIENCE FAIR, California, 2005.

- [101] "solarpowerplanetearth.com," [Online]. [Accessed 10 August 2014].
- [102] "http://www.ledroadwaylighting.com/about-us/company-overview.html," Roadway Lighting Company, 2002. [Online]. [Accessed 20 August 2014].
- [103] "http://www.campbellsci.ca/cr1000," Campbell Scientific Company. [Online]. [Accessed 20 August 2014].
- [104] "http://weatherspark.com," [Online]. [Accessed 08 August 2014].
- [105] "http://eeg.tuwien.ac.at/eeg.tuwien.ac.at_pages/events/iewt/iewt2013/uploads/presentation/Pr_35_Panzer_Christian.pdf," [Online]. [Accessed 08 August 2014].
- [106] "http://pv.nrcan.gc.ca," [Online]. [Accessed 08 August 2014].

APPENDIX A DETAILED SIMULATION AND MEASURED RESULTS

Table 34: PV daily maximum current, voltage and power

May	14th	15th	16th	17th	18th	19th	20th	21st	22nd
Current (A)	12.46	13.78	12.42	11.95	13.08	9.81	6.64	13.79	16.54
Voltage (V)	20.8	20.44	19.96	20.29	19.6	18.54	18.49	20.20	21.01
Power (W)	187.47	225.17	185.14	192.75	204.83	163.04	113.40	207.13	280.88

Table 35: PV daily maximum current, voltage and power

May	23rd	24th	25th	26th	27th	28th	29th	30th	31st
Current (A)	9.23	7.966	13.29	8.59	8.31	21.12	11.51	10.89	11.78
Voltage (V)	19.78	19.75	20.09	18.24	17.93	20.53	20	20.29	20.85
Power (W)	157.31	127.41	224.47	142.97	139.19	319.38	177.93	172.14	178.53

Table 36: PV daily maximum current, voltage and power

June	1st	2nd	3rd	4th	5th	6th	7th	8th
Current (A)	11.74	11.84	12.11	4.8	15.38	16.99	17.19	12.01
Voltage (V)	20.32	20.9	20.5	18.04	20.4	20.34	21.33	20.28
Power (W)	177.73	177.64	185.70	80.31	227.71	286.96	285.90	183.24

Table 37: Daily maximum current, voltage and power

June	9st	10th	11th	12th	13th	14th	15th	16th
Current (A)	12.38	12.03	14.01	11.36	17.02	4.153	17.01	19.87
Voltage (V)	20.76	20.36	20.15	20.64	20.52	18.42	18.25	18.89
Power (W)	190.34	178.02	222.20	171.21	262.61	68.60	269.60	297.05

Table 38: Daily produced Ah by PV

May	14th	15th	16th	17th	18th	19th	20th	21st	22nd
Produced electricity (Ah)	39.27	40.46	40.25	39.1	35.34	32	31.47	57.61	39.21

Table 39: Daily produced Ah by PV

May	23rd	24th	25th	26th	27th	28th	29th	30th	31st
Produced electricity (Ah)	37.25	38.77	33.97	23.80	26.71	62.66	41.94	37.50	38.44

Table 40: Daily produced Ah by PV

June	1st	2nd	3rd	4th	5th	6th	7th	8th
Produced electricity (Ah)	36.86	36.96	37.56	26.59	50.21	41.09	39.15	36.91

Table 41: Daily produced Ah by PV

June	9st	10th	11th	12th	13th	14th	15th	16th
Produced electricity (Ah)	36.57	37.23	38.94	36.51	39.29	16.72	29.34	56.97

Table 42: Maximum current & power during charging and discharging

	May	14th	15th	16th	17th	18th	19th	20th	21st	22nd
Charge	Current (A)	12.77	14.91	12.48	13.45	14.23	11.41	8.21	14.78	18.41
	Power (W)	179.93	209.63	177.98	184.4	195.38	157	109.11	207.13	280.88
Discharge	Current (A)	4.77	4.77	4.77	4.8	4.8	4.84	4.84	4.84	4.77
	Power (W)	58.72	58.76	58.65	58.88	58.43	59.01	58.89	58.84	58.76

Table 43: Maximum current & power during charging and discharging

	May	23rd	24th	25th	26th	27th	28th	29th	30th	31st
Charge	Current (A)	11.27	9.02	15.44	10.15	10.05	21.29	11.89	11.74	12.01
	Power (W)	157.31	127.41	224.47	142.97	139.19	319.38	177.93	172.14	178.53
Discharge	Current (A)	4.77	4.81	4.81	4.84	4.87	4.91	4.81	4.77	4.77
	Power (W)	58.84	58.90	59.02	59.07	59.01	59.15	59.08	58.84	58.86

Table 44: Maximum current & power during charging and discharging

	June	1st	2nd	3rd	4th	5th	6th	7th	8th
Charge	Current (A)	11.95	12.01	12.55	5.889	15.82	18.93	18.79	12.35
	Power (W)	177.73	177.64	185.70	80.31	227.71	286.96	285.90	183.24
Discharge	Current (A)	4.81	4.77	4.77	4.77	4.8	4.77	4.77	4.77
	Power (W)	58.97	58.88	58.87	58.84	58.77	58.91	58.81	58.98

Table 45: Maximum current & power during charging and discharging

		June	9st	10th	11th	12th	13th	14th	15th	16th
Charge	Current (A)		12.34	12.1	14.11	12	17.53	5.00	19.02	20.18
	Power (W)		190.34	178.02	222.20	171.21	262.62	68.61	269.61	297.06
Discharge	Current (A)		4.77	4.77	4.77	4.77	4.77	4.77	4.84	4.87
	Power (W)		58.79	58.79	58.91	58.80	58.85	58.87	58.84	58.99

Table 46: Initial and final voltage for charge and discharge cycles

		May	14th	15th	16th	17th	18th	19th	20th	21st	22nd
Charge	Voltage (V) Initial		12.45	12.43	12.45	12.45	12.43	12.41	12.35	12.27	12.48
	Voltage (V) Final		14.41	14.55	14.54	14.65	14.53	13.76	13.29	14.4	14.67
Discharge	Voltage (V) Initial		12.87	12.86	12.85	12.72	12.87	12.88	12.8	12.78	12.9
	Voltage (V) Final		12.25	12.22	12.26	12.25	12.25	12.17	12.14	12.08	12.3

Table 47: Initial and final voltage for charge and discharge cycles

		May	23rd	24th	25th	26th	27th	28th	29th	30th	31st
Charge	Voltage (V) Initial		12.47	12.43	12.39	12.37	12.3	12.2	12.42	12.48	12.47
	Voltage (V) Final		14.45	14.52	14.6	13.53	13.31	14.72	14.51	14.4	14.54
Discharge	Voltage (V) Initial		12.85	12.88	12.8	12.8	12.7	12.63	12.82	12.85	12.81
	Voltage (V) Final		12.27	12.22	12.22	12.17	12.09	11.99	12.26	12.3	12.26

Table 48: Initial and final voltage for charge and discharge cycles

	June	1st	2nd	3rd	4th	5th	6th	7th	8th
Charge	Voltage (V)	12.45	12.46	12.47	12.45	12.37	12.47	12.47	12.47
	Initial								
	Voltage (V)	14.46	14.59	14.69	13.3	14.62	14.88	14.81	14.33
	Final								
Discharge	Voltage (V)	12.83	12.83	12.81	12.83	12.77	12.85	12.89	12.84
	Initial								
	Voltage (V)	12.26	12.27	12.27	12.26	12.2	12.29	12.29	12.29
	Final								

Table 49: Initial and final voltage for charge and discharge cycles

	June	9st	10th	11th	12th	13th	14th	15th	16th
Charge	Voltage (V)	12.5	12.49	12.46	12.51	12.48	12.47	12.34	12.29
	Initial								
	Voltage (V)	14.55	14.52	14.82	14.58	14.75	13.18	13.44	14.53
	Final								
Discharge	Voltage (V)	12.84	12.82	12.8	12.83	12.81	12.83	12.7	12.49
	Initial								
	Voltage (V)	12.32	12.3	12.28	12.33	12.27	12.29	12.15	12.1
	Final								

Table 50: Columbic capacity (Ah) of discharge and charge cycles

May	14th	15th	16th	17th	18th	19th	20th	21st	22nd
Discharge (Ah)	44.718	46.42	44.836	44.99	44.34	46.799	48.63	46.9	45.37
Charge (Ah)	45.96	47.188	46.36	45.8	41.368	37.295	37.55	68.3	44.92

Table 51: Columbic capacity (Ah) of discharge and charge cycles

May	23rd	24th	25th	26th	27th	28th	29th	30th	31st
Discharge (Ah)	43.79	46.34	44.91	42.88	47.26	47.22	42.03	41.94	42.96
Charge (Ah)	44.67	45.95	39.74	27.15	31.41	74.41	50.56	43.78	44.52

Table 52: Columbic capacity (Ah) of discharge and charge cycles

June	1st	2nd	3rd	4th	5th	6th	7th	8th
Discharge (Ah)	41.96	41.59	42.69	45.71	43.08	47.53	44.91	41.52
Charge (Ah)	42.77	42.71	43.64	30.57	57.94	42.77	46.3	42.55

Table 53: Columbic capacity (Ah) of discharge and charge cycles

June	9st	10th	11th	12th	13th	14th	15th	16th
Discharge (Ah)	40.75	40.75	42.4	41	44.73	43.39	45.11	43.07
Charge (Ah)	41.62	41.65	45.07	41.79	45.2	18.08	33.86	66.45

Table 54: LED operating data

May	14th	15th	16th	17th	18th	19th	20th	21st	22nd
Light ON	20:20	20:17	20:25	20:25	20:21	20:12	19:56	20:04	20:23
Light OFF	5:52	6:14	6:00	6:06	5:50	6:07	6:13	5:58	6:06
Operating hour (hr)	9.53	9.95	9.58	9.68	9.48	9.88	9.28	9.9	9.72
Ah consumption	44.72	46.42	44.84	44.99	44.34	46.8	48.63	46.9	45.37

Table 55: LED operating data

May	23rd	24th	25th	26th	27th	28th	29th	30th	31st
Light ON	20:29	20:22	20:28	20:37	20:17	20:10	20:42	20:40	20:35
Light OFF	6:10	6:19	6:05	5:43	6:28	6:10	5:39	5:39	5:47
Operating hour (hr)	9.68	9.95	9.62	9.1	10.18	10	8.83	8.98	9.2
Ah consumption	43.79	46.34	44.91	42.88	47.26	47.22	42.03	41.94	42.96

Table 56: LED operating data

June	1st	2nd	3rd	4th	5th	6th	7th	8th
Light ON	20:40	20:43	20:35	20:08	20:46	20:10	20:21	20:41
Light OFF	5:39	5:38	5:45	5:58	5:56	6:29	5:59	5:37
Operating hour (hr)	8.98	8.92	9.17	9.83	9.17	10.32	9.63	9.93
Ah consumption	41.96	41.59	42.69	45.71	43.08	47.53	44.91	41.52

Table 57: LED operating data

June	9st	10th	11th	12th	13th	14th	15th	16th
Light ON	20:46	20:46	20:30	20:38	20:28	20:44	20:36	20:30
Light OFF	5:35	5:35	5:35	5:32	6:04	5:34	6:21	5:35
Operating hour (hr)	8.82	8.82	9.8	8.9	9.6	8.83	9.75	9.8
Ah consumption	40.75	40.75	42.4	41	44.73	43.39	45.11	43.07

Table 58: Wattage usage by LED lamp

May	14th	15th	16th	17th	18th	19th	20th	21st	22nd
Min (W)	58.09	58.14	57.93	58.12	58.48	58.25	58.05	58.21	58.09
Average (W)	58.42	58.46	58.28	58.43	58.12	58.59	58.53	58.50	58.43
Maximum (W)	58.72	58.76	58.65	58.88	58.43	59.01	58.89	58.84	58.76

Table 59: Wattage usage by LED lamp

May	23rd	24th	25th	26th	27th	28th	29th	30th	31st
Min (W)	58.00	58.17	58.30	58.27	58.21	58.33	58.24	58.14	58.07
Average (W)	58.44	58.53	58.67	58.70	58.62	58.75	58.66	58.51	58.49
Maximum (W)	58.84	58.90	59.02	59.07	59.01	59.15	59.08	58.84	58.86

Table 60: Wattage usage by LED lamp

June	1st	2nd	3rd	4th	5th	6th	7th	8th
Min (W)	58.27	58.13	58.09	58.19	58.07	58.09	58.15	58.16
Average (W)	58.60	58.50	58.43	58.50	58.40	58.50	58.48	58.57
Maximum (W)	58.97	58.88	58.87	58.84	58.77	58.91	58.81	58.98

Table 61: Wattage usage by LED lamp

June	9st	10th	11th	12th	13th	14th	15th	16th
Min (W)	57.88	58.02	58.15	57.89	58.13	58.14	58.20	58.28
Average (W)	58.35	58.35	58.55	58.35	58.48	58.47	58.50	58.66
Maximum (W)	58.79	58.79	58.91	58.80	58.85	58.87	58.84	58.99

Table 62: PV, ambient, box and battery temperature

Date	Battery temperature (°C)			Ambient temperature (°C)			Box temperature (°C)			PV temperature (°C)		
	Min	Avg	Max	Min	Avg	Max	Min	Avg	Max	Min	Avg	Max
	14-May	11.4	14.5	21.2	4.4	10.9	20.1	7.9	14.0	22.1	1.3	16.2
15-May	10.2	13.3	17.1	8.0	12.0	18.4	9.3	14.0	20.6	7.2	14.8	35.1
16-May	12.6	16.7	21.0	9.9	15.6	24.2	11.9	17.4	24.8	9.8	20.4	45.4
17-May	13.0	15.4	17.6	8.9	12.4	17.6	11.1	15.7	22.6	7.3	18.4	41.2
18-May	9.0	11.7	14.0	6.1	9.0	12.9	7.4	11.1	15.7	6.0	10.5	28.0
19-May	7.1	9.0	10.9	5.4	7.9	13.2	6.4	9.3	14.6	5.3	9.3	20.0
20-May	8.3	9.1	10.3	5.9	7.9	10.2	7.3	9.4	13.0	6.0	9.6	17.7
21-May	7.9	12.6	17.9	6.0	11.4	19.5	7.3	14.4	23.5	6.0	18.1	42.5
22-May	11.3	14.3	18.1	8.7	12.9	20.8	10.2	14.7	23.3	8.8	15.0	36.8
23-May	11.8	13.7	15.7	9.2	11.5	15.8	10.7	13.3	17.8	8.8	12.7	21.8
24-May	9.6	11.6	14.2	5.1	9.4	15.4	6.8	11.3	17.6	5.0	11.2	23.2
25-May	6.9	9.3	11.6	4.7	8.1	12.9	5.8	9.5	14.0	3.1	9.1	21.2
26-May	6.4	8.0	9.5	2.6	6.5	8.7	4.3	8.2	14.0	0.3	7.2	16.8
27-May	8.0	9.5	11.4	6.3	9.1	12.4	7.6	10.1	13.7	5.7	10.2	17.8
28-May	6.5	10.2	15.2	3.9	7.9	14.5	5.3	11.0	21.8	3.9	11.4	31.8
29-May	7.8	12.9	18.3	3.2	11.2	21.8	5.1	14.1	24.9	1.6	17.1	45.4
30-May	12.1	15.1	18.3	7.7	12.7	20.9	10.0	15.5	22.4	5.6	17.1	40.7
31-May	10.5	14.7	20.0	6.4	12.5	25.7	8.8	15.4	27.6	4.1	17.9	48.5
1-Jun	9.9	13.8	17.5	5.7	11.6	20.6	7.7	15.0	24.6	4.2	17.9	45.0
2-Jun	11.9	15.2	18.2	7.7	12.6	20.7	9.9	16.1	26.5	5.0	17.6	40.9
3-Jun	12.0	14.9	17.8	8.4	12.5	20.6	10.2	15.2	22.0	5.7	17.9	44.5
4-Jun	11.2	12.5	13.7	9.1	11.1	14.2	10.5	12.8	16.3	9.2	12.8	19.3
5-Jun	12.0	14.8	18.7	11.0	13.3	19.4	11.8	15.7	23.3	11.1	18.7	41.9
6-Jun	13.1	15.1	18.0	10.0	13.8	19.8	12.1	15.4	23.1	11.5	15.8	31.3
7-Jun	14.5	16.2	18.5	11.1	14.6	18.4	12.8	16.3	22.0	10.2	16.4	27.9
8-Jun	12.6	18.1	24.2	10.0	17.8	26.7	11.1	20.0	30.4	9.1	21.5	42.8
9-Jun	17.2	19.4	21.7	11.1	15.5	20.6	14.0	19.8	26.5	8.4	20.5	42.1
10-Jun	15.1	19.0	22.9	11.7	17.5	26.1	13.5	19.5	26.8	9.9	21.7	49.4
11-Jun	14.7	19.2	23.9	10.8	17.9	25.6	12.4	20.5	30.0	9.6	21.7	42.8
12-Jun	15.4	18.9	21.6	10.9	15.1	21.3	13.0	18.5	24.7	10.8	19.8	38.9

Date	Battery temperature (°C)			Ambient temperature (°C)			Box temperature (°C)			PV temperature (°C)		
	Min	Avg	Max	Min	Avg	Max	Min	Avg	Max	Min	Avg	Max
	13-Jun	12.4	14.3	16.2	10.2	12.0	16.3	11.6	14.3	19.4	9.8	15.3
14-Jun	12.6	13.2	14.0	11.1	12.6	14.4	12.1	13.4	15.8	10.3	13.1	18.6
15-Jun	12.6	14.6	17.7	11.6	14.3	20.7	12.5	15.5	22.7	11.7	15.6	31.9
16-Jun	13.3	15.9	19.8	11.2	14.6	20.8	12.3	16.6	25.1	10.6	15.8	28.4

APPENDIX B MATLAB CODES FOR CHARGE CONTROLLER AND BATTERY COMPONENTS

Charge controller MATLAB code:

```
Impp = trnInputs(1);
current = trnInputs(2);
signall = trnInputs(3);
load = trnInputs(4);
sooc = trnInputs(5);
V = trnInputs(6);
SOC1 = trnInputs(7);
SOC2 = trnInputs(8);
SOC3 = trnInputs(9);
if signall == 1
    if sooc > SOC1
        I=-1*(load/V);
        if I > -4.47
            I= - 4.47;
        end
    elseif sooc <= SOC1
        I=0;
    end
elseif signall == 0;
    if sooc <= SOC2
        I = Impp;
    elseif sooc > SOC2 && sooc < SOC3
        I =current;
    elseif sooc >= SOC3
        if current > 0.2
            I=0.2;
        else
            I=current;
        end
    end
end
trnOutputs(1) = I;
mFileErrorCode = 0;
```

Battery component MATLAB code:

```
signall= trnInputs(1);
I = trnInputs(2);
T = trnInputs(3);
I10 = 22.9;
C10 = 229;
C=229;
Inicharge = 200;
Tref = 25;
CellNum=6;
if (trnTime - trnStartTime) < 1.5*trnTimeStep
    Ah=Inicharge;
```

```

        soc=1;
    end
    Ah = Ah+( I * trnTimeStep);
    if signall==1
        e=-1*(I/I10);
        c=real((1.67*C10*(1+(0.005*(T-Tref)))/(1+(0.67*(e^0.9)))));
        soc=Ah/c;
        sooc=Ah/C;
        V=CellNum*(real((2.085-0.12*(1-soc))-(-
1*I/C10)*((4/(1+(I^1.3)))+(0.27/((soc)^1.5))+0.02)*(1-0.007*(T-
Tref))));
    end
    if signall==0
        e=(I/I10);
        c=real((1.67*C10*(1+(0.005*(T-Tref)))/(1+(0.67*(e^0.9)))));
        eta=1-exp((20.73/(e+0.55))*((soc)-1));
        soc=(Ah/c)*eta;
        sooc=(Ah/C);
        V=real (CellNum*((2+0.16*soc)+(I/C10)*((6/(1+(I^0.86)))+(0.48/((1-
soc)^1.2))+0.036)*(1-(0.025*(T-Tref))));
    end
    if V >= 14.2;
        V=14.2;
    end
    if sooc >=0.9
        V=14.2;
    end
    trnOutputs(1)=V;
    trnOutputs(2)=sooc;
    trnOutputs(3)=Ah;
    mFileErrorCode = 0;

```


APPENDIX C IPN PROREMOTE SETTING MENUS

Top menu

BATTERY	The values are related to battery voltage and net current respectively.
INPUT CHG	Values related to input and output current respectively
BATTERY CAPACITY	The values in these boxes indicate remaining capacity of the battery in percentage or number of Ah from full based on Ah counting.
BATTERY AMP-HRS FROM FULL	
AUX BAT AUX CHG	Based on selected function of Charge controller (charging auxiliary battery or accommodating required power for connected load) auxiliary battery voltage or load control status is shown respectively.
LOAD CONTROL OUTPUT	
EQLIZE NOW AT ... V	Equalization cycle would be controlled through this box by adjusting internal time accumulator or manually control the end.
ENTER ADVANCED DISPLAY/SETUP	Access to advanced display setup menu is provided through this box.

Advanced display menu

LAST FULL CHARGE

LAST EQUALIZE

The respective boxes show number of days since last full charge or equalize. The counter starts to work after applying the battery and transition occurs every 24 hours.

MAX BAT VOLTS

MIN BAT VOLTS

The maximum and minimum detected battery voltage is logged since last cleared.

TOTAL CHG AMP-HR

This box shows total amount of captured Amp-hours since last cleared.

LIFETIME BAT AH

Due to this feature, Battery life time could be estimated through capturing total discharge Amp-hours since last cleared

BAT TEMPERATURE

Shows measured temperature of battery pack through installed temperature sensor.

VIEW CHARGE UNIT

STATTUS

The detected values for PV input current and voltage as well as output current are available through this box

ENTER SETUP MENU

The respective box provides access to Setup menu in order to more detailed adjustment.

Setup menu

BAT AMP-HRS

The respective box must be adjusted regarding rated capacity of battery at 20 °C and 20 hours discharge

CHG Efficiency

The adjusted value in this box related to efficiency of battery charging and has notable impact on accuracy of estimating remained battery charge. Charge efficiency can be set manually or automatically based on battery operation during various

SELF-DISCHG

Similar to charge efficiency, adjusted value for monthly self-discharge is effective on predicting the amount of energy stored in the battery.

AUX OUT OFF
SETPOINT

AUX OUT ON
SETPOINT

As mentioned earlier based on selected function, accommodating required power for attached load or charging auxiliary battery can be controlled between on/off mode

POST-DUSK LIGHTS

Based on time controlling feature of charge controller post-Dusk and pre-Dawn timer can be set to appropriate time values based on night time duration.

PRE-DAWN

BAT CHARGE
PARAMETER MENU

Access to voltage set points for controlling the charging process is provided through this tab.

Battery charge parameter menu

ACCEPT CHG VOLTAGE	<p>During charging process transition from acceptance mode to bulk occurs when battery voltage hit the acceptance voltage which can be set between 10 and 80 V according to battery specification data sheet. Acceptance voltage is associated with</p>
FLOAT CHG VOLTAGE	<p>For increasing the battery life time charging process divided into two/three stages. Battery voltage should be kept constant during second phase of charging when SOC increases from 70 to 90%. Prospective voltage can be set between 10 and 80 V through this</p>
EQUALIZ VOLTAGE	
EQUALIZ TIME	<p>In the case that equalization process is required, voltage, duration and the interval between each cycle can be set through these three tabs.</p>
AUTO EQUALIZ	
T-COMP SLOPE	<p>For more precise operation, voltage drop versus temperature can be set between 0 and 8mV/C per cell.</p>
FLOAT CURRENT	<p>Transition from second stage (Acceptance mode) to third stage (Float mode) occurs when battery current drop to certain value. Prospective current set point can be set between 0.1 and 10 Amp per each 100 Ah of battery capacity.</p>
FLOAT CURRENT	<p>In addition to current set point float stage can be controlled by setting acceptance charge time between 0 and 10 hours.</p>